2016

Stimuli Responsive Nanoparticle for Cancer Targeted Therapy

Huacheng He
University of South Carolina

STIMULI RESPONSIVE NANOPARTICLE FOR CANCER TARGETED THERAPY

by

Huacheng He

Bachelor of Engineering
Zhejiang University, 2009

Submitted in Partial Fulfillment of the Requirements

For the Degree of Doctor of Philosophy in

Pharmaceutical Sciences

College of Pharmacy

University of South Carolina

2016

Accepted by:

Peisheng Xu, Major Professor

Campbell McInnes, Committee Member

Kim Creek, Committee Member

Patrick Woster, Committee Member

Hui Wang, Committee Member

Lacy Ford, Senior Vice Provost and Dean of Graduate Studies

DEDICATION

This dissertation is dedicated to my supportive wife, Jiang, and my parents for their endless love, support and encouragement.

ACKNOWLEDGEMENTS

I am profoundly grateful to my advisor, Dr. Peisheng Xu for his mentorship, support, and encouragement throughout my graduate training. He always inspires me to think independently, intrigues me to pursue a career of science. He is not only an excellent teacher but also a closer friend who gives me great assistance, making my oversea life much easier.

I would like to express my acknowledgement to my committee members, Dr. Campbell McInnes, Dr. Kim Creek, Dr. Patrick Woster, Dr. Hui Wang for their time, suggestions and support.

I would like to acknowledge all the faculty, staff and students in South Carolina College of Pharmacy for making my oversea study life richer and more fruitful.

I would also like to acknowledge the following professors, colleagues, and former lab members who have given me so many helps and mentorship: Dr. Anna-Liisa Nieminen, Dr. Eleni Markoutsa, Dr. Diego Altomare, Dr. Ufuk Ozer, Dr. Remant K.C, Dr. Gary Schools, Bei Cheng and Bindu Thapa.

Finally, I am deeply indebted to my family: my parents for their love and unconditional support, my wife, Jiang, for her incredible sacrifices, encouragement and support during this challenging time.

ABSTRACT

Nanoparticle is the particle with a size in the range from several nanometers to hundreds of nanometers. It has been extensively used for cancer diagnosis and therapy. However, it is still a great challenge to fabricate nanoparticles with spatiotemporally controllable delivery of anticancer drugs to tumors and with high therapeutic efficacy. This thesis mainly focuses on the development of stimuli responsive nanoparticles for cancer targeted therapy. These nanoparticles either response to internal stimuli such as pH and redox potential or external stimuli like temperature and light could effectively target tumors and control the release of anticancer drugs there to improve their anticancer efficacy as well decrease adverse effects.

We firstly developed a poly[(2-(pyridin-2-yldisulfanyl)ethyl acrylate)-co-[poly(ethylene glycol)]] (PDA-PEG) polymer and found that this polymer when combined with copper could efficiently kill a wide spectrum of cancer cells, including drug resistant cancer cells, while sparing normal cells. Next, we used this polymer or its derivatives to fabricate a series of stimuli responsive nanogels for targeted photodynamic therapy (PDT). These nanogels could efficiently target tumors under the help of targeting ligands and control photosensitizers release in the tumor by response to pH, redox potential and temperature, and finally induce high anticancer efficacy.

To further improve the therapeutic efficacy, a polydopamine coated poly(lactic-co-glycolic acid) nanoparticle was developed for chemo-thermal therapy. This nanoparticle could respond to near infrared light (NIR) to release the anticancer drug

(doxorubicin) in the tumor and effectively eradicate head and neck tumor in a xenograft mouse model by combining the NIR-mediated photothermal therapy and doxorubicin induced chemotherapy.

TABLE OF CONTENTS

DEDICATION III

ACKNOWLEDGEMENTS IV

ABSTRACT V

LIST OF FIGURES IX

CHAPTER 1: STIMULI RESPONSIVE NANOPARTICLE FOR CANCER THERAPY 1

1.1 CANCER AND CURRENT CANCER THERAPY 1

1.2 NANOPARTICLE FOR CANCER THERAPY 3

1.3 PLAN OF RESEARCH 13

1.4 REFERENCES 16

CHAPTER 2: CANCER CELL SELECTIVE-KILLING POLYMER/COPPER COMBINATION 21

2.1 INTRODUCTION 21

2.2 EXPERIMENTS 23

2.3 RESULTS AND DISCUSSION 32

2.4 CONCLUSIONS 47

2.5 REFERENCES 49

CHAPTER 3: SELF-QUENCHING BIOACTIVATABLE NANOGEL FOR TARGETED PHOTODYNAMIC THERAPY 52

3.1 INTRODUCTION 52

3.2 EXPERIMENTS 56

3.3 Results and Discussion 64

3.4 Conclusions 81

3.5 References 82

Chapter 4: Triple-responsive Expansile Nanogel for Tumor and Mitochondria Targeted Photosensitizer Delivery 85

4.1 Introduction 85

4.2 Experiments 87

4.3 Results and Discussion 95

4.4 Conclusions 108

4.5 References 109

Chapter 5: Mussel Inspired PLGA/polydopamine Core-shell Nanoparticle for Light Induced Cancer Thermochemotherapy 111

5.1 Introduction 111

5.2 Experiments 112

5.3 Results and discussion 120

5.4 Conclusions 130

5.5 References 131

Chapter 6: Summary and Future Directions 133

6.1 Summary 133

6.2 Innovation and Significance 134

6.3 Future Directions 135

Appendix: Permission to Reprint 137

LIST OF FIGURES

Figure 1.1 Illustration of the in vivo fate of the nanoparticle and its mechanism for cancer targeted therapy 10

Figure 2.1 Cytotoxicity of DTP for different cell lines. 22

Figure 2.2 Representative ^{1}H-NMR spectrum and GPC curve for PDA-PEG polymer... 33

Figure 2.3 TEM images of nanoparticle fabricated from PDA-PEG..... 34

Figure 2.4 The size distribution of nanoparticles formed from PDA-PEG polymer and PDAPEG/Cu^{2+} acquired by dynamic light scattering 34

Figure 2.5 Cytotoxicity of PDA-PEG nanoparticle for different cell lines. 36

Figure 2.6 Cytotoxicity of PDA-PEG/Cu^{2+} combination for normal and cancer cells..... 36

Figure 2.7 The concentration effect of $CuCl_2$ on the cytotoxicity 37

Figure 2.8 Fluorescence images of cancer cells after culturing with different concentrations of PDA-PEG/Cu^{2+} combination 38

Figure 2.9 Flow cytometry spectra of SKOV-3 and NIH 3T3 cells and confocal images of cellular uptake of nanoparticles in SKOV-3 cells..... 40

Figure 2.10 The flow cytometry spectra of SKOV-3 and NIH 3T3 cells treated with Cy5 labeled PDA-PEG nanoparticles 41

Figure 2.11 The release kinetic of pyridine-2-thiol liberating from PDA-PEG 42

Figure 2.12 The effect of GSH-MME on the cytotoxicity of PDA-PEG/Cu^{2+} 44

Figure 2.13 The effect of BSO on the cytotoxicity of PDA-PEG/Cu^{2+} 44

Figure 2.14 RNA expression in response to PDA-PEG/Cu^{2+} treatment..... 46

Figure 2.15 Cell cycle analysis of SKOV-3 cells after treated with PDA-PEG/Cu^{2+}. 47

Scheme 3.1 Schematic illustration of the self-quenching bioactivatable nanogel for targeted photodynamic therapy 55

Scheme 3.2 Illustration of the synthesis of polymers and the fabrication of PhA nanogels 65

Figure 3.1 ^{1}H-NMR spectra of PhA, PDA-PEG, PDA-PEG-PhA and PDA-PEG-AEME 66

Figure 3.2 Size and surface charge of PhA nanogels 68

Figure 3.3 Absorption, fluorescence and photoactivity 71

Figure 3.4 Cellular uptake and intracellular localization of nanogels 75

Figure 3.5 *In vitro* cytotoxicity of PhA, Pha-NG and PhA-ENG 77

Figure 3.6 *In vivo* distribution of PhA nanogels 79

Figure 3.7 Antitumor activity of free PhA and PhA nanogels 80

Figure 4.1 Schematic illustration of the synthesis of MBA-PDA-PEG-PNiPMA polymer and the fabrication of MBA-Pc 4-TRN nanogels 87

Figure 4.2 ^{1}H NMR and GPC spectra of PDA-PEG-PNiPMA polymer 96

Figure 4.3 The z-average size of TRN in response to the change of temperature, the addition of DTT (C), and the change of pH 97

Figure 4.4 Stability of TRN at 37 °C monitored by dynamic light scattering 99

Figure 4.5 The Pc 4 release kinetics of TRN at different conditions 100

Figure 4.6 The expression of sigma-2 receptor in head and neck cancer and its effect on the cellular uptake of MBA-Pc 4-TRN 102

Figure 4.7 Subcellular co-localization of Pc 4 loaded TRN with lysosome and mitochondria 104

Figure 4.8 Cellular uptake of Pc 4 after 4 and 20 h of culture 105

Figure 5.1 Fabrication of PhA-ENG, proposed cellular uptake and TEM images 120

Figure 5.2 Physical properties of nanoparticles fabricated based on PLGA polymer. ... 121

Figure 5.3 The photothermal effect of DOX@PLGA/PD on medium temperature elevation, drug release kinetics, and cell viability 124

Figure 5.4 Confocal images, flow cytometry spectra, and cytotoxicity of DOX@PLGA/PD-C treated UMSCC 22A cells 126

Figure 5.5 Tumor response after receiving different treatments..... 127

Figure 5.6 The TEM images of heart tissue sections and H&E staining images of liver and tumor tissue sections 129

CHAPTER 1

STIMULI RESPONSIVE NANOPARTICLE FOR CANCER THERAPY

1.1 CANCER AND CURRENT CANCER THERAPY

Cancer is a group of diseases characterized by uncontrolled growth and spread of abnormal cells, which has become one of the leading causes of death in both developing and developed countries. According to the latest report by World Health Organization, 14.1 million new cancer cases were diagnosed and 8.2 million people died from cancer worldwide in 2012, and these numbers are still increasing continuously and expected to rise to 19.3 million for new diagnosed cancer cases each year by 2025.[1] The high incidence and mortality of cancer strain heavily on the world health-care system and are projected to cost the world approximately 458 billion U.S dollars for cancer prevention, diagnosis, treatment and other cancer caused economic issues in 2030.[2] As the world population ageing, unhealthy eating habits globally spreading and risk factors steadily increasing such as tobacco use, the situation for cancer therapy become more and more harsh and urgent.

Currently, the widely used cancer treatments including surgery, radiotherapy and chemotherapy. In surgery, tumors are directly removed by surgeon using scalpels, while in radiotherapy and chemotherapy tumors are exposed to high dose of X- or gamma ray, or anticancer drugs respectively, both of which finally induce the death of cancer cells. All of these treatment modalities have been proved to be effective for cancer therapy and

have saved or prolonged millions of patients' lives in the past decades. However, these treatments still have lots of limitations. It is extremely difficult for surgeons to cut off the entire tumor from the patient body especially in the late stage when the tumor is too big. The tumor left in the patient body after surgery can easily initiate tumor recurrence, metastasis and eventually cause patients' death. Thus radiotherapy and chemotherapy are extensively used after surgery, since further X-ray irradiation or anticancer drug treatment will help destruct the rest of tumor in the patient body after surgery and inhibit tumor growth and metastasis. Yet radiotherapy and chemotherapy themselves have severe side effects. Due to the use of ionizing laser, the radiotherapy generally will cause serious damage to normal tissues neighboring the tumor.[3] In chemotherapy, anticancer drugs usually evenly distribute to both tumor and normal tissues, and the nonspecific accumulation of anticancer drugs in normal tissues always induce severe systemic toxicity. For example, the anthracycline anticancer drug doxorubicin which is an effective chemotherapeutic agent and frequently used for various malignancies have been reported to induce fatal heart failure (cardiomyopathy).[4] Consequently, some cancer patients are died from these side effects instead of dying from cancer itself. Besides the side effects of radioactive beams and anticancer drugs retarding the application of radiotherapy and chemotherapy, cancer cells itself also makes some adjustments to reduce the efficacy of these treatments and threaten patients' lives. For instance, multi-drug resistance protein 1 (MDR1) is found overexpressed in many tumors and its overexpression promotes elimination of various anticancer drugs out of cancer cells such as taxanes, topoisomeraseinhibitors and antimetabolites, and thus dramatically decreases anticancer efficacy by lowering intracellular drug concentration.[5] Other mechanisms,

including drug inactivation,[6] drug targets alteration,[7] DNA damage repair[8] and dysfunction of cell apoptosis pathway,[9] are also widely developed among tumors, making chemotherapy fail. Because of all reasons mentioned above, exploring alternative modalities to improve anticancer effectiveness as well as reduce adverse effects is extremely necessary and urgent. Thus, nanomedicine, as a novel strategy for the treatment of cancer has been proposed and explored.

1.2 NANOPARTICLE FOR CANCER THERAPY

1.2.1 Nanoparticle and its advantages and limitations for cancer therapy

Nanoparticles are particles with a size in the nanometer range from several nanometer to hundreds of nanometers, including polymer conjugate, micelles, dendrimers, nanogels, liposomes, quantum dots, gold nanoparticles and others.[10] In the chemotherapy scenario, anticancer drugs are loaded into nanoparticles which will serve as carriers to efficiently deliver the drugs to the tumor and release drugs effectively to kill cancer cells. There are several advantages of nanoparticle based chemotherapy over conventional chemotherapy for cancer treatment.[11,12] Firstly, as the majority of anticancer drugs are hydrophobic, their systemic applications are hindered. The application of nanoparticles will improve these drugs' aqueous solubility by providing a hydrophobic internal minienvironment for them, and prevent their precipitation and premature degradation by isolating them from the biological environment. Meanwhile, nanoparticles can prolong the circulation time of the drugs in the blood stream and thus increase their opportunity to reach the tumor to take effect. Furthermore, nanoparticles can also overcome drug resistance and improve the drug's anticancer efficacy because compared to free drug the nanoparticle enters cancer cells by a different pathway which bypasses

the MDR1 mediated drug efflux. During the past decades, nanoparticles have got phenomenal progress and remarkably improved the treatment effectiveness for cancer therapy. Till now, several nanoparticles have been approved by FDA and use clinically, including Doxil® and Abraxane®.

However, there are still many shortages existed for nanoparticle based chemotherapy. In one hand, the premature release of anticancer drugs in the blood stream can result in nonspecific distribution of anticancer drugs in normal tissues, increasing the risk of systemic toxicity.[13] In the other hand, the slow drug release in the tumor site can limit drug efficacy due to its low active drug concentration.[14] It is very challenging in balancing the drug release of nanoparticles in blood and in tumor since no or minimal drug release is wanted in the blood stream while rapid and high amount of drug release in tumor is expected. Moreover, due to the size, surface charge and other effects, the nanoparticle sometimes has very low cellular uptake.[15] This becomes extremely critical for those drugs whose anticancer effects should be only intracellularly activated. The low cellular uptake usually induces negligible efficacy. Therefore, nanoparticles with advanced functionality is essentially needed to improve their anticancer performance. These nanoparticles should be extremely stable in the circulation process, highly accumulated in tumor, and efficiently enter the cancer cells, where rapid drug release occurs, and reach enhanced anticancer effect. Fortunately, the unique cancer physiobiological characteristics provide the basis for researchers to develop such kind of highly functionalized nanoparticles.

1.2.2 Cancer physiobiological characteristics and nanoparticle design

Enhanced permeability and retention effect and tumor accumulation of nanoparticles

The most well-known property of the cancer is the enhanced permeability and retention effect (EPR effect), which has been discovered for more than 30 years. In the mid-1980s, Matsumura et al. found that proteins larger than 30 kDa could preferentially accumulate in tumor interstitium and remain there for prolonged periods of time. They ascribed this tumoritropic accumulation to the presence of fenestrations in the imperfect blood vessels and the prolonged retention to the poor lymphatic drainage in tumor.[16] Since then, the mechanism of EPR effects has been extensively investigated and more fundamental knowledge about EPR has been unveiled.[17] When tumor grows to a certain size, it cannot get enough oxygen and nutrition from its surrounding normal vasculature for its further proliferation. At this time point, the dying cancer cells will secrete growth factors to trigger the budding of new blood vessels from the existing capillaries.[18] This process is called angiogenesis and it promotes the rapid generation of irregular blood vessels which induces the formation of fenestrations due to the discontinuousness of epithelium and the lack of the basal membrane in the blood vessels.[19] When nanoparticles reach to the tumor, they can easily extravagate to the tumor from the porous blood vessels due to their small size (<200 nm) comparing to the pore size in the blood vessels (~200-2000 nm).[17,20] This explains the enhanced permeability portion of EPR effect. For the enhanced retention, it is because of the deficiency of the lymphatic system in the tumor, which only allow extravasated solutes and colloids return to circulation by themselves.[17,21] As small molecules can easily diffuse back to blood, nanoparticles, due to their larger hydrodynamic size, they are trapped in the tumor interstitium for a

prolonged time. Thanks to the EPR effect, nanoparticles can achieve a high specificity in delivering anticancer drugs to tumor. In fact, almost all currently used nanoparticles, their tumor specific accumulation is greatly relied on the EPR effect. That is why now EPR effect has become the central dogma for nanoparticle based anticancer drug delivery and has been widely used to explain and design nanoparticles for efficient tumor therapy.

Acidic pH and pH responsive nanoparticles

The second important physiobiological property for tumor is the acidic pH in tumor environment. Tumor stroma usually has a pH in the range of 6.5-6.8, which is lower than the pH in blood and other normal tissues (~7.4).[22] The low pH in tumor is ascribable to the production of large amounts of lactate by cancer cells through "aerobic glycolysis", which was firstly discovered by Otto Warburg's in 1924.[23] The difference of pH between the tumor and normal tissue can be utilized to guide the design of pH responsive nanoparticles, which are stable in blood stream while release anticancer drugs in low pH tumor stroma. The pH responsiveness will decrease the side effects as well as enhance the anticancer efficacy of nanoparticles since unwanted drug leaky in blood stream can be minimized and high dose of active drug can be reached at tumor due to a pH triggered drug release. To fabricate such kind of nanoparticles, two strategies are currently widely applied, either using physical interaction or chemical bonds. Nanoparticles formed through physical interaction usually base on the hydrophobic interaction between carrier materials and anticancer drugs. These nanoparticles generally contain an amphiphilic polymer which can bury anticancer drugs in its hydrophobic core and release them in tumor by changing itself to hydrophilic polymer at low pH.[24] Beside of physical interaction, some acidic liable chemical bonds are also incorporated to make

pH responsive nanoparticles. These bonds including ester bond, amide, acetal and ketal are relative stable in physiological condition, while degradable in low pH.[25] Nanoparticles contain these bonds can break up at tumor site through the bond degradation and thus release a high amounts of anticancer drugs for enhanced cancer therapy.[26]

Upregulated glutathione and redox responsive nanoparticles

Glutathione (GSH) is a tripeptide of glutamate, cysteine and glycine existing at high concentration in virtually all mammalian tissues. It plays an important role in nutrient metabolism, antioxidant defense, and regulation of cellular processes, such as cell proliferation, differentiation and apoptosis. Disturbance of GSH homeostasis is tightly associated with progression of many diseases including cancer. A great number of clinical data have revealed that GSH level is elevated up to 10 folds in many types of tumors, including liver tumor, breast tumor, lung tumor, neck and head tumor, gastrointestinal tumor and gynecological tumor.[27] Compared to normal cells, cancer cells also exhibit 7-10 fold higher intracellular GSH concentration.[28] From the genetic view, the high GSH in tumor is ascribable to genes that express GSH-transferases (GST) with reduced enzymatic activity. GST decreases GSH level by catalyzes the conjugation of GSH with many exogenous and endogenous electrophilic substrates. The reduction of GST activity in tumor lowers the consumption of GSH and thus promotes its elevation.[29] The high GSH level both in tumor and cancer cells provide another trigger to induce tumor specific drug release, therefore GSH or redox potential responsive nanoparticles have been developed.[30] This kind of nanoparticle generally have disulfide bonds or other redox sensitive bonds which can be quickly cleaved only at the presence of high GSH.

Since the relative low GSH in normal tissue and blood stream (2-20 μM), premature release of anticancer drug can be minimized in those tissues, while rapid drug release will occur in tumor due to its high GSH (2-10 mM).[31] The tumor specific drug release can lead to enhanced cancer therapy with minimal adverse effects.

Cu elevation and anti-angiogenesis

Copper is an important trace metal that plays critical roles in maintaining normal biological functions. Elevated copper concentration (up to 2–3 fold) is frequently observed in a wide spectrum of tumors including ovarian, breast, cervical, prostate and leukemia.[32] Although the detailed molecular mechanism for copper increase is still not clear, sufficient amount of evidence suggests that copper elevation is highly associated with tumor angiogenesis.[33] Angiogenesis is the process of development of new blood vessels. In normal cells, it is precisely regulated by a complex interaction and balance between endogenous stimulators and inhibitors. In tumor, however, the synthesis of the stimulators either by tumor itself or by endothelial cells is elevated to improve the rapid generation of new blood vessels to supply tumor with enough oxygen and nutrition for proliferation. The stimulators includes Vascular Endothelial Growth Factor (VEGF), Tumor Necrosis Factor a (TNF-a), Epidermal Growth Factor (EGF), copper and others. And this probably is one of the reasons that lead to the copper increase in tumor. The high copper concentration induces the tumor progression as well as metastasis. Therefore, depleting copper in tumor will be a promising alternative strategy to control tumor growth.[34] In fact, the elevated copper in tumor has already been developed as a target for cancer therapy since many researchers found that copper chelators which form

complex with copper could effectively inhibit the growth of tumor by the removal of copper from tumors to impede the tumor angiogenesis (anti-angiogenesis).[35]

Receptor overexpression and tumor targeting

Although nanoparticles can passively accumulate in tumor by EPR effect, their anticancer efficacy may still be very low if only few nanoparticles enter cells where anticancer drugs take into effect. Hence, enhanced cellular uptake is high demanded. Currently, the main strategy is to decorate nanoparticles with targeting ligands to improve their cellular uptake efficiency. The targeting ligands include proteins, antibodies, peptides, sugars, nucleic acids and small molecules.[17] The mechanism behinds the ligand mediated cellular uptake is the recognition of ligands by its target substrates (receptors). As numerous paper reported, many cancers overexpress specific receptors on their cell surfaces. For example, epidermal growth factor receptor (EGFR) is found overexpressed in cervical, head and neck, ovarian, bladder and esophageal cancer.[36] The elevated expression of EGFR increases the sensitivity of cancer cells to ambient level of growth factors that normally would not trigger proliferation. For nanoparticle, the high density of receptors in cancer cells will promote a strong interaction between the cell and the nanoparticle, increasing the opportunity of the nanoparticle entering the cells through receptor mediated endocytosis.

Based on above mentioned tumor characteristics, stimuli responsive tumor targeted nanoparticles are created and their tumor specific targeting and drug release is summarized in **Figure 1.1.**[11] The whole scenario is as follows: the ligand modified nanoparticle will specifically accumulate in tumor by EPR effect (passive targeting). When nanoparticles reach the tumor, due to the low pH or high GSH level there, they will

be degraded and anticancer drugs (yellow dots) will be released and enter cells to take effect. In some situations, the pH and GSH may not be strong enough to break up the nanoparticles in extracellular environment, then the nanoparticles will enter the cells through the ligand-receptor interaction (active targeting). Upon cellular uptake, because of the extremely low pH (4-5) in endosomes/lysosomes or high GSH in cytosol, the nanoparticles will be destroyed and drugs will be liberated to kill cancer cells. In contrast to free drugs, the tumor specific accumulation and controlled drug release of nanoparticles will impose minimal toxicity to normal tissues while generate significantly high anticancer efficacy.

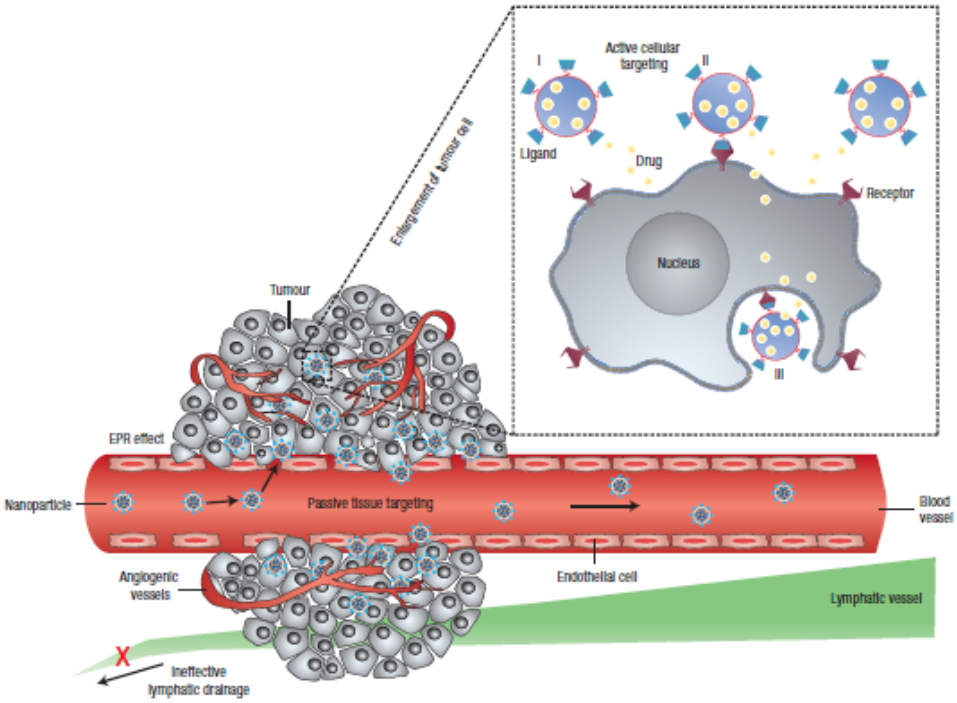

Figure 1.1 Illustration of the *in vivo* fate of the nanoparticle and its mechanism for cancer targeted therapy. Reprinted by permission from Macmillan Publishers Ltd: [Nature Nanotechnology] (Ref.11), copyright (2007).

1.2.3 Advanced nanoparticles for cancer therapy

As we know, tumors are heterogeneous and dynamically changing to adapt to their environments. They can develop drug resistance after initial treatment of anticancer drugs due to physiobiological alteration. Therefore, it is sometimes very difficult to treat tumor with chemotherapy. Although nanoparticles exhibit improved performance, their efficacy may still be destructed due to the heterogeneity and dynamics of tumors. Furthermore, single responsiveness of nanoparticles may not efficient enough to release sufficient amounts of anticancer drug to kill cancer cells. As these issues have arisen, developing advanced nanoparticles endowed with more functions will be extremely necessary. These advanced nanoparticles include multi-responsive nanoparticles, multi-targeting nanoparticles, and nanoparticle for combined therapy. For multi-responsive nanoparticles, two or more stimuli responsiveness will be incorporated into one nanoparticle, such as pH and redox dual responsiveness, pH, redox and temperature triple responsiveness. This kind of nanoparticles can response to different stimuli simultaneously and improve the drug release profile. Xu et al. reported a pH and redox responsive nanogel.[37] This nanogel contained ester bonds and disulfide bonds and can be degraded at low pH and high GSH, respectively. Because of the dual responsiveness, the nanogel showed a more controllable drug release profile which has low drug release at neutral pH while release more drugs at pH 5.0 and further release was reached at high GSH condition. This well controlled release made the nanogel has much higher anticancer efficacy. Since tumors undergo dynamically changing, their receptor expression is also altered spatiotemporally, which may decrease tumor targeting effect of nanoparticles. To overcome this issue, Karathanasis et al. conjugated two peptides

targeting P-selectin and $\alpha_v\beta_3$ integrin to the nanoparticle to guarantee the effectiveness of targeting ligands at different tumor sites and stages of breast cancer, which generally have varied receptor expression level.[38] Results revealed that the dual targeting nanoparticle had much better tumor homing performance than single ligand labeled nanoparticle because either one or both of the two targeting ligands can take effect to improve the cellular uptake of nanoparticle no matter the spatiotemporal changes of receptors in the tumor.

Drug resistance of tumor is a big challenge associated with chemotherapy. Currently, the most effective way to treat cancer with drug resistance is using combination therapy. In combination therapy, two or more treatments with different anticancer mechanisms are applied. As the tumor become resistance to one treatment, it still can be cured by the other one, inducing enhanced anticancer efficacy because of the beneficial interaction between treatments. Nanoparticles either loaded with two or more anticancer drugs or functionalized with different treatment modalities can realize the combination therapy. As reported, co-encapsulation of doxorubicin and 17-AAG or doxorubicin and camptothecin had showed enhanced cancer therapy ascribing to the synergistic effect between drugs.[39] Not only drug and drug interaction exhibits synergistic effect, two different treatment strategies also showed synergism in killing cancer cells. For example, Yang et al. used gold nanorod loaded mesoporous silica (GNR@$mSiO_2$) to deliver doxorubicin to treat lung cancer by combining chemotherapy (doxorubicin) with near infra-red (NIR) light induced photothermal therapy.[40] *In vivo* data showed that under a 808 nm laser irradiation, the nanoparticle could rapidly heat the tumor to 66 ºC and induce photothermal therapy (PTT), following the increased release of doxorubicin from

the nanoparticle for chemotherapy. Due to the great synergistic effect between PTT and chemotherapy, the nanoparticle finally reach a 66.5% tumor inhibition rate which is much better than free doxorubicin and combination treatment of GNR@$mSiO_2$ and laser. Since the high effectiveness of combination therapy, more and more researches are focusing on this cancer treatment regime. Recently, nanoparticles with combination property have been being extensively investigated to combat cancer.

1.3 PLAN OF RESEARCH

The overall goal of this research is to develop stimuli responsive nanoparticles to realize one or several following aspects: 1) controlled release; 2) enhanced anticancer efficacy; 3) minimized side effects. The studies described in this dissertation investigated the following hypotheses:

1. Therapeutic agents which target copper will result in cancer specific killing effect.
2. Loading chemotherapeutic agents into a polymer containing stimuli sensitive bonds such as disulfide bonds, ester bonds and temperature sensitive segment will achieve stimuli responsive nanoparticle for controlled drug release.
3. Modification of nanoparticle with targeting ligands will increase the cellular uptake and obtain enhanced anticancer efficacy.
4. Combination therapy will achieve enhanced anticancer effect.

To evaluate the hypotheses above mentioned, a research plan including specific aims and major objectives to achieve these aims was devised.

Specific Aim 1. Synthesize poly[(2-(pyridin-2-yldisulfanyl)ethyl acrylate)-co-[poly(ethylene glycol)]] (PDA-PEG) polymer and investigate its cytotoxicity toward normal and cancer cell lines.

a. Synthesize PDA-PEG with free radical polymerization and evaluate its cytotoxicity in numerous cancer and normal cell lines by MTT assay

b. Study the cellular uptake behaviour, gene expression and cell cycles of cancer and normal cell lines after treatment of PDA-PEG/copper to reveal the mechanism of cytotoxicity of the polymer/copper combination.

Specific Aim 2. Conjugate photosensitizer pheophorbide a (PhA) to PDA-PEG for fabrication of redox potential responsive nanogel for cancer targeted photodynamic therapy (PDT).

a. Conjugate PhA to PDA-PEG via disulfide bonds and fabricating the polymer into nanogel by the formation of disulfide crosslinking. Modify the nanogel with targeting ligand.

b. Investigate the redox potential responsiveness of the nanogel and study its impact on PhA release,

c. Investigate the influence of targeting ligands on the cellular uptake, intracellular distribution and *in vitro* PDT efficacy.

d. Evaluate the *in vivo* biodistribution, PDT efficacy and systematic toxicity of the nanogel.

Specific Aim 3. Synthesize poly[(2-(pyridin-2-yldisulfanyl)ethyl acrylate)-co-[poly(ethylene glycol)]]-co-[poly (N-Isopropyl methacrylamide)]

(PDA-PEG-PNiMA) and fabricate it into a pH, redox potential and temperature responsive nanogel for cancer targeted PDT.

a. Synthesize PDA-PEG-PNiMA by free radical polymerization and make the polymer into nanogel by disfulide crosslinking. Modify the nanogel with targeting ligands.
b. Investigate the responsiveness of the nanogel to pH, redox potential and temperature and study its influence on the drug release.
c. Investigate the impact of the targeting ligand on the cellular uptake, intracellular localization, and *in vitro* PDT.
d. Investigate the *in vivo* biodistribution and PDT efficacy of the nanogel

Specific Aim 4. Fabricate polydopamine coated PLGA nanoparticle for controlled drug release and light induced thermochemotherapy.

a. Fabricate doxorubicin loaded PLGA nanoparticle and conjugate targeting ligand to the surface of the nanoparticle through a polydopamine layer.
b. Study the influence of light irradiation on the temperature of the nanoparticle and its impact on the drug release profile.
c. Investigate the influence of the targeting ligand on cellular uptake and evaluate the *in vitro* anticancer efficacy of the nanoparticle when combines with light.
d. Study the in vivo anticancer efficacy and cardiotoxicity of the nanoparticle.

1.4 REFERENCES

(1)S. B. W and W. C. P *World Cancer Report 2014*; International Agency for Research on Cancer (I A R C) (UN), 2014.

(2)C. Cancer Progress Report Steering,C. L. Arteaga,P. C. Adamson,J. A. Engelman,M. Foti,R. B. Gaynor,S. G. Hilsenbeck,P. J. Limburg,S. W. Lowe,E. R. Mardis,S. Ramsey,T. R. Rebbeck,A. L. Richardson,E. H. Rubin,G. J. Weiner,A. Staff,S. M. Sweeney,K. Honey,J. Bachen,P. Driscoll,J. Hobin,J. Ingram,R. Kalamegham,R. Lobb,J. G. Retzlaff,M. L. Watts and N. R. Fuller, *Clin. Cancer Res.*, 2014, **20**, S1-S112.

(3)A. Master,M. Livingston and A. Sen Gupta, *J. Controlled Release,* 2013, **168**, 88-102.

(4)K. Chatterjee,J. Zhang,N. Honbo and J. S. Karliner, *Cardiology,* 2010, **115**, 155-162.

(5)C. Holohan,S. Van Schaeybroeck,D. B. Longley and P. G. Johnston, *Nat. Rev. Cancer,* 2013, **13**, 714-726.

(6)C. Meijer,N. H. Mulder,H. Timmer-Bosscha,W. J. Sluiter,G. J. Meersma and E. G. E. de Vries, *Cancer Res.,* 1992, **52**, 6885-6889.

(7)S. Kobayashi ,T. J. Boggon ,T. Dayaram ,P. A. Jänne ,O. Kocher ,M. Meyerson ,B. E. Johnson ,M. J. Eck ,D. G. Tenen and B. Halmos *New Engl. J. Med.,* 2005, **352**, 786-792.

(8)S. Fan,W. S. El-Deiry,I. Bae,J. Freeman,D. Jondle,K. Bhatia,A. J. Fornace,I. Magrath,K. W. Kohn and P. M. O'Connor, *Cancer Res.,* 1994, **54**, 5824-5830.

(9)S. Chen,Y. Dai,H. Harada,P. Dent and S. Grant, *Cancer Res.,* 2007, **67**, 782-791.

(10) R. Duncan, *Nat. Rev. Cancer,* 2006, **6**, 688-701; J. Gong,M. Chen,Y. Zheng,S. Wang and Y. Wang, *J. Controlled Release,* 2012, **159**, 312-323; P. Kesharwani,K. Jain and N. K. Jain, *Prog. Polym. Sci.,* 2014, **39**, 268-307; R. T. Chacko,J. Ventura,J. Zhuang and S. Thayumanavan, *Adv. Drug Delivery Rev.,* 2012, **64**, 836-851; T. M. Allen and P.

R. Cullis, *Adv. Drug Delivery Rev.,* 2013, **65**, 36-48; C. E. Probst,P. Zrazhevskiy,V. Bagalkot and X. Gao, *Adv. Drug Delivery Rev.,* 2013, **65**, 703-718; E. C. Dreaden,L. A. Austin,M. A. Mackey and M. A. El-Sayed, *Ther. Delivery,* 2012, **3**, 457-478.

(11) D. Peer,J. M. Karp,S. Hong,O. C. Farokhzad,R. Margalit and R. Langer, *Nat. Nanotechnol.,* 2007, **2**, 751-760.

(12) Z. Chen, *Trends Mol. Med.,* 2010, **16**, 594-602; X. Dong and R. J. Mumper, *Nanomedicine (London, U. K..),* 2010, **5**, 597-615.

(13) S. C. Owen,D. P. Y. Chan and M. S. Shoichet, *Nano Today,* 2012, **7**, 53-65.

(14) A. A. Manzoor,L. H. Lindner,C. D. Landon,J.-Y. Park,A. J. Simnick,M. R. Dreher,S. Das,G. Hanna,W. Park,A. Chilkoti,G. A. Koning,T. L. M. ten Hagen,D. Needham and M. W. Dewhirst, *Cancer Res.,* 2012, **72**, 5566-5575.

(15) Y. Jiang,S. Huo,T. Mizuhara,R. Das,Y.-W. Lee,S. Hou,D. F. Moyano,B. Duncan,X.-J. Liang and V. M. Rotello, *ACS Nano,* 2015, **9**, 9986-9993.

(16) Y. Matsumura and H. Maeda, *Cancer Res.,* 1986, **46**, 6387-6392.

(17) N. Bertrand,J. Wu,X. Xu,N. Kamaly and O. C. Farokhzad, *Adv. Drug Delivery Rev.,* 2014, **66**, 2-25.

(18) D. Bates,N. Hillman,B. Williams,C. Neal and T. Pocock, *J. Anat.,* 2002, **200**, 581-597.

(19) R. K. Jain, *Nat. Med.,* 1998, **4**, 655-657; R. K. Jain and T. Stylianopoulos, *Nat. Rev. Clin. Oncol.,* 2010, **7**, 653-664.

(20) S. K. Hobbs,W. L. Monsky,F. Yuan,W. G. Roberts,L. Griffith,V. P. Torchilin and R. K. Jain, *Proc. Natl. Acad. Sci.,* 1998, **95**, 4607-4612.

(21) T. P. Padera,B. R. Stoll,J. B. Tooredman,D. Capen,E. di Tomaso and R. K. Jain, *Nature,* 2004, **427**, 695-695.

(22) Y. Wang,K. Zhou,G. Huang,C. Hensley,X. Huang,X. Ma,T. Zhao,B. D. Sumer,R. J. DeBerardinis and J. Gao, *Nat. Mater.,* 2014, **13**, 204-212.

(23) R. A. Gatenby and R. J. Gillies, *Nat. Rev. Cancer,* 2004, **4**, 891-899; M. G. Vander Heiden,L. C. Cantley and C. B. Thompson, *Science,* 2009, **324**, 1029-1033.

(24) K. H. Min,J.-H. Kim,S. M. Bae,H. Shin,M. S. Kim,S. Park,H. Lee,R.-W. Park,I.-S. Kim,K. Kim,I. C. Kwon,S. Y. Jeong and D. S. Lee, *J. Controlled Release,* 2010, **144**, 259-266.

(25) M. Kanamala,W. R. Wilson,M. Yang,B. D. Palmer and Z. Wu, *Biomaterials,* 2016, **85**, 152-167.

(26) S.-S. Han,Z.-Y. Li,J.-Y. Zhu,K. Han,Z.-Y. Zeng,W. Hong,W.-X. Li,H.-Z. Jia,Y. Liu,R.-X. Zhuo and X.-Z. Zhang, *Small,* 2015, **11**, 2543-2554; Y. Gu,Y. Zhong,F. Meng,R. Cheng,C. Deng and Z. Zhong, *Biomacromolecules,* 2013, **14**, 2772-2780.

(27) M. P. Gamcsik,M. S. Kasibhatla,S. D. Teeter and O. M. Colvin, *Biomarkers.,* 2012, **17**, 671-691.

(28) Y.-w. Hu,Y.-z. Du,N. Liu,X. Liu,T.-t. Meng,B.-l. Cheng,J.-b. He,J. You,H. Yuan and F.-q. Hu, *J. Controlled Release,* 2015, **206**, 91-100.

(29) G. K. Balendiran,R. Dabur and D. Fraser, *Cell Biochem. Funct.,* 2004, **22**, 343-352.

(30) Y.-C. Wang,F. Wang,T.-M. Sun and J. Wang, *Bioconjugate. Chem.,* 2011, **22**, 1939-1945; Y. Yuan,S. Xu,C.-J. Zhang,R. Zhang and B. Liu, *J. Mater. Chem. B,* 2016, **4**, 169-176; J. Wang,X. Sun,W. Mao,W. Sun,J. Tang,M. Sui,Y. Shen and Z. Gu, *Adv. Mater.,* 2013, **25**, 3670-3676.

(31) W. Chen,P. Zhong,F. Meng,R. Cheng,C. Deng,J. Feijen and Z. Zhong, *J. Controlled Release,* 2013, **169**, 171-179.

(32) H. He,D. Altomare,U. Ozer,H. Xu,K. Creek,H. Chen and P. Xu, *Biomater. Sci.,* 2016, **4**, 115-120.

(33) A. Gupte and R. J. Mumper, *Cancer Treat. Rev.,* 2009, **35**, 32-46;J.Wang,C. Luo,C. Shan,Q. You,J. Lu,S. Elf,Y. Zhou,Y. Wen,J. L. Vinkenborg,J. Fan,H. Kang,R. Lin,D. Han,Y. Xie,J. Karpus,S. Chen,S. Ouyang,C. Luan,N. Zhang,H. Ding,M. Merkx,H. Liu,J. Chen,H. Jiang and C. He, *Nat. Chem.,* 2015, **7**, 968-979.

(34) K. Garber, *Science,* 2015, **349**, 129-129.

(35) H. M. Alvarez,Y. Xue,C. D. Robinson,M. A. Canalizo-Hernández,R. G. Marvin,R. A. Kelly,A. Mondragón,J. E. Penner-Hahn and T. V. O'Halloran, *Science,* 2010, **327**, 331-334; G. J. Brewer,R. D. Dick,D. K. Grover,V. LeClaire,M. Tseng,M. Wicha,K. Pienta,B. G. Redman,T. Jahan,V. K. Sondak,M. Strawderman,G. LeCarpentier and S. D. Merajver, *Clin. Cancer Res.,* 2000, **6**, 1-10.

(36) M. Schrevel,A. Gorter,S. M. Kolkman-Uljee,J. B. M. Z. Trimbos,G. J. Fleuren and E. S. Jordanova, *Modern. Pathol.,* 2011, **24**, 720-728; R. I. Nicholson,J. M. W. Gee and M. E. Harper, *Eur. J. Cancer,* 2001, **37,** Supplement 4, 9-15.

(37) R. Bahadur K. C and P. Xu, *Adv. Mater.,* 2012, **24**, 6479-6483.

(38) E. Doolittle,P. M. Peiris,G. Doron,A. Goldberg,S. Tucci,S. Rao,S. Shah,M. Sylvestre,P. Govender,O. Turan,Z. Lee,W. P. Schiemann and E. Karathanasis, *ACS Nano,* 2015, **9**, 8012-8021.

(39) S. S. Desale,S. M. Raja,J. O. Kim,B. Mohapatra,K. S. Soni,H. Luan,S. H. Williams,T. A. Bielecki,D. Feng,M. Storck,V. Band,S. M. Cohen,H. Band and T. K.

Bronich, *J. Controlled Release,* 2015, **208**, 59-66; K. M. Camacho,S. Kumar,S. Menegatti,D. R. Vogus,A. C. Anselmo and S. Mitragotri, *J. Controlled Release,* 2015, **210**, 198-207.

(40) S. Shen,H. Tang,X. Zhang,J. Ren,Z. Pang,D. Wang,H. Gao,Y. Qian,X. Jiang and W. Yang, *Biomaterials,* 2013, **34**, 3150-3158.

CHAPTER 2

CANCER CELL SELECTIVE-KILLING POLYMER/COPPER COMBINATION[1]

2.1 INTRODUCTION

Although various anticancer drugs have been developed to conquer cancer, a large number of cancer patients ultimately still lost their battle against it.[1] There are two major causes for the failure, drug resistance of cancer cells and side effects of anticancer drugs.[2] Because of the inherited or acquired multidrug resistance, cancer cells survive after receiving the original effective drug,[3] which results in the recurrence of the cancer and eventually kills cancer patients. The selectivity of anticancer drugs used in chemotherapy is predominantly relying on the proliferation rate difference between normal cells and cancer cells.[4] Most cancer cells are fast growing.[5] However, besides cancer cells, normal cells in the digestive tract, bone marrow, hair follicles, and reproductive system are also vulnerable to anticancer drugs that targeting quick proliferating cells due to their fast renewal nature. Furthermore, some anticancer drugs even compromise the function of heart, nervous system, and kidneys.

To increase the selectivity of anticancer drug for cancer cells, various approaches have been explored, including utilizing the specific receptors expression level difference between normal and cancer cells,[6] as well as the tumor unique physiological properties such as low pH,[7] high GSH,[8] and changed metal ion concentrations.[9] Among them,

[1]H.He, D. Altomare, U. Ozer, H. Xu, K. Creek, H. Chen and P. Xu. 2016. *Biomater. Sci.* 4: 115-120.

Reprinted here with permission of publisher.

copper concentration in tumors has attracted extreme high interest recently. Copper is an important trace metal that plays critical roles in maintaining normal biological functions. Elevated copper concentration (up to 2-3 fold) is frequently observed in a wide spectrum of tumors including ovarian, breast, cervical, prostate and leukemia.[10] High copper concentration facilitates tumor angiogenesis. Depletion of copper by copper chelators such as D-penicillamine, trientine, and disulfiram has been proved effective in inhibiting angiogenesis and killing cancer cells both *in vitro* and *in vivo*.[11] Chelators can form complex with copper by thiol, amine, and pyridine ring to reduce copper concentration in the tumor, which eventually result in the death of cancer cells.[12] Thus, several clinic trials involve the copper chelators have been conducted.[13] However, due to the non-specific tissue distribution and rapid clearance of chelators, none or only little beneficial was observed in those trials.

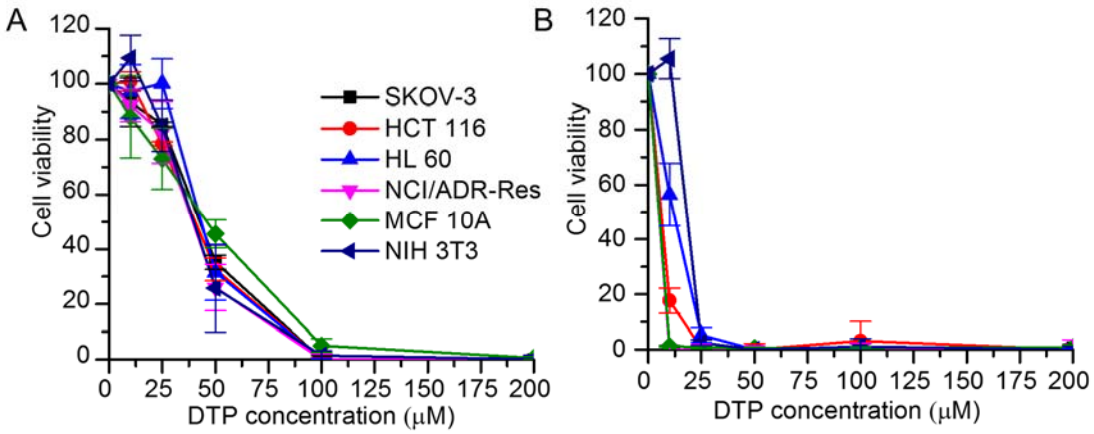

Figure 2.1 Cytotoxicity of DTP for different cell lines at the absence (A) and presence (B) of 10 μM $CuCl_2$. Data represent the means ± SD, n = 3.

Our preliminary study found that the addition of copper ions to 2, 2′-Dithiodipyridine (DTP) could significantly boost its cytotoxicity for cancer cells and normal cells (**Figure 2.1**). To endow high density of pyridine-2-thiol, the intracellular

metabolite of DTP, we designed a poly[(2-(pyridin-2-yldisulfanyl)ethyl acrylate)-co-[poly(ethylene glycol)]] (PDA-PEG) polymer. PDA-PEG was synthesized through free radical polymerization according to our published method.[8] The pyridine rings in PDA can complex with Cu^{2+}, turning the polymer into a multi-chelator system.

2.2 EXPERIMENTS

2.2.1 Materials and reagents

Aldrithiol-2 and Silica gel (Spherical, 100 mm) were purchased from Tokyo Chemical Industry Co., LTD (Harborgate Street, Portland, OR). 2-Mercaptoethenol, DL-dithiothreitol (DTT), tris(2-carboxyethyl)phosphine (TCEP), 2, 2-Azobisisobutyronitrile (AIBN), (3-(4,5-dimethylthiazol-2-yl)-2,5-diphenyltetrazolium bromide (MTT), Propidium Iodide (PI) and Poly(ethylene glycol)methacrylate (Mn=360 Da) were purchased from Sigma Aldrich Chemical Co. (St. Louis, MO). Buthionine sulfoximine (BSO) and Glutathione ethyl ester (GSH-MEE) were purchased from Cayman Chemical (Ann Arbor, Michigan). Penicillin (10,000 U/mL), streptomycin (10,000 mg/mL), 0.25% trypsin-EDTA, Dulbecco's Modified Eagle Medium (with L-glutamine) and fetal bovine serum (FBS) were obtained from American Type Culture Collection (ATCC, Manassas, VA). 5-(and-6)-chloromethyl-2',7'-dichlorodihydrofluorescein diacetate, acetyl ester (CM-H_2DCFDA), Molecular probes and RNase were purchased from Life Technologies (Grand Island, NY). GSH-Glo™ Glutathione Assay kit was purchased from Promega Corporation (Madison, WI). Cy5-NHS was purchased from Lumiprobe Corporation (Hallandale Beach, FL). All the other solvents used in this research were purchased from Sigma Aldrich Chemical Co. (St.Louis, MO) and used without further purification unless otherwise noted.

2.2.2 Synthesis of PDA-PEG

PDA-PEG polymer was synthesized according to our previous reports. Briefly, PDA (241.3 mg (1mmol), 482.6 mg (2 mmol) or 965.2 mg (4 mmol),) and PEG360 (1 mmol, 360 g) were dissolved in 10 mL degassed anisole. 2,2-Azobisisobutyronitrile (AIBN, 14 mg (0.085 mmol), 21 mg (0.126 mmol) or 35 mg (0.213 mmol)) in 1 mL degassed anisole was then added, and the reaction mixture was stirred for 24 h at 65 ºC. The final product was precipitated (3×) in ice cold ether and dried for 48 h in vacuum. The structure of PDA-PEG was confirmed by ^{1}H-NMR, and its molecular weight and polydispersity were evaluated by gel permeation chromatography (GPC).

2.2.3 PDA-PEG-Cy5 synthesis

PDA-PEG was modified by Cy5 for cellular uptake study. Briefly, cysteamine (0.11 mg, 5% PDA function group) in 500 μL DMSO was added dropwise into 20 mg PDA-PEG in 500 μL DSMO and the reaction mixture was left at room temperature overnight. After overnight reaction, Cy5 NHS ester (0.39 mg in 390 μL DMSO) was added and the mixture was left for reacting overnight, following a thoroughly dialysis towards DMSO to remove free Cy5. The concentration of Cy5 in the final product was measured by a microplate reader (SpectraMax® M5, Molecular Devices Inc) at λ_{ex}640 and λ_{em}680.

2.2.4 PDA quantification in PDA-PEG polymer

Two methods were used to measure PDA concentration in the polymer. In the first method, PDA-PEG (50 μg/mL in DMSO) was incubated with tris(2-carboxyethyl)phosphine (TCEP, 10 mM, 20 mM and 50 mM) for 1 hour at room

temperature, and then the amount of pyridine-2-thione released was quantified through UV-Vis spectrophotometer at λ = 375 nm and correlated to PDA amount (ε, molar absorption coefficient = 8080 $M^{-1}cm^{-1}$). In the second method, a calibration curve of pyridine-2-thione was firstly established and then applied to calculate the PDA concentration in the polymer. In brief, 100 μg aldrithiol-2 was dissolved in 1 mL DMSO and completely converted to pyridine-2-thione by adding excess TCEP (13.1 mg, 100×). The reaction mixture was then diluted in DMSO to obtain a serial of concentrations of pyridine-2-thione with UV-Vis absorbance between 0.1 and 1 at 375 nm. Based on the UV-Vis absorbance, the calibration curve was established. Then PDA-PEG (50 μg/mL in DMSO) was incubated with 10, 20 and 50 mM TCEP for 1 h and PDA concentration in the polymer was calculated according to the calibration curve after measuring the UV-Vis absorbance of the polymer solution.

2.2.5 TEM and DLS

The size and morphology of PDA-PEG in PBS is characterized by transmission electron microscopy (TEM) and dynamic light scattering (DLS). In brief, 1 mg PDA-PEG was dissolved in 1 mL PBS with or without copper chloride ($CuCl_2$, 10 μM). Then the PDA-PEG solution was measurement by DLS (Zetasizer Nano ZS, Malvern Instruments Ltd), or loaded onto carbon coated copper grids, dried and observed directly under TEM (Hitachi H8000, Hitachi High Technologies America, Inc.).

2.2.6 Intracellular GSH measurement

Tumor and normal cells were seeded in 96-well white plate (5,000 cells/well) overnight prior to the study. BSO (1 mM) or GSH-MEE (5 mM) in culture medium was added. For control group, only fresh culture medium was added. Cells were incubated for

8 h, and the intracellular GSH concentration was measured by GSH-Glo™ Glutathione Assay according to the manufacturer's instruction.

2.2.7 In vitro Cytotoxicity MTT Assay

In vitro cytotoxicity of PDA-PEG was tested in cancer cell lines (MDA-MB-231, SKOV-3, NCI/ADR-Res, UMSCC 22A, HCT 116 and HL 60) and normal cell lines (CONA, NIH 3T3, MCF 10A, KC and BNL CL.2). Cells were seeded in 96-well plate (20,000 cells/well) for 24 h prior to the study. Then a serial of concentrations of PDA-PEG in culture medium was added, supplementing with or without $CuCl_2$ (10 μM). The cells were then incubated 48 h in in 95/5% air/CO_2 at 37 ºC. After 48h, MTT reagent (100 μL, 10%(w/w) in medium) was added and incubated for 4h, following the addition of MTT stop solution and the measurement of the optical density of the medium using a microplate reader (ELX808, Bio-Tech Instrument, Inc) at λ = 595 nm.

2.2.8 Intracellular GSH effect to cytotoxicity

To test the effect of intracellular GSH effect to the cytotoxicity of PDA-PEG, intracellular GSH concentration was inhibited or promoted by BSO and GSH-MEE, respectively. In brief, cells were seeded in 96-well plate (20,000 cells/well) for 24 h prior to the study. To investigate the PDA-PEG cytotoxicity responding to reduced intracellular GSH, cells was treated with BSO (1 mM) for 24 h and then varied concentrations of PDA-PEG with or without 10 μM $CuCl_2$ were added and incubated for another 48 h. To investigate the PDA-PEG cytotoxicity responding to increased intracellular GSH, cells were treated at the same time with GSH-MEE (5 mM) and varied concentration of PDA-PEG with or without 10 μM $CuCl_2$ for 48 h. For both experiments, the cell viability was finally quantified by MTT assay.

2.2.9 Cellular Uptake Confocal microscopy

SKOV-3 (200,000 cells/dish) were seeded in 35mm^2 Petri dishes (Mat Tek, MA, USA) overnight. Prior to adding polymer, certain dishes were added with 5,5'-dithiobis-(2-nitrobenzoic acid) (DTNB, 0.6 mg in 75 μL PBS) to block the thiol groups on the cell surface. Then PDA-PEG-Cy5 in 5 μL DMSO was added (equivalent to 0.1 μg/mL Cy5). After 1 h incubation under a humidified atmosphere of 95/5% air/CO_2. Cells were washed by PBS (3×), fixed with formaldehyde (4.5 % in PBS) and stained with Hoechst 33342 (final concentration 1 μg/mL). Then cells were analyzed under a confocal microscope (LSM 700, Carl-Zeiss Inc.).

2.2.10 Flow cytometry

SKOV-3 and NIH 3T3 cells (300,000 cells/well) were seeded in 6-well plates overnight. Certain wells were then added with DTNB (0.6 mg in 75 μL PBS) to block the thiol groups on the cell surface, following the addition of PDA-PEG-Cy5 in 5 μL DMSO (equivalent to 1 μg/mL Cy5). After 1 h, cells were washed, trypsinized and resuspened in PBS. Cy5 positive cell population was quantified at λ_{ex}640 and λ_{em}675 nm using flow cytometry (BD Accuri C6, BD Biosciences).

2.2.11 Intracellular ROS measurement by flow cytometry and fluorescence microscopy

MDA-MB-231 and HCT 116 were seeded in 24-well plate (80,000 cells/well) or 6-well plate (300,000 cells/well) for 24 h prior to the study. PDA-PEG (83.15 μM, DTP equivalent) with or without 10 μM $CuCl_2$ were added into plates and cells were incubated for 18 h. For flow cytometry, cells in 6-well plate were trypsinized, collected and incubated for 30 min with CM-H_2DCFDA (100 μM in PBS) at 37 ^oC. For positive

control, cells were treated with H_2O_2 (1 mM) for 30 min before trypsinization. After CM-H_2DCFDA staining, cells were washed by PBS (3×) and intracellular ROS was immediately quantified by flow cytometry (Ex=488 nm, Em=515-540 nm). For fluorescence microscopy, cells in 24-well plate were washed by PBS (3×) and stained with CM-H_2DCFDA (100 μM in PBS) for 30 min at 37 ºC. For positive control, cells were treated with H_2O_2 (1 mM) for 30 min before CM-H_2DCFDA staining. After CM-H_2DCFDA staining, cells were washed by PBS (3×) and immediately observed under fluorescence microscopy using GFP channel.

2.2.12 Selective Cell Killing

NIH3T3, NCI/ADR-RES, SKOV-3 and UMSCC 22A were trypsinized and washed by PBS (3×) and resuspended in 1 mL PBS supplemented with Cell Tracker™ deep red dye (2 μM), blue dye (50 μM), green CMFDA dye (25 μM) and orange CMTMR dye (25 μM), respectively. All cells were stained for 30 min at 37 ºC and washed by PBS (3×) and resuspended in 2 mL DMEM culture medium. Cells were then counted and seeded in 24-well plate separately or together. Four wells for each individual cell line and cell mixture. Cell density was 10,000 cells/well for individual cell and 40,000 cells/well for cell mixture. All cells were incubated for 24 h under a humidified atmosphere of 95/5% air/CO_2 before polymer treatment. After 24 h, culture medium was removed and replaced with fresh medium containing different concentrations of PDA-PEG (equivalent to 16.6-83.15 μM PDA) at the presence of 10 μM $CuCl_2$. After 24 h, cells were directly observed under the fluorescence microscopy (Olympus IX81, Olympus America Inc).

2.2.13 Microarray Assay RNA isolation

SKOV-3, NCI/ADR-RES, MCF-7 and MCF 10A (5,000,000 cells/well) were seeded in 100 mm Petri dishes (four dishes for each cell line) overnight under a humidified atmosphere of 95/5% air/CO_2. Culture medium was then replaced with fresh one with or without PDA-PEG (50 μM PDA) at the presence of 10 μM $CuCl_2$. Cells were incubated for another 12 h and total RNA for gene expression analysis was isolated from cell line samples using miRNeasy Mini Kit (QIAGEN, Cat#. 217004) according to the manufacturer's instructions. Briefly, cells were scraped with 700 μL of QIAzol reagent, collected in eppendorf tube, lysed by vortexing and homogenized by centrifugation through QIAshredder columns (QIAGEN, Cat#. 79656). After addition of 140 μL of chloroform, the homogenate was vigorously shaken for 15 s and centrifuged at 12,000 g for 15 min at 4°C. The RNA-containing aqueous phase was transferred to a new tube and RNA was precipitated with 525 μL of 100% ethanol. Subsequently, the sample was transfer to a RNeasy Mini spin column and centrifuged at 12,000 g for 15 s at room temperature. In the next step, RNA samples were on-column DNase treated and posteriorly washed with RPE buffer. Then, RNA was eluted from the column with 30 μL of RNase free water and quantified using a spectrophotometer. RNA quantity was assessed using an Agilent 2100 Bioanalyzer and RNA Integrity Numbers (RIN) ranged from 9.2 to 10.0.

2.2.14 mRNA labeling and hybridization

Microarrays experiments were performed using Agilent's platform. Total RNA samples were amplified and labeled using Agilent's Low Input Quick Amp Labeling Kit (Cat. # 5190-2306) according to the manufacturer recommendations. Briefly, mRNA

contained in 200 ng of total RNA was converted into cDNA using a poly-dT primer that also contains the T7 RNA polymerase promoter sequence. Subsequently, T7 RNA polymerase was added to cDNA samples to amplify original mRNA molecules and to simultaneously incorporate cyanine 3- or cyanine 5-labeled CTP (cRNA) into the amplification product. In addition, Agilent RNA spike-in controls (Cat. # 5188-5279) were added to samples prior cDNA synthesis and were used as experimental quality control. In the next step, labeled RNA molecules were purified using Qiagen's RNeasy Mini Kit (Cat. # 74104). After spectrophotometric assessment of dye incorporation and cRNA yield, samples were store at -80 °C until hybridization. Labeled cRNA samples were hybridized to SurePrint G3 Human Gene Expression 8x60K v2 Microarrays (Cat. # G4858A-039494) at 65 °C for 17 h using Agilent's Gene Expression Hybridization Kit (Cat. # 5188-5242) according to the manufacturer's recommendations. Two (2) control sample replicates we hybridized against two (2) polymer treated sample replicates in a dye swap design. After washes, arrays were scanned using an Agilent DNA Microarray Scanner System (Cat. # G2565CA).

2.2.15 Data analysis

Data was extracted from images with Feature Extractor Software version 10.7.3.1 (Agilent). In this process, background correction using additive and multiplicative detrending algorithms was performed. In addition, linear and LOWESS methods were used for dye normalization. Subsequently, data was uploaded into GeneSpring GX version 13.0 for analysis. In this process, data was log2 transformed, quantile normalized and base line transformed using the median of all samples. Then, data was filtered by flags in a way that 100% of the samples in at least one of the two treatment groups have a

"detected" flag. Differentially expressed genes were determined using a moderated t-test statistics setting as cutoff values a p-value of 0.001 and a fold of 3.0. Pathway analysis was also performed with Genespring GX using BioCarta, KEGG, NCI and Pathway Commons databases.

2.2.16 Cell Cycle Analysis

SKOV-3 cell (300,000 cells/well) were seeded in 6-well plates overnight. The culture medium was then replaced by fresh one with PDA-PEG polymer (equivalent to 83.15 μM PDA) at the presence or absence of 10 μM $CuCl_2$. The cell was cultured for 12 h under a humidified atmosphere of 95/5% air/CO_2. Then cells in each well were collected after trypsinization. Cells were wash with PBS (1×) and fixed by 70 % ice cold methanol for 5 min. After the fixation, cells were wash by PBS (1×) and resuspended in 250 μL RNase (100 μg/mL in PBS) for 15 min at 37 ºC. Cells were wash by PBS (1×) again and stained by propidium iodide (PI, 100 μg/mL in PBS) for 1 h on ice. Cells were finally washed and measured by flow cytometry (Ex=488 nm, Em=585 nm).

2.2.17 PDA-PEG Stability Study In vitro

The stability of PDA-PEG was investigated at the presence of varied concentrations of GSH to mimic the conditions in the body. Briefly, 50 μg PDA-PEG was dissolved in 1 mL 10 mM phosphate buffer saline with 10 μM $CuCl_2$ and varied concentrations of GSH (0, 0.01, 0.1, 1 and 10 mM). The UV-Vis absorbance of the polymer at 0, 0.5, 1, 1.5 and 2 h after adding GSH was measured by a UV-Vis spectrophotometer and normalized by comparing to the maximum absorbance of the polymer.

2.3 RESULTS AND DISCUSSION

The successful synthesis of the polymer was verified by ^{1}H-NMR (**Figure 2.2A**) and gel permeation chromatography (GPC) (**Figure 2.2B**). The ^{1}H NMR result revealed that the actual ratio between PDA and mPEG in the final PDA-PEG polymer was close to their feeding ratios (1:1). GPC showed that the molecular weight of PDA-PEG polymer was 41.8 kDa. Due to the co-existing of hydrophobic PDA and hydrophilic PEG, the amphiphilic PDA-PEG self-assembles into nanoparticle in aqueous solution. Zeta sizer revealed that PDA-PEG nanoparticles had a hydrodynamic size of 87.64 ± 2.06 nm and carried negative surface charge (-15.4 ± 2.05 mV). The morphology of PDA-PEG nanoparticle was also confirmed by TEM, which showed a spherical shape with a size around 80 nm (**Figure 2.3A**). After the addition of Cu^{2+} ($CuCl_2$, 10 μM), the hydrodynamic size of the nanoparticles increased to 196.4 ± 0.07 nm (**Figure 2.4**), while becoming less negatively charged (-5.47 ± 0.86 mV). Due to the interaction between Cu^{2+} and pyridine ring made the PDA segment more hydrophilic so that the core became less condensed (**Figure 2.3B**), which led to the increase of the particle size.[14] The formation of nanoparticle will endow two advantages for cancer therapy. First, due to the existence of PEG corona, the circulation time of the polymer in the blood stream can be greatly extended. Second, by taking advantage of the leaky structure of the capillaries in the tumor tissue, the formed PDA-PEG/Cu^{2+} nanoparticle can be enriched in the tumor through the so called enhanced permeability and retention (EPR) effect.

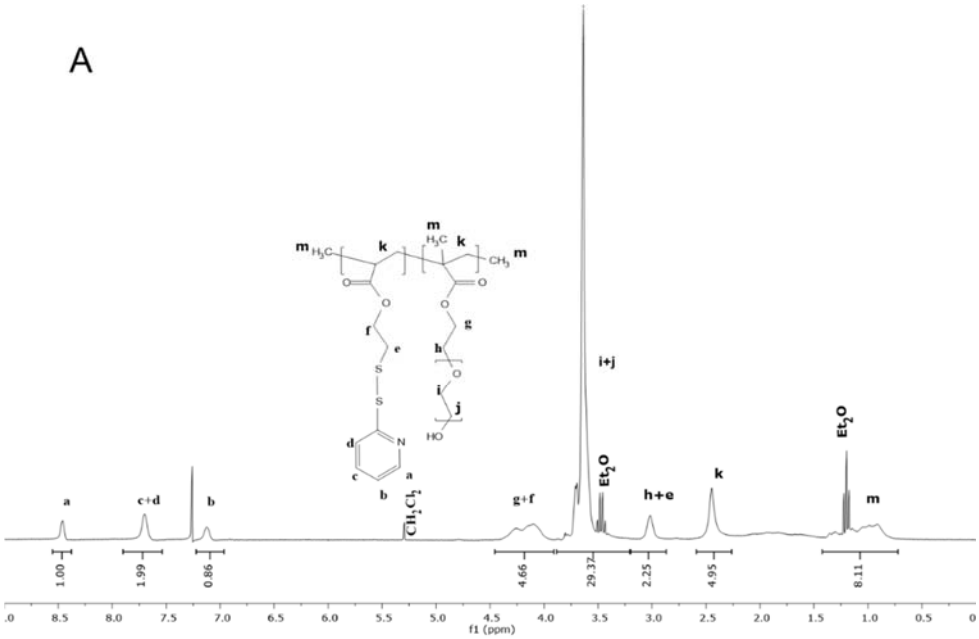

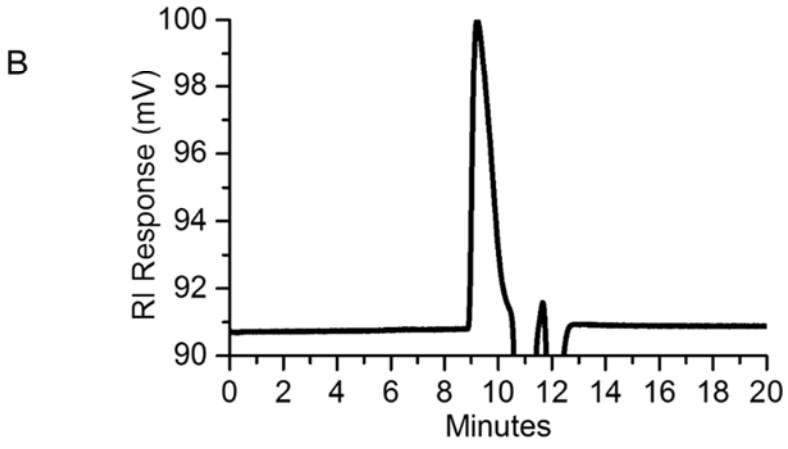

.

Figure 2.2 Representative ^{1}H-NMR spectrum (A) and GPC curve (B) for PDA-PEG polymer. The NMR spectrum was acquired in $CDCl_3$

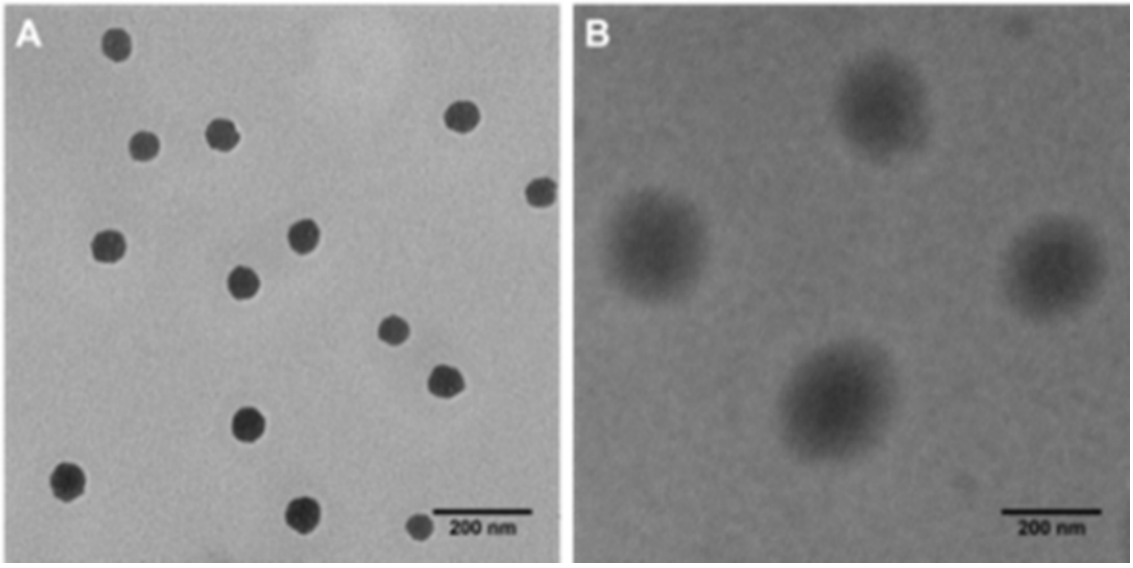

Figure 2.3 TEM images of nanoparticle fabricated from PDA-PEG alone (A), and PDA-PEG/Cu^{2+} combination (B). Scale bars are 200 nm.

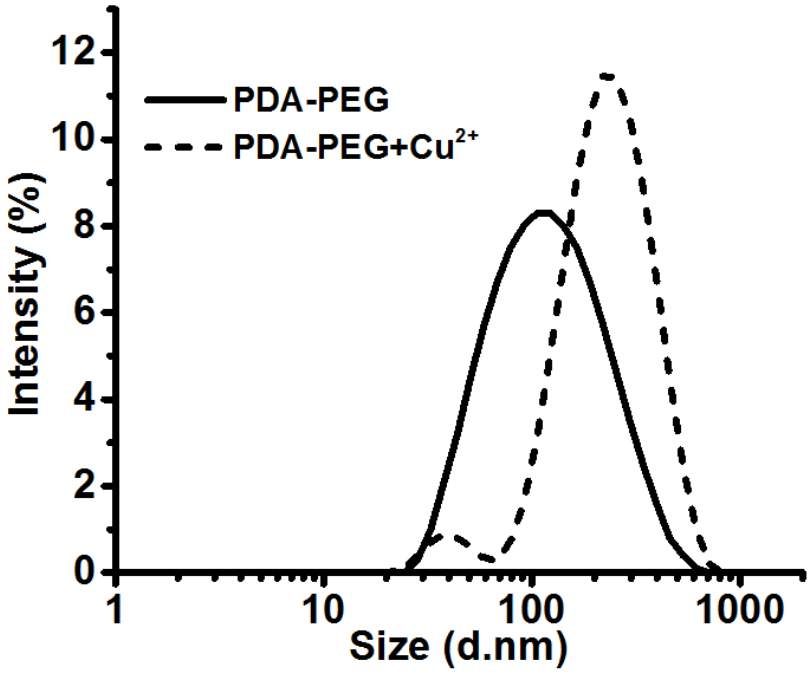

Figure 2.4 The size distribution of nanoparticles formed from PDA-PEG polymer and PDAPEG/Cu^{2+} acquired by dynamic light scattering.

To validate whether the polymer form of DTP chelator possesses similar cell killing capacity as its small molecular counterpart, cell proliferation assay was employed in 7 cancer cell lines, 5 normal cell lines, and a NIH 3T3 cell line, an immortalized cell line derived from normal cells. As expected, PDA-PEG nanoparticle did not show obvious toxicity up to the equivalent DTP concentration of 40 μM for all tested cells (**Figure 2.5**). Similar as DTP, the addition of Cu^{2+} dramatically enhanced the potency of PDA-PEG nanoparticles for cancer cells (**Figure 2.6**). The IC_{50} of PDA-PEG/Cu^{2+} for SKOV-3, NCI/ADR-Res, MDA-MB-231, and UMSCC 22A cells were less than 6 μM (**Table 2.1**), and with a IC_{95} less than 20 μM. Contrary to its small molecule counterpart (**Figure 2.1B**), the cell killing effect of PDA-PEG/Cu^{2+} for cancer cells and normal cells are significantly different. **Figure 2.6** also showed that PDA-PEG/Cu^{2+} combination is non-toxicity to normal cells, including keratinocytes, fibroblasts, breast epithelial cells, colon cells, and hepatocytes, up to 80 μM. The IC_{50} values for normal cells were 10-70 fold higher than those for cancer cells (**Table 2.1**). All these suggested that PDA-PEG/Cu^{2+} could selectively kill cancer cells, including drug resistant cancer cells, while sparing normal ones. In addition, **Figure 2.7** also revealed that the cytotoxicity of PDA-PEG/Cu^{2+} for cancer cells increases with the increase of Cu^{2+} concentration, while not showing influence on normal cells.

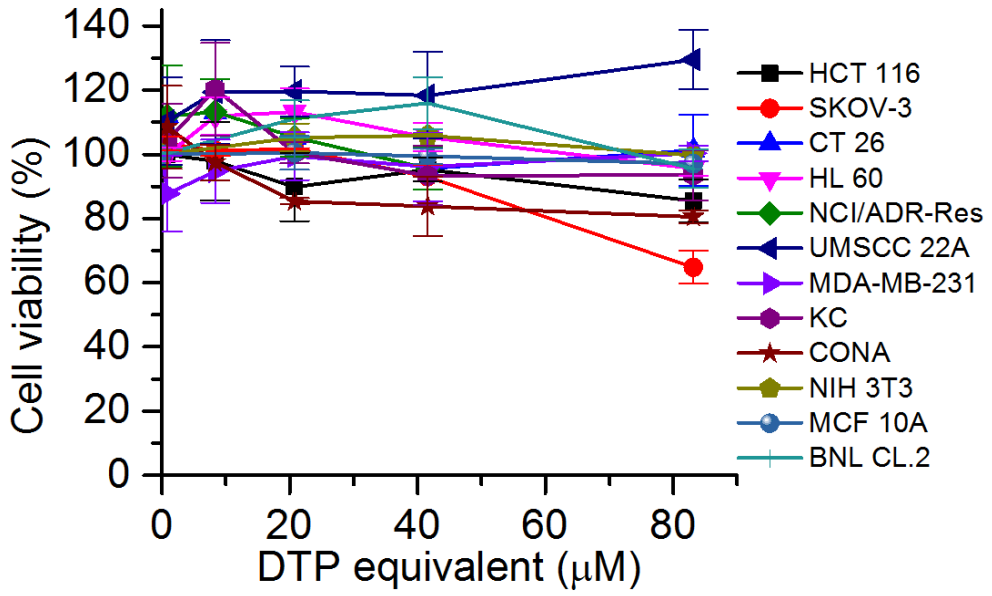

Figure 2.5 Cytotoxicity of PDA-PEG nanoparticle for different cell lines without the addition of 10 μM $CuCl_2$. Data represent the means ± SD, n = 3.

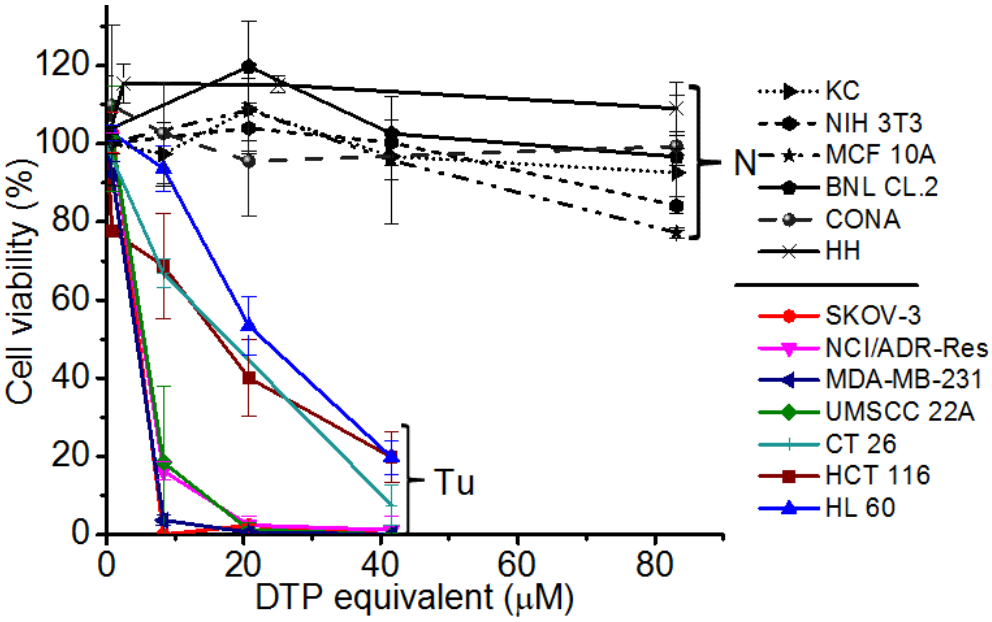

Figure 2.6 Cytotoxicity of PDA-PEG/Cu^{2+} combination for normal (N) and cancer (Tu) cells. Normal cells include KC (human keratinocyte), NIH 3T3 (murine fibroblast), MCF 10A (human breast epithelial cell), BNL CL.2 (murine liver cell), CONA (CCD 841 CoN, human colon cell), and HH (human hepatocyte). Data represent the means ± SD, n=3.

Table 2.1 The IC50s of PDA-PEG/Cu^{2+} nano-complex for normal and cancer cell lines. IC50s were calculated based on MTT results by IBM SPSS Statistics software.

Cell lines	IC_{50} (μM)
MDA-MB-231	2.32±0.0.33
SKOV-3	3.83±0.58
NCI/ADR-RES	4.72±0.045
UMSCC 22A	5.34±0.51
CT 26	10.56±0.90
HCT 116	11.45±5.35
HL60	22.90±0.83
HH	>831.5
BNL CL.2	552.02±72.50
CONA	289.91±70.00
KC	202.47±26.56
NIH3T3	158.70±17.13
MCF 10A	135.37±10.80

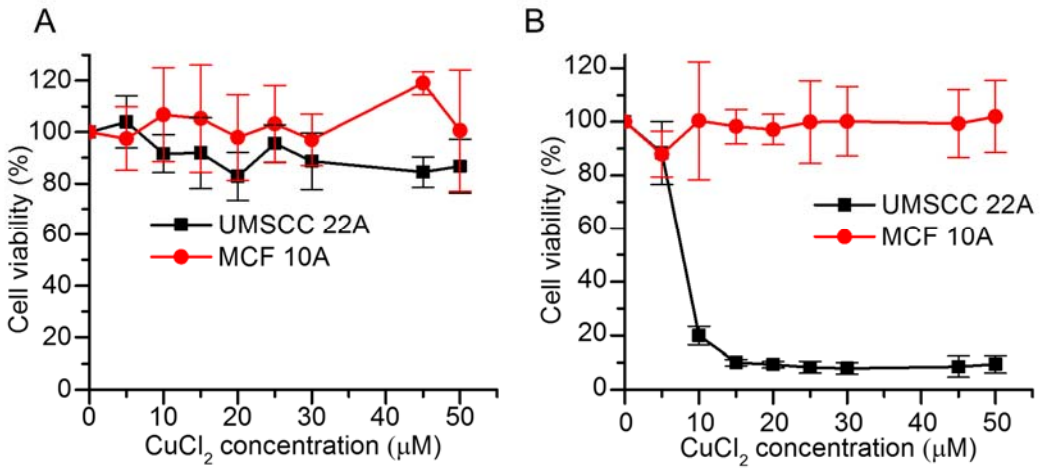

Figure 2.7 The concentration effect of $CuCl_2$ on the cytotoxicity of medium (A) and PDA-PEG (B). PDA-PEG (8.32 μM, equivalent to DTP) was mixed with different concentrations of $CuCl_2$ and incubated with UMSCC 22A and MCF 10A for 48 h. Data represent the means ± SD, n=3.

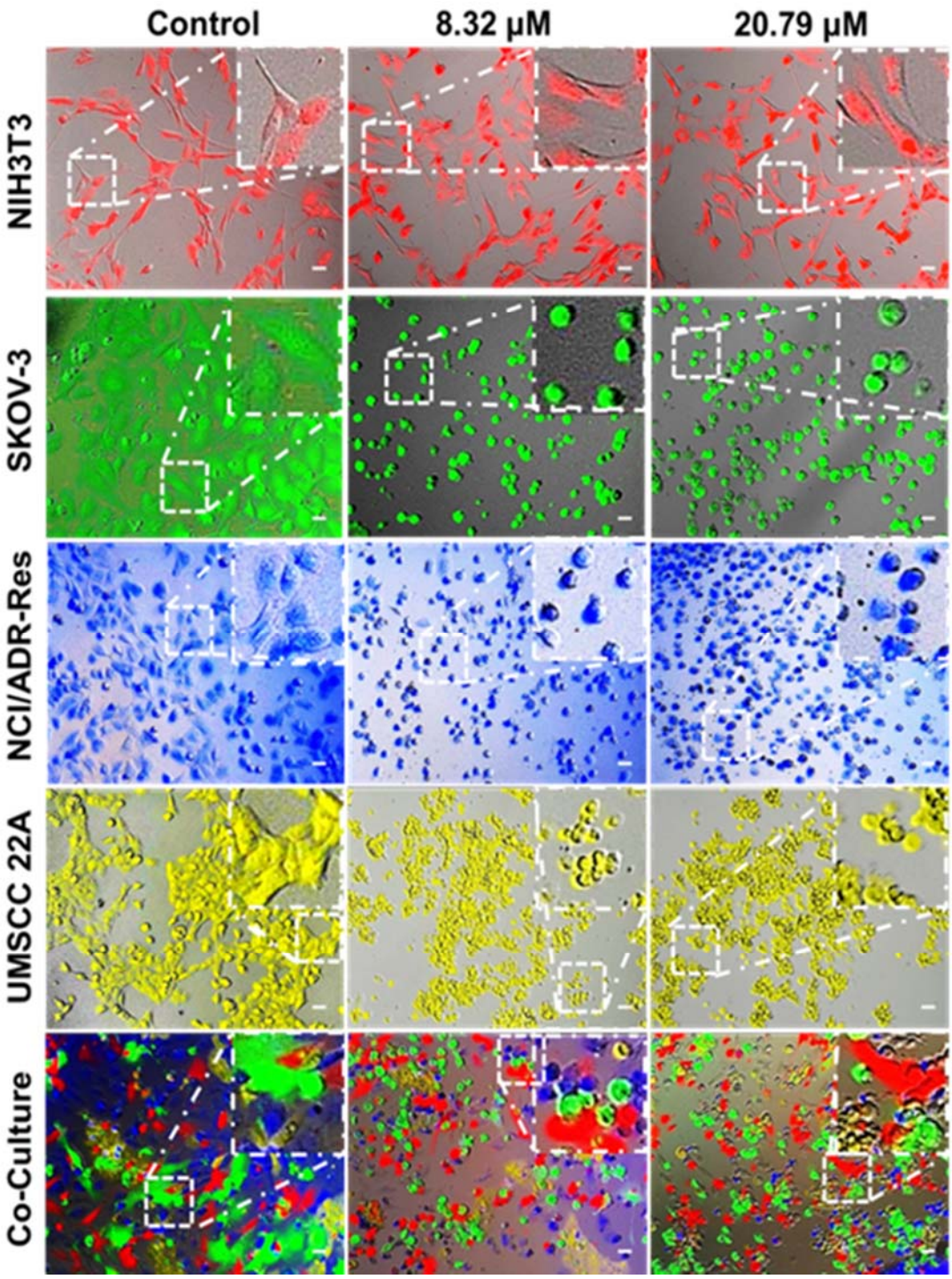

Figure 2.8 Fluorescence images of cancer cells after culturing with different concentrations of PDA-PEG/Cu^{2+} combination. NIH 3T3, NCI/ADR-Res, SKOV-3 and UMSCC 22A were pre-stained with Cell Tracker™ deep red, blue, green CMFDA and orange CMTMR dye, respectively, and imaged 24 h after the treatment. The scale bars were 40 μm.

To further validate that the PDA-PEG/Cu^{2+} combination can specifically kill cancer cells versus normal ones, NIH 3T3, SKOV-3, NCI/ADR-Res, and UMSCC 22A cells were stained with different color fluorescent dyes. NIH 3T3 cell was selected as a representative normal cell because its comparable growth rate and suitability for co-culture with cancer cells in DMEM medium. **Figure 2.8** showed that all cells except NIH 3T3 were rounded up after treated with 8.3 μM of PDA-PEG/Cu^{2+}, indicating these cells were not in healthy status. On the contrary, NIH 3T3 cells still kept its original stretched cell shape at 20.79 μM. All these images visually confirmed the MTT results in **Figure 2.6** This phenomenon was also observed in the multiple cell lines co-culture model (bottom row of **Figure 2.8**), where only NIH 3T3 cells kept their original spindle morphology, indicating that the PDA-PEG/Cu^{2+} combination could selectively kill cancer cells while sparing normal cells in a more disease relevant co-culture model.

To probe the mechanism for PDA-PEG/Cu^{2+} selectively killing cancer cells, we first investigated the cellular uptake of PDA-PEG and PDA-PEG/Cu^{2+} nanoparticle with flow cytometry and confocal microscopy. **Figure 2.9A** showed that the nanoparticles fabricated from Cy5 labeled PDA-PEG and PDA-PEG/Cu^{2+} combination entered cells with identical manners, suggesting that the addition of copper ions did not affect its entering cells. In addition, these nanoparticles showed similar efficiency in entering normal cells (NIH 3T3) and cancer cells (SKOV-3). Therefore, the uptake of PDA-PEG/Cu^{2+} wasn't the reason for its cancer-cell-selectivity. 5,5'-Dithio-bis-(2-nitrobenzoic acid) (DTNB) is a compound binds the free thiol groups on the surface of cell membrane. The addition of DTNB significantly inhibited the cellular uptake of PDA-PEG (**Figure 2.9B**), suggesting that PDA-PEG entering cells via exofacial thiol mediated endocytosis.

We think this is because PDA-PEG polymer contains high density of thiol-reactive PDA segment, which can react with exofacial thiols through thiol-disulfide exchange reaction to facilitate cellular uptake. Similar blocking effect was also observed in NIH 3T3 cells treated with DTNB (**Figure 2.10**).

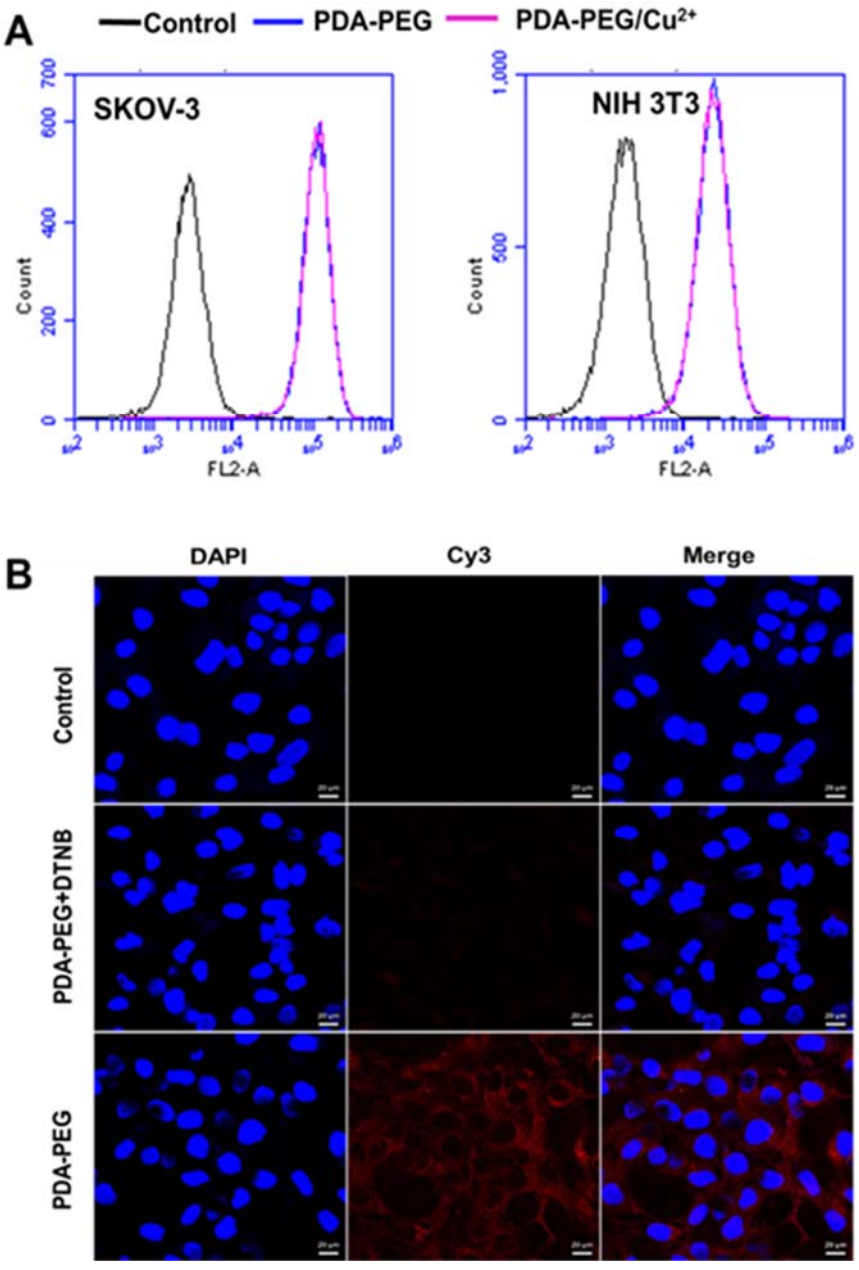

Figure 2.9 Flow cytometry spectra of SKOV-3 and NIH 3T3 cells (A) and confocal images of cellular uptake of nanoparticles in SKOV-3 cells (B). Cellular uptake assays were carried out 1 h after the addition of nanoparticles. Scale bars were 20 μm.

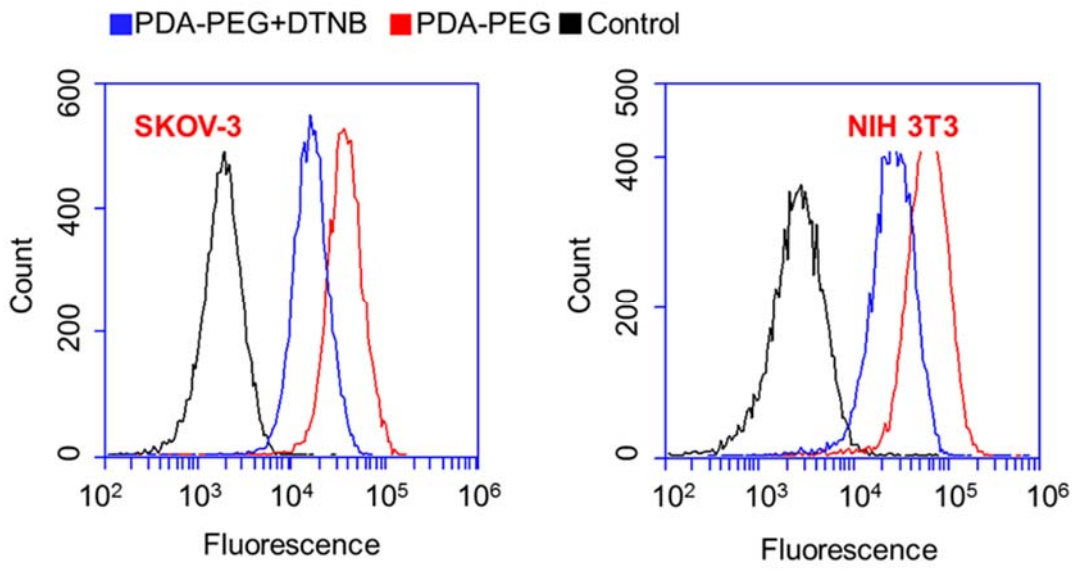

Figure 2.10 The flow cytometry spectra of SKOV-3 (Left) and NIH 3T3 (Right) cells treated with Cy5 labeled PDA-PEG nanoparticles. Cellular uptake assays were carried out 1 h after the addition of nanoparticles.

Our previous study found that polymer-drug conjugates linked through disulfide bond could quickly release its payload by cleaving the disulfide bond with the help of intracellular elevated glutathione (GSH).[6] As pyridine-Cu complex analogues had been reported highly toxic and extensively studied as anticancer drugs, the release of pyridine-Cu complex probably induced cell death.[14] The high cytotoxicity of DTP/copper combination also suggested that pyridine-2-thiol/copper combination could be the active segment for its cytotoxicity. To study the release kinetics of the PDA-PEG/Cu^{2+} nanoparticles, samples were dispersed in phosphate buffers supplemented with different levels of GSH as well as serum containing media to mimic the plasma and intracellular environment. **Figure 2.11A** showed that PDA-PEG/Cu^{2+} is extremely stable at a low reducing environment ([GSH] < 0.1 mM), such as the plasma, where has a GSH level less than 5 μM.[15] However, almost all pyridine-2-thiol segments could be instantly released from PDA-PEG at the GSH level of 10 mM, indicating its super responsiveness to the

intracellular reducing condition. Furthermore, the polymer/copper combination was very stable in 50% serum containing medium, only 12.92% pyridine-2-thiol was released after 7 days of incubation (**Figure 2.11B**), suggesting its great stability during blood circulation.

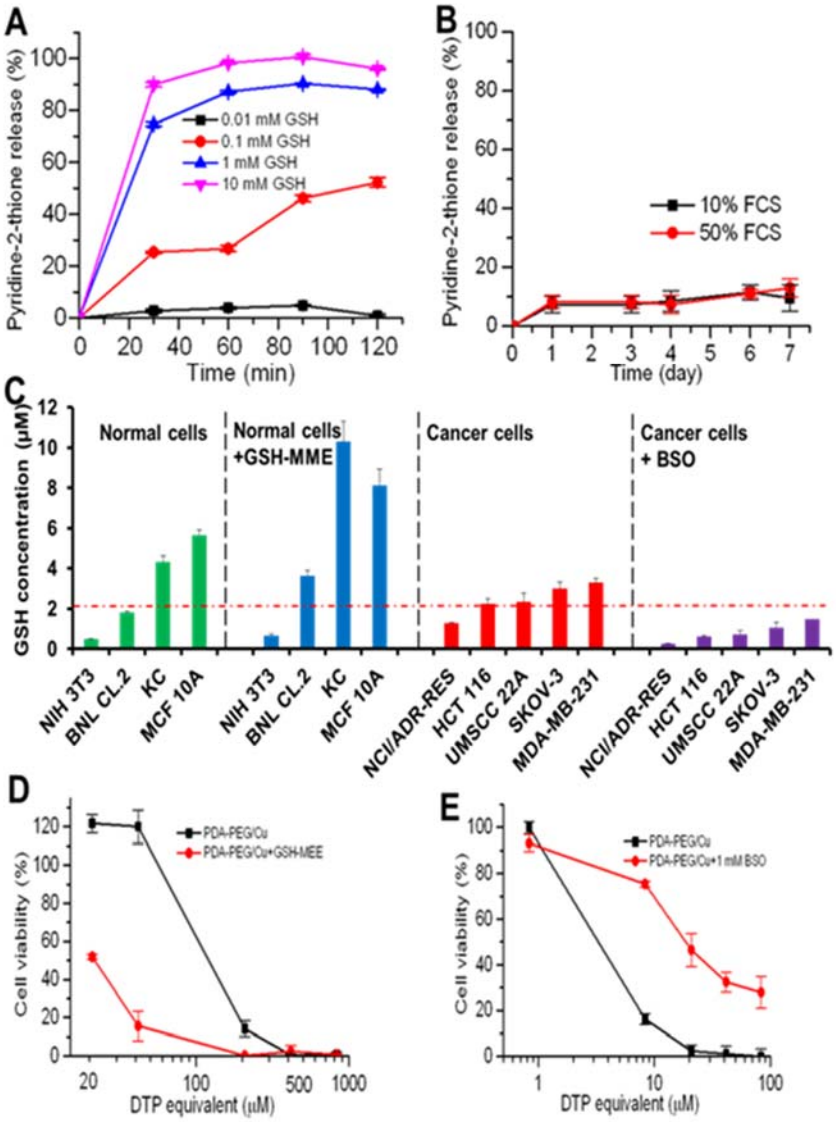

Figure 2.11 The release kinetic of pyridine-2-thiol liberating from PDA-PEG at different GSH levels (A) and in serum containing media (B), the GSH level in different cell lines and response to the addition of GSH-MME and BSO (C), GSH-MME effect on the cytotoxicity of PDA-PEG/Cu^{2+} for MCF10A cells (D), and BSO effect on the cytotoxicity of PDA-PEG/Cu^{2+} combination for NCI/ADR-Res cells (E). Data represent the means ± SD, n=3.

Since there was no significant difference between normal cells and cancer cells in uptaking PDA-PEG/Cu^{2+} nanoparticle, we postulate that the observed cancer-cell-selective-killing effect was due to the intrinsic difference between normal and cancer cells. It has been reported that GSH levels in tumor tissues, such as ovarian, head and neck, breast, and lung cancer are higher than that in normal tissues.[16] To probe whether the high GSH level is also prevail in cancer cells *in vitro*, GSH-Glo™ Glutathione Assay was employed. Interestingly, **Figure 2.11C** revealed that, the GSH level range in normal cells is relatively broad, ranging from 0.48 to 5.65 μM, while most tested cancer cell lines displayed relatively high GSH level (> 2 μM), suggesting that intracellular GSH level could be a valid target for cancer targeted therapy. To prove that, glutathione-monomethylester (GSH-MME, 5 mM) and buthionine sulfoxamine (BSO, 1 mM) were employed to boost or deplete the intracellular GSH level in normal cells (NIH 3T3, BNL CL.2, KC, and MCF 10A) or cancer cells (NCI/ADR-Res, HCT 116, UMSCC 22A, SKOV-3, and MDA-MB-231), respectively.[17] After the addition of GSH-MME all normal cells exhibited higher intracellular GSH level **(Figure 2.11C).** As expected, these cells became more vulnerable to the polymer/copper combination treatment (**Figure 2.11D and 2.12**). On the contrary, BSO treated NCI/ADR-Res, UMSCC 22A, and SKOV-3 cells displayed declined GSH level. Interestingly, only NCI/ADR-Res cells became more tolerant to the polymer/copper combination treatment (**Figure 2.11E**), while the other two cancer cell lines kept their sensitivity to the treatment (**Figure 2.13)**. Based on these results shown in **Figure 2.11**, we conclude that intracellular GSH level is not the sole cause for the cancer-cell-selective-killing effect of PDA-PEG/Cu^{2+} nanoparticles.

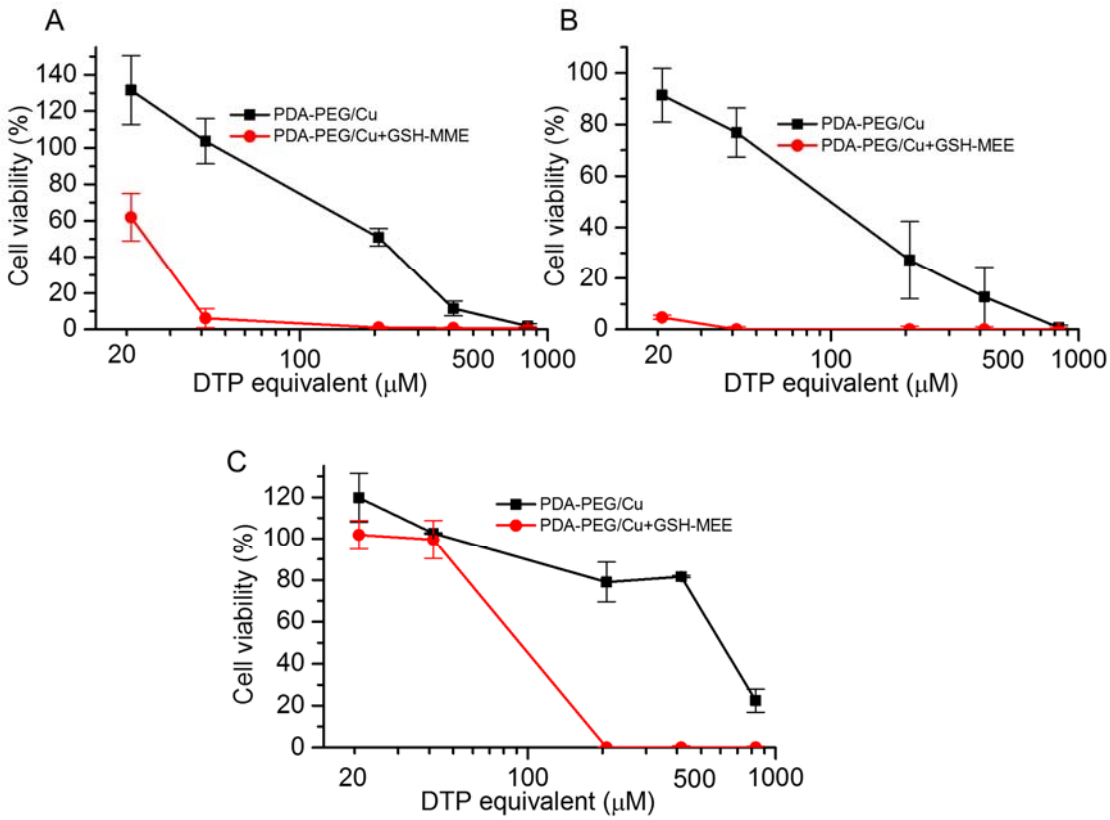

Figure 2.12 The effect of GSH-MME on the cytotoxicity of PDA-PEG/Cu^{2+} for KC (A), NIH 3T3 (B), and BNL.CL.2 (C) cells. Data represent the means ± SD, n=3.

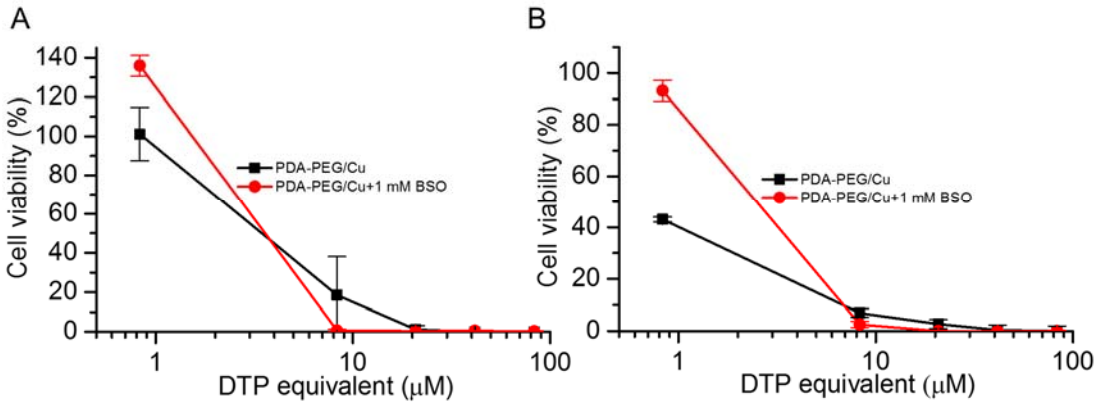

Figure 2.13 The effect of BSO on the cytotoxicity of PDA-PEG/Cu^{2+} for UMSCC 22A (A) and SKOV-3 cells. Data represent the means ± SD, n=3.

Among those tested cells, there were several exceptions. First, MCF 10A and KC exhibited higher GSH level than other normal cells and cancer cell, while not sensitive to PDA-PEG/Cu^{2+} treatment. Second, NCI/ADR-Res cells showed lower GSH level than

other cancer cells, but still vulnerable to the treatment. Third, SKOV-3 and UMSCC 22A cells displayed lower GSH level after BSO treatment, however, the decreased GSH level only slightly abolished their response to PDA-PEG/Cu^{2+} **(Figure 2.13**). To solve these puzzles, we further investigated the gene response to PDA-PEG/Cu^{2+} treatment in MCF 10A, NCI/ADR-Res, and SKOV-3 cells through RNA microarray analysis. Cells were treated with PDA-PEG/Cu^{2+} for 12 h before the RNA extraction. Microarray analysis data revealed that, for untreated cells, the RNA levels of oncogenes (CIRBP and STMN1) were upregulated, while tumor suppressor genes (CDKN1C and GADD45B) were downregulated in both ovarian cancer cell lines (**Figure 2.14A**). Surprisingly, PDA-PEG/Cu^{2+} treatment reversed the above gene expression pattern by downregulating the RNA level of CIRBP and STMN1 (>3 folds), while upregulating CDKN1C and GADD45B (>5 folds) (**Figure 2.14B**). Interestingly, no obvious expression level change of these genes was detected in the normal breast cell line. Other studies showed that oncogenes (CIRBP[18] and STMN1[19]) are upregulated while tumor suppressor genes (CDKN1C[20] and GADD45B[21]) are downregulated in various types of cancers. Since the upregulated oncogenes and downregulated tumor suppressor genes stimulate cancer cell proliferation and promote tumor growth, reversing those malregulated genes through PDA-PEG/Cu^{2+} treatment would result in cancer cells apoptosis. For MCF 10A cells, although the high level of GSH could release large amount of pyridine-2-thiol intracellularly, cells still survived due to that those oncogenes and tumor suppressor genes are not sensitive to the treatment. For NCI/ADR-Res cells, whose GSH level is relatively low but still high enough to release needed pyridine-2-thiol to regulate their oncogenes and tumor suppressor genes due to its high sensitivity. Similarly, BSO

decreased the GSH level in SKOV-3 and UMSCC 22A cells, while the resulted GSH level is still high enough to release pyridine-2-thiol to regulate their oncogenes and tumor suppressor genes. Therefore, the cancer-cell-selective-killing property of PDA-PEG/Cu^{2+} is the combination effects of high intracellular GSH level and the malregulation of oncogenes and tumor suppressor genes in cancer cells.

A

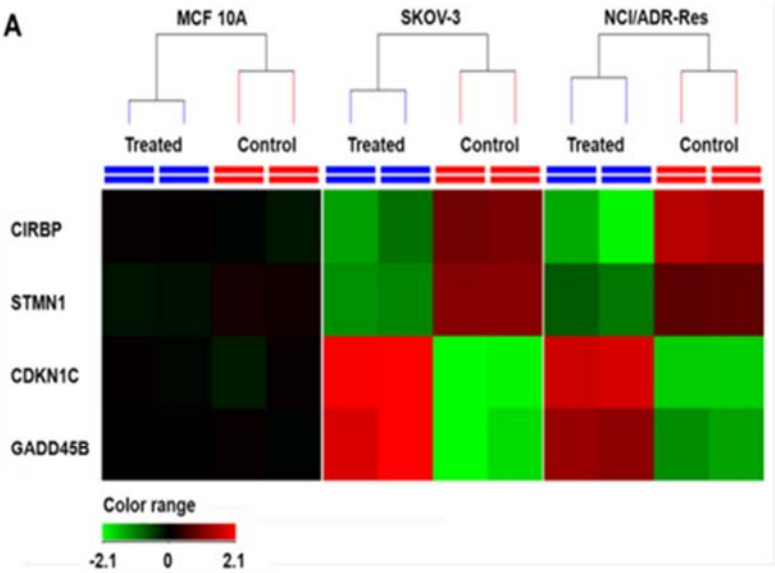

B

	SKOV-3	NCI/ADR-Res	MCF10A
Oncogene	Fold of change		
CIRBP	4.25 ↓	9.04 ↓	1.11 ↓
STMN1	4.74 ↓	3.10 ↓	1.22 ↓
Tumor suppressor gene			
CDKN1C(p57)	20.55 ↑	10.72 ↑	1.06 ↑
GADD45B	16 ↑	5.45 ↑	1.01 ↑

Figure 2.14 RNA expression in response to PDA-PEG/Cu^{2+} treatment. Cells were treated with 41.58 μM of PDA-PEG/Cu^{2+} for 12 h. (A) Heatmap RNA level with and without drug treatment. Red: upregulation; green: downregulation; black: no change. (B) Genes alteration fold after treatment.

CDKN1C is an inhibitor for G1 cyclin/Cdk complexes and causes cell arrest in G1 phase.[20] To investigate the effect of CDKN1C up-regulation after PDA-PEG/Cu^{2+} treatment, cell cycle analysis was employed. **Figure 2.15** showed that PDA-PEG/Cu^{2+}

inhibited cell division and arrested cancer cells in G1 phase, which could induce cell apoptosis. As expected, PDA-PEG polymer or Cu^{2+} ion alone did not show any effect on the cell cycle distribution of SKOV-3 cells.

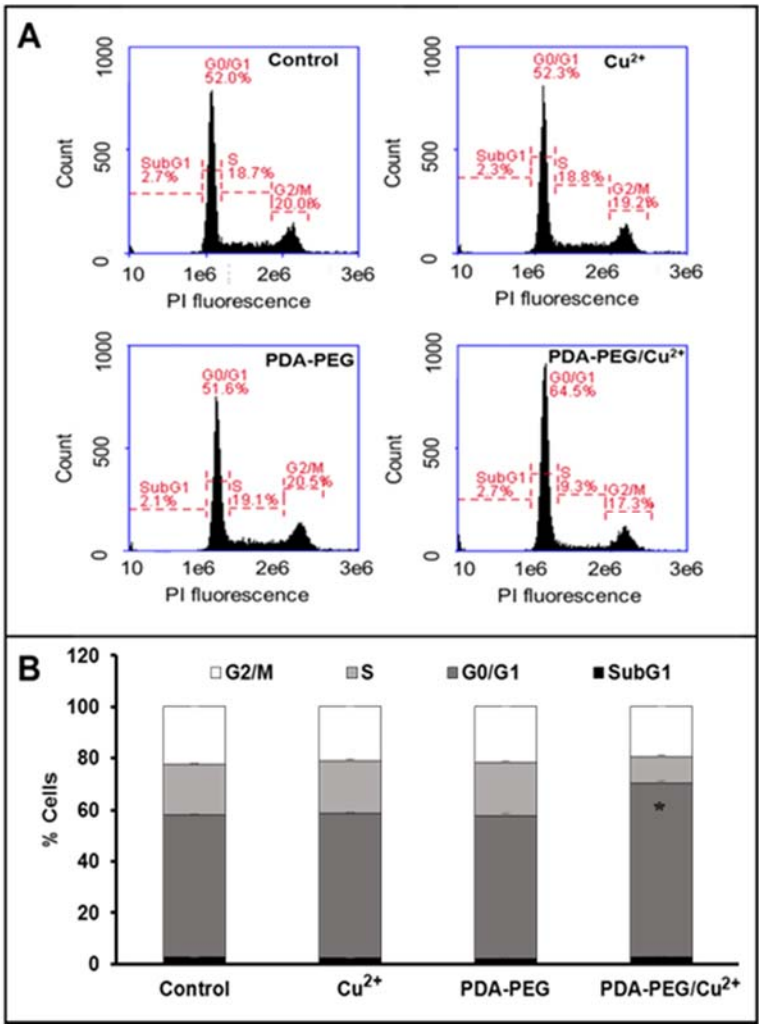

Figure 2.15 Cell cycle analysis of SKOV-3 cells after treated with 41.58 μM of PDA-PEG/Cu^{2+} for 12 h. Flow cytometry spectra (A) and quantitative analysis (B) of cell cycle. Data represent the means ± SD, n=3, **P*<0.01.

2.4 CONCLUSIONS

In summary, we developed a cancer-cell-selective-killing nanoparticle from PDA-PEG/Cu^{2+} combination aiming for safe and effective cancer therapy. The polymer/Cu^{2+} based nanoparticle entered cells through the interaction with exofacial thiols, and

subsequently released pyridine-2-thiol/Cu complex to kill cells. Due to the difference in the intracellular GSH level as well as the expression level of oncogenes (CIRBP and STMN1) and tumor suppressor genes (CDKN1C and GADD45B) between normal and cancer cells, the PDA-PEG/Cu^{2+} exhibited high selectivity in killing a broad spectrum of cancer cells, including drug resistant one, while sparing normal cells. Therefore, PDA-PEG/Cu^{2+} nanoparticle will provide a new paradigm for the cure of ovarian and other cancers. The ongoing research will investigate the cell killing mechanism of PDA-PEG/Cu^{2+} in molecular level and test whether the cancer-cell-selective-killing effect of PDA-PEG/Cu^{2+} can be translated into a safe and effective cancer treatment tool *in vivo*.

2.5 REFERENCES

(1) R. Siegel, J. Ma, Z. Zou and A. Jemal, *CA Cancer J. Clin.*, 2014, **64**, 9-29.

(2) C. Holohan, S. Van Schaeybroeck, D. B. Longley and P. G. Johnston, *Nat. Rev. Cancer*, 2013, **13**, 714-726; X.-J. Liang, C. Chen, Y. Zhao and P. Wang, in *Multi-Drug Resistance in Cancer*, ed. J. Zhou, Humana Press, 2010, vol. 596, ch. 21, pp. 467-488.

(3) E. K. Pauwels, P. Erba, G. Mariani and C. M. Gomes, *Drug News Perspect.*, 2007, **20**, 371-377.

(4) K. Masui, B. Gini, J. Wykosky, C. Zanca, P. S. Mischel, F. B. Furnari and W. K. Cavenee, *Carcinogenesis*, 2013, **34**, 725-738.

(5) P. M. Herst, J. E. Davis, P. Neeson, M. V. Berridge and D. S. Ritchie, *Haematologica*, 2009, **94**, 928-934; T. J. Mitchison, *Mol. Biol. Cell*, 2012, **23**, 1-6.

(6) H. He, A. W. Cattran, T. Nguyen, A.-L. Nieminen and P. Xu, *Biomaterials*, 2014, **35**, 9546-9553; B. K. Remant, V. Chandrashekaran, B. Cheng, H. Chen, M. M. Pena, J. Zhang, J. Montgomery and P. Xu, *Mol. Pharm.*, 2014, **11**, 1897-1905.

(7) D. Ling, W. Park, S.-j. Park, Y. Lu, K. S. Kim, M. J. Hackett, B. H. Kim, H. Yim, Y. S. Jeon, K. Na and T. Hyeon, *J. Am. Chem. Soc.*, 2014, **136**, 5647-5655; H.-m. Ding and Y.-q. Ma, *Sci. Rep.*, 2013, **3**, 2804.

(8) R. Bahadur K. C and P. Xu, *Adv. Mater.*, 2012, **24**, 6479-6483; B. Cheng, B. Thapa, R. K. C and P. Xu, *J. Mater. Chem. B,* 2015, **3**, 25-29.

(9) A. Gupte, S. Wadhwa and R. J. Mumper, *Bioconjug. Chem.*, 2008, **19**, 1382-1388; A. Gupte and R. J. Mumper, *Free Radic. Biol. Med.*, 2007, **43**, 1271-1278.

(10) A. Gupte and R. J. Mumper, *Cancer Treat. Rev.*, 2009, **35**, 32-46.

(11) F. Wang, P. Jiao, M. Qi, M. Frezza, Q. P. Dou and B. Yan, *Curr. Med. Chem.*, 2010, **17**, 2685-2698; D. Chen and Q. P. Dou, *Expert Opin. Ther. Targets*, 2008, **12**, 739-748.

(12) D. J. Lewis, P. Deshmukh, A. A. Tedstone, F. Tuna and P. O'Brien, *Chem. Comm.*, 2014, **50**, 13334-13337; C. Santini, M. Pellei, V. Gandin, M. Porchia, F. Tisato and C. Marzano, *Chem. Rev.*, 2013, **114**, 815-862.

(13) S. Brem, S. A. Grossman, K. A. Carson, P. New, S. Phuphanich, J. B. Alavi, T. Mikkelsen, J. D. Fisher and f. t. N. A. t. B. T. T. C. Consortium, *Neuro.Oncol.*, 2005, **7**, 246-253; M. T. Schweizer, J. Lin, A. Blackford, A. Bardia, S. King, A. J. Armstrong, M. A. Rudek, S. Yegnasubramanian and M. A. Carducci, *Prostate Cancer Prostatic Dis.*, 2013, **16**, 357-361.

(14) I. Kinoshita, L. James Wright, S. Kubo, K. Kimura, A. Sakata, T. Yano, R. Miyamoto, T. Nishioka and K. Isobe, *Dalton Trans.*, 2003, 1993-2003.

(15) M. E. Anderson, *Methods Enzymol.*, 1985, **113**, 548-555.

(16) M. P. Gamcsik, M. S. Kasibhatla, S. D. Teeter and O. M. Colvin, *Biomarkers*, 2012, **17**, 671-691.

(17) P. Xu, G. K. Quick and Y. Yeo, *Biomaterials*, 2009, **30**, 5834-5843.

(18) T. Sakurai, H. Kashida, T. Watanabe, S. Hagiwara, T. Mizushima, H. Iijima, N. Nishida, H. Higashitsuji, J. Fujita and M. Kudo, *Cancer Res.*, 2014, **74**, 6119-6128; T. Sakurai, N. Yada, T. Watanabe, T. Arizumi, S. Hagiwara, K. Ueshima, N. Nishida, J. Fujita and M. Kudo, *Cancer Sci.*, 2015, **106**, 352-8.

(19) J. Akhtar, Z. Wang, C. Yu, C.-S. Li, Y.-L. Shi and H.-J. Liu, *BMC Cancer*, 2014, **14**, 28; B. E. Batsaikhan, K. Yoshikawa, N. Kurita, T. Iwata, C. Takasu, H. Kashihara and M. Shimada, *Anticancer Res.*, 2014, **34**, 4217-4221.

(20) E. Kavanagh and B. Joseph, *Biochim. Biophys. Acta*, 2011, **1816**, 50-56; A. Borriello, I. Caldarelli, D. Bencivenga, M. Criscuolo, V. Cucciolla, A. Tramontano, A. Oliva, S. Perrotta and F. Della Ragione, *Mol. Cancer Res.*, 2011, **9**, 1269-1284

(21) L. Zhang, Z. Yang and Y. Liu, *Exp. Biol. Med. (Maywood)*, 2014, **239**, 773-778; R. E. Tamura, J. F. de Vasconcellos, D. Sarkar, T. A. Libermann, P. B. Fisher and L. F. Zerbini, *Curr. Mol. Med.*, 2012, **12**, 634-651.

CHAPTER 3

SELF-QUENCHING BIOACTIVATABLE NANOGEL FOR TARGETED PHOTODYNAMIC THERAPY

3.1 INTRODUCTIOIN

Photodynamic therapy (PDT) has attracted extensive study in the past several decades, as an alternative or adjunctive therapy to conventional cancer treatment modalities.[1] It involves three components: photosensitizer (PS), PS-activating light and oxygen.[2] During PDT, PS is firstly localized to tumor, following the illumination of tumor with light of a specific wavelength to activate the PS. Then the activated PS transfers its energy to molecular oxygen to generate cytotoxic reactive oxygen species (ROS) to destruct tumor vasculature and kill cancer cells.[3] As all three components are necessary for PDT to take effect, the nonspecific accumulation of PS alone will not cause systemic toxicity while at the absence of PS the nonspecific irradiation of PS activating light on internal healthy organs is not harmful, making PDT greatly advantageous over traditional chemotherapy and radiotherapy.[4]

In the past decades, PDT has been proved to be effective in treating certain superficial cancers, such as Barrett's esophagus,[5] skin cancer[6] and head and neck cancers,[7] to which PS activating light is easily accessible. However, PDT still has yet to be clinically accepted as a first-line oncological intervention due to several limitations, including the low aqueous solubility and limited tumor accumulation of PS. The

application of nanoparticles, including polymer conjugates,[8] micelles,[9] dendrimers[10] and nanogels,[11] significantly drive the development of PDT in overcoming some of those challenges. Loading PS to nano-carriers usually improves the water solubility and serum stability of PS, making it suitable for systemic application. Furthermore, the nanoparticle can specifically accumulated in tumor tissue through passive and/or active targeting effect and thus increase the local concentration of PS in tumor, which finally produces a high PDT efficacy with reduced adverse effects.[12]

Another challenge associated with PDT is the photosensitivity reaction, which can cause serious skin and eye irradiation due to the activation of photosensitizers after exposure of these areas to sunlight.[13] Patients received PDT have to stay away from light for several months. As free PSs exhibit photosensitivity reaction, their phototoxicity can be greatly reduced by encapsulating them into nanoparticles due to the aggregation induced photoquenching similar to the fluorescence resonance energy transfer (FRET) effect, which results in the generation of less singlet oxygen ($^1O_2$), one of the cell toxic reactive oxygen species.[14] However, these nanoparticles can also inhibit the production of $^1O_2$ at tumor because of the incomplete release of PSs and thus significantly reduce the PDT efficacy.[15] To overcome these issues, some stimuli responsive nanoparticles have been developed. These nanoparticles can release PSs efficiently at tumor site by response to pH,[16] glutathione (GSH),[17] and enzymes[18] and therefore restore the PDT efficacy of PSs. Among them, GSH responsive nanoparticles have received great attention. GSH is a tripeptide which has a high intracellular concentration (2-10 mM).[19] It can be used as a biological trigger to induce drug release in nanoparticle through the cleavage of disulfide bonds. Huh et al. reported a polymer conjugate which used disulfide bonds to link glycol

chitosan and Pheophorbide a (PhA), a second generation of PSs.[20] The conjugate could form micelles by self-assembly and exhibited a reduction of phototoxicity at low GSH condition due to the aggregation of PhA, while its PDT effect was restored upon cellular uptake because of the release of PhA at high intracellular GSH condition. Na et al. also reported a nanoparticle based on disulfide linked pullulan-PhA conjugate and revealed the GSH induced PDT effect.[21] However, the serum stability of these nanoparticles are extremely concerned since they are either micelles or physically crosslinked colloids which may break up and release out free PhA during blood circulation and would induce photosensitivity reaction and damage normal tissues. Alternative nanoparticles with high serum stability combined with GSH responsiveness are significantly demanded.

In our group, we previously have developed a series of GSH responsive nanogels based on poly[(2-(pyridin-2-yldisulfanyl) ethyl acrylate)-co-[poly(ethylene glycol)]] (PDA-PEG).[22] The PDA-PEG polymer contains numerous 2-mercaptopyridine groups which can be easily replaced with other molecules to form a polymer-drug conjugate linked by disulfide bond. The polymer-drug conjugate can be easily made into disulfide crosslinked nanogel by simply adding a reducing agent. These nanogel have been proved to be stable in blood stream condition while rapidly release drug after exposure to intracellular GSH, making the polymer an ideal carrier materials to fabricate activatable nanogels for PDT.

Herein, we developed a self-quenching bioactivatable nanogel for targeted photodynamic therapy (**Scheme 3.1**). PhA was firstly conjugated to PDA-PEG polymer through disulfide bond, and then the PhA conjugated polymer was fabricated into nanogel by disulfide crosslinking. The formation of the nanogel would induce the

fluorescence quenching of PhA due to its self-aggregation, which resulted in a dramatic inhibition of the generation of singlet oxygen. The nanogel was further decorated with targeting ligand to improve its cellular uptake and tumor homing ability in a head and neck tumor model. After systemic administration, in the blood stream where the GSH concentration is low (2-20 μM),[19] the nanogel would stay in its quenching status, thus the phototoxicity to normal tissues would be greatly reduced. When the nanogel accumulated in tumor tissues and efficiently entered cancer cells by EPR effect and ligand-receptor interaction, the nanogel would be rapidly and fully activated because of the elevated GSH concentration, and finally produced high singlet oxygen for tumor destruction upon laser irradiation.

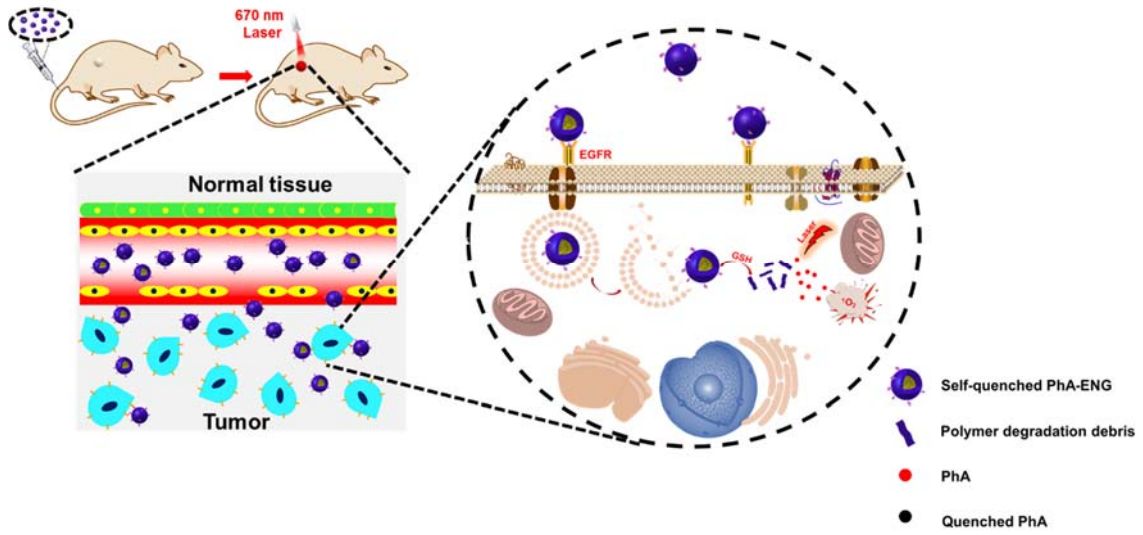

Scheme 3.1 Schematic illustration of the self-quenching bioactivatable nanogel for targeted photodynamic therapy.

3.2 EXPERIMENTS

3.2.1 Materials and Reagents

Aldrithiol-2 and Silica gel (Spherical, 100 mm) were purchased from Tokyo Chemical Industry Co., LTD (Harborgate Street, Portland, OR). 2-Mercaptoethenol, DL-dithiothreitol (DTT), tris(2-carboxyethyl)phosphine (TCEP), 2, 2-Azobisisobutyronitrile (AIBN), Poly(ethylene glycol)methacrylate (Mn=360 Da, PEG360), 9,10-dimethylanthracene (DMA) and Thiazolyl Blue Tetrazolium Bromide (MTT) were purchased from Sigma Aldrich Chemical Co. (St. Louis, MO). Pheophorbide A (PhA) was purchased from Frontier Scientific, Inc (Logan, UT). Penicillin (10,000 U/mL), streptomycin (10,000 mg/mL), 0.25% trypsin-EDTA, Dulbecco's Modified Eagle Medium (with L-glutamine) and fetal bovine serum (FBS) were obtained from American Type Culture Collection (ATCC, Manassas, VA). Anti-EGFR Affibody® Molecule was purchased from Abcam plc. (Cambridge, MA). All the other solvents used in this research were purchased from Sigma Aldrich Chemical Co. (St. Louis, MO) and used without further purification unless otherwise noted.

3.2.2 PDA-PEG-PhA polymer synthesis

PhA was covalently conjugated to PDA-PEG polymer. Briefly, PDA-PEG (20 mg in 250 μL DMSO) was firstly reacted with cysteamine hydrochloride (1.857 mg in 250 μL DMSO, 60% PDA function group) over night at room temperature. TEA (20 μL) and PhA (16.13 mg in 200 μL DMSO) activated by EDC (10.44 mg in 200 μL DMSO) and NHS (6.27 mg in 200 μL DMSO) were then added. The reaction mixture was stirred over night at room temperature, followed by a thorough dialysis in DMSO (MW CO=6,000

Da) to remove unconjugated PhA. The resulted PDA-PEG-PhA DMSO solution was directly used for nanogel fabrication.

3.2.3 PDA-PEG-AEME polymer synthesis

The synthesis of PDA-PEG-AEME polymer was similar as the synthesis of PDA-PEG polymer. Briefly, PDA (125 mg, 0.52 mmol) and PEG360 (187.5 mg, 0.52 mmol) were firstly dissolved in 5 mL degassed anisole, following the addition of 2-aminoethyl methacrylate hydrochloride (AEME, 8.28 mg, 0.05 mmol) in 1 mL CH_3OH. AIBN (7 mg, 0.0425 mmol) in 1 mL degassed anisole was then added, and the reaction mixture was stirred for 24 hours at 65 ºC. The final product was precipitated (3×) in ice cold ether and dried for 48 h in vacuum.

3.2.4 PDA quantification in polymer

For the quantification of PDA in the polymer, PDA-PEG, PDA-PEG-PhA or PDA-PEG-AEME (50 μg/mL in DMSO) was incubated with tris(2-carboxyethyl)phosphine (TCEP, 10 mM and 20 mM) for 1 hour at room temperature, and then the amount of 2-pyridinethione released was quantified through UV-Vis spectrophotometer (DU® 650 Spectrophotometer, Beckman Coulter, Inc.) at λ = 375 nm (ε, molar absorption coefficient = 8080 $M^{-1}cm^{-1}$)

3.2.5 PDA-PEG-PhA nanogel fabrication (PhA-NG)

PDA-PEG-PhA (2.0 mg in 500 μL DMSO) and PDA-PEG-AEME (1 mg in 50 μL DMSO) was firstly mixed well. TCEP (110.4 μg in 20 μL DMSO) was then added and the final mixture solution was immediately added dropwise into 5 mL ddH2O and stirred overnight night in a glass vial with open cap to form the nanogel. The nanogel was

further purified by dialysis in DMSO to remove free PhA and then PBS (pH 7.4, 10 mM) to change the solvent. The nanoparticle size, zeta potential and morphology were measured by DLS (Zetasizer Nano ZS, Malvern Instruments Ltd) and TEM (Hitachi H8000, Hitachi High Technologies America, Inc.), respectively.

3.2.6 EGFR conjugation to the nanogel (PhA-ENG)

Mal-PEG-COOH (Mw=3,500 Da, 500 μg in 100 μL DMSO) was firstly activated by EDC (100 μg in 100 μL DMSO) and NHS (60 μg in 100 μL DMSO) and added into the PhA-NG (0.6 mg polymer in 2 mL PBS). The mixture was stirred at 4 ºC overnight and then dialyzed in PBS to remove unreacted Mal-PEG3500-COOH (MW CO=6,000 Da). The conjugation of anti-EFGR affibody to the nanogel was realized by the reaction between maleimide and thiol group. Briefly, Anti-EGFR Affibody® Molecule (20, 100 and 500 μg, respectively) was firstly pretreated with 20 mM DTT to expose the reactive cysteine residue and then added to the nanogel (~0.3 mg in 1 mL PBS) and reacted overnight at 4 ºC to obtain the PhA-ENG. The nanogel was purified by passing through Sephadex® G-25 column (Sigma-Aldrich Co. LLC) to remove unconjugated affibody and filtrated through 0.22 μm filter.

3.2.7 UV-Vis spectra investigation

PhA and PhA-NG were dissolved in DMSO and TCEP was added to achieve a final concentration of 10 mM. The UV-Vis spectra of PhA and PhA-NG were recorded by UV-Vis spectroscopy (DU® 650 Spectrophotometer, Beckman Coulter, Inc).

3.2.8 PhA quantification in the nanogel

PhA concentration in the nanogel was quantified by UV-Vis spectrophotometer. In brief, the nanogel was diluted in DMSO with 50 mM and 100 mM TCEP for 2 h to release PhA. The absorbance at 670 nm was then recorded and PhA concentration was calculated according to a pre-generated calibration curve.

3.2.9 PhA nanogel fluorescence kinetic profile study

The kinetic profile of the nanogel was investigated by measuring the PhA fluorescence at different GSH concentration. Briefly, PhA-NG was diluted in PBS supplemented with 1% Tween 80 and 10 mM EDTA to yield a final PhA concentration of 800 nM. To mimic the tumor and normal tissue reducing conditions, GSH (100 μM and 10 mM) was added into the nanogel and incubated at 37 ℃. At pre-determined time points, 1 mL sample was retrieved and frozen in liquid nitrogen immediately. At the end of the experiment, all samples were thawed at 37 ℃ quickly and their fluorescence were measured by a plate reader (Ex=405 nm, Em=680 nm, Molecular Devices SpectraMax M2, Molecular Devices, LLC).

3.2.10 Determination of singlet oxygen generation

Singlet oxygen generation was determined by monitoring the decrease of fluorescence intensity of 9,10-dimethylanthracene (DMA) as a singlet oxygen sensor. Briefly, PhA, PhA-NG, PhA-NG supplemented with 10 mM GSH were diluted in PBS with 1% Tween 80 and 10 mM EDTA to get a final PhA concentration of 800 nM. All samples were incubated at 37 ºC for 1 h, 3 h and 5 h, respectively. DMA was then added (final concentration was 25 μM), following the irradiation under a 670 nm laser (15

mW/cm^2, Intense HPD 7404 diode laser, Intense Ltd.). At every minute interval, 200 μL sample was retrieved and the fluorescence intensity of DMA was measured by a microplate reader (Ex=370 nm, Em=535 nm, Beckman Coulter DTX 880 Multimode Detector, Beckman Coulter, Inc). The singlet oxygen quantum (SOQ) yield was calculated as follows:

$$\emptyset_\Delta = \frac{K_S}{K_R} \times \frac{A_R}{A_S} \times ref.\emptyset_\Delta \qquad (2\text{-}1)$$

where A is absorbance at 670 nm and K is the slope of the absorbance curve; S and R represent the sample and the reference, respectively. The SOQ ($\emptyset_\Delta$) of each sample was calculated from the reference $\emptyset_\Delta$value (PhA 0.52: $ref.\emptyset_\Delta$).

3.2.11 GSH-mediated photoactivity of PhA-NG

The fluorescence emission spectra of the PhA-NG was studied by fluorescence spectroscopy. In briefly, PhA-NG equivalent to 800 nM PhA was suspended in PBS or PBS supplemented with 1% Tween 80 and were added with GSH at concentration of 10 μM, 100 μM, 1 mM, 10 mM, 25 mM and 50 mM. Then nanogel solution was incubated at 37 ºC for 1 h and its fluorescence emission spectra was recorded by Varian Cary Eclipse Fluorescence Spectrophotometer (Agilent technologies, Inc.) with an excitation wavelength at 405 nm.

The activatable photoactivity of PhA-NG depending on the gradient of GSH concentrations were investigated. In brief, PhA-NG with the equivalent PhA concentration to 800 nM in PBS supplemented with 1% Tween 80 was exposed to different concentrations of GSH (0.01-50 mM) and incubated at 37 ºC for 1 h, 2 h, and 4 h. The nanogel was then loaded into a black 96-well plate and the fluorescence imaging

was taken by IVIS spectrum fluorescence and bioluminescence imaging system (Ex=430 nm, Em=680 nm, PerkinElmer Inc.).

3.2.12 Confocal microscopy

UMSCC 22A (200,000 cells/dish) were seeded in 35mm^2 Petri dishes (Mat Tek, MA, USA) overnight. PhA, PhA-NG and PhA-ENG were then diluted in culture medium and added into the dishes with the final equivalent PhA concentration at 800 nM in each dish. After 3 h of incubation under a humidified atmosphere of 95/5% air/CO_2, cells were washed by PBS (3×), fixed with formaldehyde (4.5 % in PBS), and then cells were analyzed under a confocal microscope (LSM 700, Carl-Zeiss Inc.).

3.2.13 Flow cytometry

UMSCC 22A cells (300,000 cells/well) were seeded in a 6-well plate overnight. PhA, PhA-NG and PhA-ENG were then diluted in culture medium and added into the plate with the final PhA concentration of 800 nM in each well. After 3 h incubation under a humidified atmosphere of 95/5% air/CO_2, cells were washed by PBS, trypsinized and resuspened in PBS. PhA positive cell population was quantified at λ_{ex}488 and λ_{em}670 nm using flow cytometry (BD Accuri C6, BD Biosciences).

3.2.13 Subcellular co-localization

UMSCC 22A cells (150,000 cells/dish) were seeded in 35mm^2 Petri dishes (Mat Tek, MA, USA) overnight and incubated with PhA-ENG at indicated times. Before imaging, fresh FBS-free medium supplemented with Insulin-Transferrin-Selenium-X (ITX) reagent was added. Cells were loaded with MitoTracker Green (MTG, 500 nM) and LysoTracker Green (LTG, 500 nM) respectively to assess the co-localization of PhA-

ENG with mitochondria and lysosomes. Cells were placed in an environmental chamber at 37 °C and analyzed by laser scanning confocal microscope (LSM 510, Carl-Zeiss Inc). A 63× N.A. 1.4 oil immersion planapochromat objective was used for all experiments. LTG, TMRM and PhA fluorescence was imaged using 488 nm excitation/500–530-nm emission, 543 nm excitation/565-615 nm emission and 580 nm excitation/650-710 nm emission, respectively. All images were processed by ImageJ software to calculate the co-localization coefficients.

3.2.14 In vitro phototoxicity

In vitro phototoxicity of PhA nanogels were tested in UMSCC 22A cell line. Cells were seeded in two 96-well plates (20,000 cells/well) for 24 h prior to the study. After that, culture medium was removed and replaced with fresh medium including a serial of concentrations of PhA, PhA-NG and PhA-ENG. After 24 h incubation, cells in one plate were exposed to 670 nm laser for irradiation (800 mJ/cm^2), and followed by continued for another 24 h of incubation in 95/5% air/CO_2 at 37 ºC. For another plate, cells were kept incubation in dark for total 48 h. Finally, for both plates, MTT reagent (100 μL, 10%(w/w) in medium) was added and incubated for 4h, followed the addition of MTT stop solution and the measurement of the optical density of the medium using a microplate reader (ELX808, Bio-Tech Instrument, Inc) at λ = 595 nm.

3.2.15 Serum Stability

The stability of the nanogel was evaluated in 10% serum condition. Briefly, PhA-NG was diluted in PBS supplemented with 10% FBS and 0.05% sodium azide. The final concentration of PhA was 800 nM. The nanogel was incubated at 37 ºC for up to 7 days. The size of the nanogel was monitored by DLS every day.

3.2.16 Animal experiment

All animal procedures were conducted in accordance with NIH regulations and approved by the Institutional Animal Care and Use Committee of the University of South Carolina.

Tumor model

UMSCC 22A cells suspended in DMEM medium at the density of 1.5×10^6/100 μL were inoculated subcutaneously in flanks of female Balb/c nude mice (8-10 week old, ~20 g, The Jackson Laboratory). The tumor volume were measured by a digital caliper and calculated according to the following formula: Tumor volume = (tumor length) × (tumor width)^2/2.

Biodistribution of nanogel

When the tumor reached to 50~150 mm^3, PhA, PhA-NG and PhA-ENG were administered by retro-orbital injection (100 μL, PhA concentration equal to 1 mg/kg). For control group, same volume of PBS was injected. After injection, mice were imaged by IVIS imaging system (IVIS Lumina III In Vivo Imaging System, Perkin, Ex=620 nm, Em=670 nm) at predetermined time points. All the image analyses were performed using a Living Image Software (IVIS Imaging Systems).

In vivo antitumor efficacy

When the tumor reached to 50~150 mm^3, PhA, PhA-NG and PhA-ENG were administered by retro-orbital injection (100 μL, PhA concentration equal to 1 mg/kg). At 24 h post-injection, tumors were irradiated with a 670 nm laser at a light density of 38.0 mW/cm^2 for 5 min. Then the tumor volume (V) and bodyweight (m) of the mice were

measured every three days up to 21 days. The relative tumor volume expressed as V/V_0 (V_0 was the tumor volume when the treatment was initiated) was used to represent the tumor size change during the whole treatment process. After 21 days, the mice were sacrificed and the blood, tumor, liver, heart, lung, kidneys and spleen were collected for further analysis. All organs were firstly fixed in 10% neutral buffered formalin for 48 h and then washed with PBS and finally kept in 70% ethanol at 4 ^{o}C.

Histological Examinations

The formalin fixed organs were embedded in OCT gel, sectioned into ~5 μm, stained with hematoxylin and eosin (H&E) and analyzed under light microscopy (Leica DM1000 LED, Leica Microsystems Inc.). The histology was performed in a blinded fashion by professional personnel in the University of South Carolina.

3.3 RESULTS AND DISCUSSION

3.3.1 Polymer synthesis and nanogel fabrication

In order to prepare the PhA encapsulated nanogel, two polymers were synthesized and post-modified. Poly[(2-(pyridin-2-yldisulfanyl) ethyl acrylate)-co-[poly(ethylene glycol)]] (PDA-PEG) was firstly polymerized according to our previous reports[11,22,23] and subsequently modified by replacing 60% of the PDA segment of the polymer with cysteamine through a thiol-disulfide exchange reaction to incorporate the amine functional group to yield PDA-PEG-NH_2. The second polymer, poly[(2-(pyridin-2-yldisulfanyl) ethyl acrylate)-co-[poly(ethylene glycol)]-co-[poly(2-aminoethyl methacrylate)]] (PDA-PEG-AEME) was synthesized the same as PDA-PEG but including 10% 2-aminoethyl methacrylate monomer in the initial monomer solution

(**Scheme 3.2B**). Both polymers' structures were verified by ^{1}H-NMR (**Figure 3.1**). PhA was connected to PDA-PEG-NH_2 through an amide bond through the coupling reaction between amine and carboxyl groups. ^{1}H-NMR result proved the successful conjugation of PhA to the polymer since the polymer conjugate (PDA-PEG-PhA) included peaks at 9.65 ppm, 9.19 ppm, 8.71 ppm and 6.21 ppm which were the characteristic peaks belonging to PhA, and peaks at 8.50 ppm, 7.79 ppm and 7.29 ppm which were the characteristic peaks of pyridine ring from the PDA segment of PDA-PEG (**Figure 3.1A**).

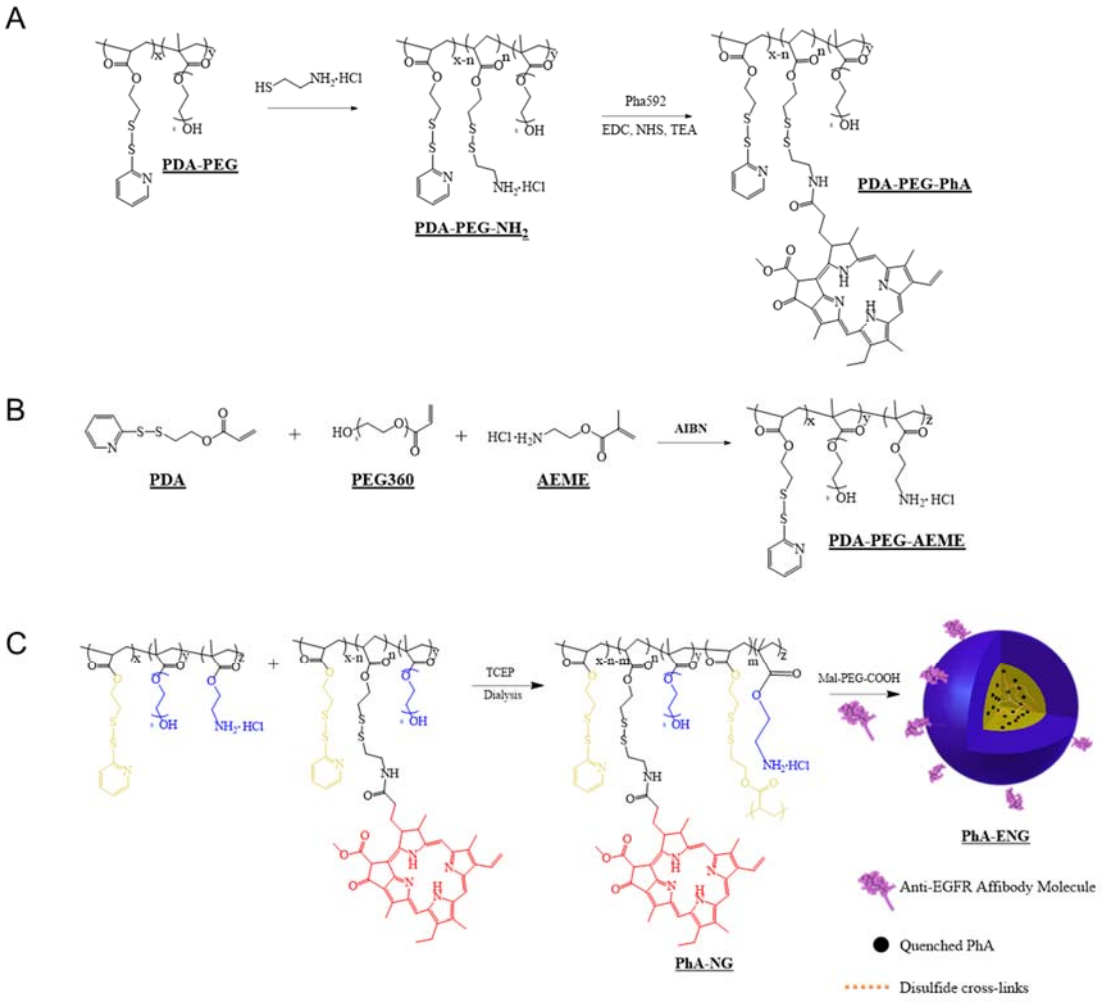

Scheme 3.2 Illustration of the synthesis of polymers and the fabrication of PhA nanogels

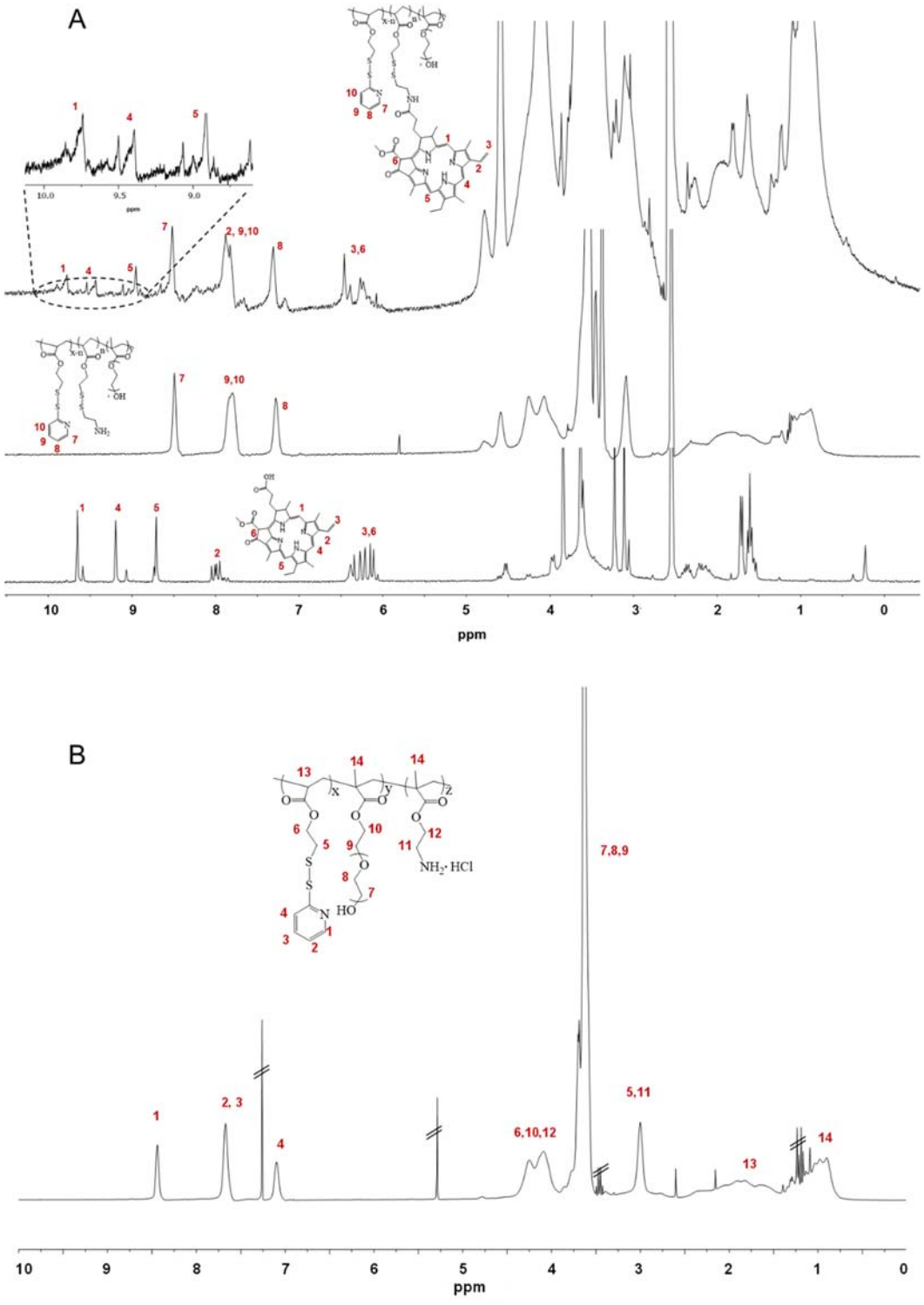

Figure 3.1 ^{1}H-NMR spectra: (A) PhA, PDA-PEG and PDA-PEG-PhA (from bottom to top); (B) PDA-PEG-AEME

PhA nanogel (PhA-NG) was formed through disulfide cross-linking which was generated by the addition of a predetermined amount of tris(2-carboxyethyl)phosphine (TCEP) into the PDA-PEG-PhA and PDA-PEG-AEME polymer mixture (**Scheme 3.2C**). The addition of PDA-PEG-AEME endowed PhA-NG containing amine functional group on its surface, making post-modification of the nanogel much easier. Zetasizer analysis revealed that the nanogel had a hydrodynamic size of 129.3 ± 1.13 nm and carried a near neutral surface charge (0.219 ± 0.830 mV) (**Figure 3.2A and 3.2B**). Transmission electron microscopy (TEM) indicated a spherical morphology of the nanogel with a size around 50 nm (**Figure 3.2C**). We further tested the responsiveness of the nanogel to redox potential since we previously had reported that disulfide crosslinked nanogel was sensitive to redox potential.[11,22] To mimic the cellular high GSH reducing environment, the nanogel was dispersed in 10 mM DTT solution, which resulted in a dramatic size increase due to the breakage of disulfide bond and the aggregation of the nanogel (**Figure 3.2C**), proving the responsiveness of the nanogel to redox potential. Next, PhA-NG was further decorated with targeting ligand to improve its cellular uptake. As reported that protruding ligands from nanoparticle's surface could achieve much better targeting effect due to the relative high opportunity for the ligands to interact with receptors,[24] a bifunctional PEG with both carboxyl and maleimide functional groups on its ends (Mal-PEG-COOH, Mw=3400 Da) was employed. The carboxyl group of Mal-PEG-COOH was firstly reacted with amine group of the nanogel, introducing maleimide to the nanogel's surface. Then thoil containing targeting ligand was anchored to the nanogel by thiol-maleimide Michael addition reaction. Anti-EGFR Affibody® molecule was a specific affinity ligand selected against the extra cellular domain of the Epidermal

Growth Factor Receptor (EGFR) which was highly overexpressed on many cancers including the head and neck cancer.[25] Thus, Anti-EGFR Affibody® molecule was selected as the targeting ligand for our study. The affibody was initially activated to expose the thiol functional group and then conjugated to the nanogel (**Scheme 3.2C**). The EGFR targeting nanogel (PhA-ENG) showed an increased hydrodynamic size (178.8 ± 4.81 nm) compared to PhA-NG with a slightly negatively charged surface (-7.95 ± 4.04 mV) (**Figure 3.2A and 3.2B**).

A

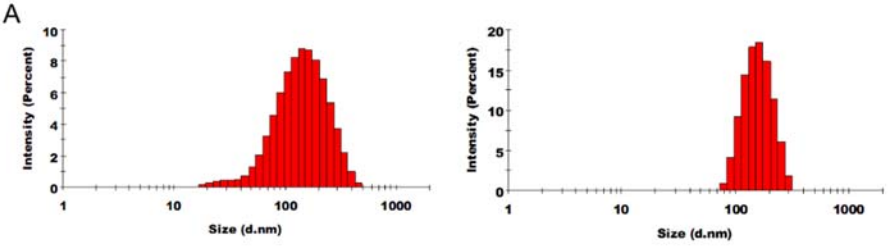

B

Nanogels	Size (nm)	PDI	Zeta potential (mV)
PhA-NG	129.3 ± 1.13	0.282 ± 0.038	0.219 ± 0.830
PhA-ENG	178.8 ± 4.81	0.217 ± 0.017	-7.95 ± 4.04

C

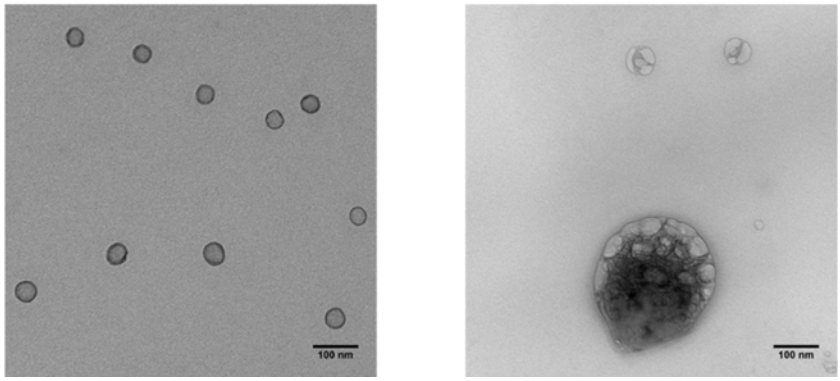

Figure 3.2 Size and surface charge of PhA nanogels. (A) Size distribution of PhA-NG (left) and PhA-ENG measured by Zetasizer based on dynamic light scattering (DLS). (B) Summary of size, PDI and zeta potential of PhA nanogels. Results are obtained from Zetasizer. (C) Representative TEM images of PhA-NG before (left) and after adding 10 mM GSH. Scale bars are 100 nm.

3.3.2 Absorption, fluorescence and photoactivity of the nanogel

As a chlorophyllide derivative, PhA has characteristic UV-Vis spectra, which has been used to verify the existing status of PhA in the nanoparticles.[26] Therefore, we firstly studied the UV-Vis spectra of PhA-NG. As shown in **Figure 3.3A**, in DMSO, the nanogel and free PhA has very similar UV-Vis spectra which includes the intense Soret band in the near-UV and the relatively weak Q-band in the visible region, and the Q-band spectra of the nanogel was not affected by the addition of the reducing agent TCEP, denoting that the disulfide bond would not change the spectrometric characteristics of PhA itself. The same phenomenon was also observed by Wool Lim Kim et al..[26] In PBS, the Q-band of the nanogel exhibited an obvious bathochromic shift to 672 nm due to the self-aggregation of PhA in the nanogel. However, the absorbance intensity of the nanogel was remarkably stronger than that of free PhA at 672 nm, indicating that the nanogel enhanced PhA's aqueous solubility, making PhA more suitable for systematic application.

The aggregation of PhA in nanogel would induce fluorescence quenching which has been reported widely.[15] The photoquenching could affect the photodynamic activity of a photosensitizer, and thus reduce PDT associated side effects. Thus we further investigated the fluorescence properties of PhA-NG. Fluorescence spectroscopy result revealed that PhA-NG really had very low fluorescence intensity in PBS buffer due to the aggregation induced quenching (**Figure 3.3B**, gray line). We further tested the effect of a biological molecular GSH on the nanogel's fluorescence since GSH would break down the nanogel, terminate the aggregation of PhA and recover PhA's fluorescence by freeing PhA to the solution. Since free PhA itself forms dimer in aqueous condition leading to

low fluorescence,[27] 1% Tween 80 was supplemented in the nanogel solution to inhibit the dimeric form of PhA after adding GSH. As shown in **Figure 3.3B**, the addition of 1% Tween 80 increased the fluorescence of the nanogel, probably because of the disturbance of Tween 80 reduced hydrophobic interaction and π-π stacking among PhA molecules inside the nanogel. However, due to the restriction of PhA within the nanogel, its fluorescence was still dramatically quenched. The recovery of PhA fluorescence by GSH in the nanogel was concentration depended, as shown in **Figure 3.3B**. At low GSH concentration such as 10 μM, 100 μM and 1 mM, no or very slight fluorescence increase was observed, probably because of few GSH diffusing into the nanogel to attack disulfide bonds. When the GSH concentration increased to 10 mM, a sharp fluorescence increase was observed and it was continuously growing as GSH elevated to 25 mM and reached its maximum as no fluorescence increased as GSH raised to 50 mM. Fluorescence imaging further confirmed the spectroscopy result that GSH could activate PhA in the nanogel. As shown in **Figure 3.3C**, at low GSH concentrations (<10 mM), very dim images were exhibited, revealing that PhA was in its quenching status. As GSH increased to 10, 25 and 50 mM, bright fluorescence images were achieved, indicating the release of PhA from the nanogel turning into its activated form. The GSH-mediated activation of PhA will be extremely important for the nanogel to be used for PDT since the nanogel will remain in its inactivated status and thus reduce non-specific light irradiation to normal tissues (e.g. blood, skin and eye) due to the low GSH concentration there, while upon accumulation in tumor tissue through EPR effect, the nanogel will turn to its activated form under the influence of high GSH level and be ready for PDT.

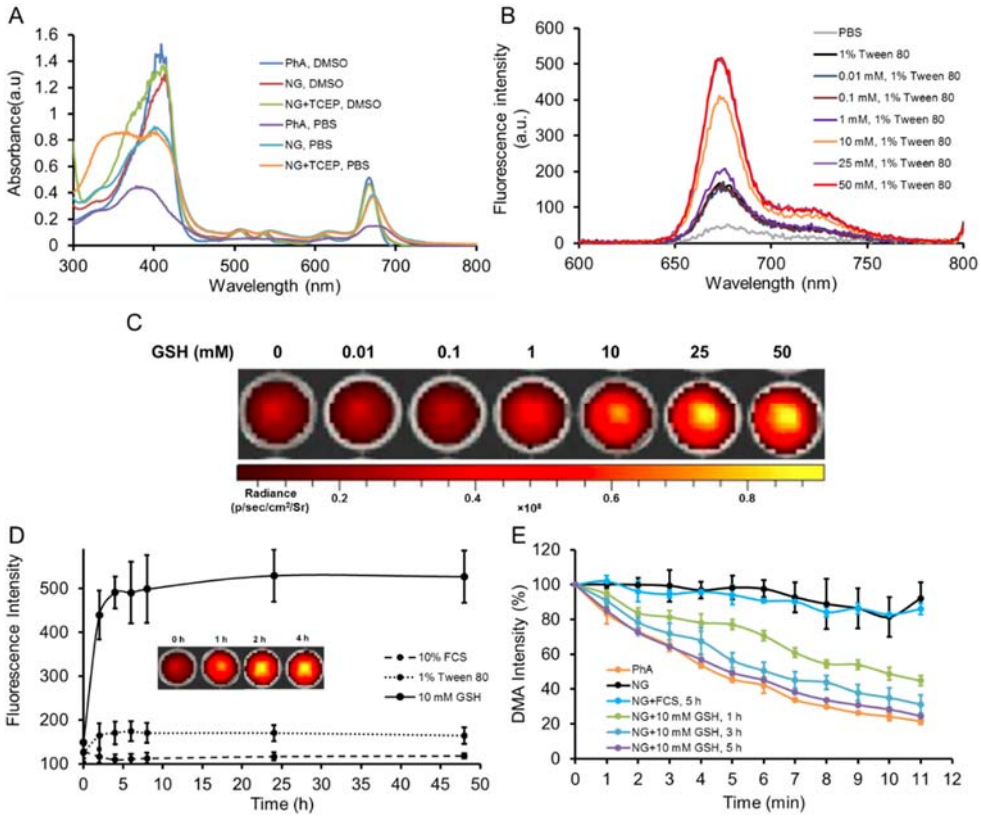

Figure 3.3 Absorption, fluorescence and photoactivity. (A) UV-Vis spectra of free PhA and PhA-NG in DMSO and PBS, respectively. The PhA equivalent concentration was 800 nM. TCEP was applied as a reducing agent to cleave disulfide bonds to release PhA from the nanogel; (B) Fluorescence emission spectra of PhA-NG in different condition. The nanogel was firstly dispersed in PBS or PBS containing 1% Tween. 0-50 mM GSH was then added and treat for 1 h. The spectra were achieved at an excitation wavelength at 405 nm by fluorescence spectrophotometer. (C) Fluorescence images of PhA-NG after treated with 0-50 mM GSH for 1 h in PBS 7.4 supplemented with 1% Tween 80. The images were taken in IVIS Lumina III In Vivo Imaging System (excitation at 405 nm and emission at 680 nm). PhA concertation was equal to 800 nM. (D) GSH effect on the fluorescence intensity change of PhA-NG. The nanogel was dispersed in PBS with 1% Tween 80 with PhA concentration of 800 nM, and GSH equal to 10 mM was added to mimic the tumor environment. FCS (10%) was also added to mimic the blood stream condition. The fluorescence intensity was measured by a plate reader (Ex=405 nm, Em=680 nm). Inset was the representative images visually exhibited the fluorescence change of PhA-NG as the incubation time increasing at the presence of 10 mM GSH. (E) Change of fluorescence of DMA due to the generation of singlet oxygen by PhA-NG. The nanogel was in 1% Tween PBS buffer without GSH or plus 10% FCS and 10 mM GSH and incubated for varied times (1 to 5 h). Then 25 μM DMA was added and the nanogel was exposed to 670 nm laser irradiation (15 mW/cm^2) up to 11 min. The fluorescence of DMA at each minute was measured by a plate reader (Ex=370 nm, Em=530 nm).

Ideally, the nanogel should be stable enough during circulation period after systemic administration while rapidly being activated by GSH as it locates to tumor. In general, the GSH level in tumor tissue or cancer cells is in the range of millimolar (2-20 mM).[19] Therefore, we further kinetically studied the process of fluorescence activation of PhA-NG in 1% Tween PBS at the presence of 10 mM GSH to mimic the tumor environment. To mimic the blood stream condition, the nanogel was directly dispersed in 10% serum. As shown in **Figure 3.3D**, the nanogel's fluorescence increased rapidly after the addition of 10 mM GSH, and almost 90% of PhA fluorescence had been recovered at 4 h, after which the fluorescence slowly proceeded to a plateau to get a 4.3 fold fluorescence increase compared to the nanogel in 1% Tween 80 without GSH. In contrast, the nanogel's fluorescence had no obvious increase even after 48 h at the presence of serum, indicating that the nanogel could maintain its self-quenching status during the blood circulation process. Inset in **Figure 3.3D** showed the fluorescence images of the nanogel at different time points after the treatment of GSH. The nanogel exhibited a increasing of image brightness as time went on, which further confirmed that the nanogel was rapidly and continuously activated by high GSH in tumor.

The activation of PhA-NG by GSH is expected to be applicable for PDT since the monomerized PhA could generate singlet oxygen ($^1O_2$) under laser irradiation. The singlet oxygen is one type of reactive oxygen species (ROS) and it governs the PDT efficacy of PhA. By comparing the capacity of $^1O_2$ generation of PhA-NG with that of free PhA, the PDT potential of the nanogel could be initially assessed before processing to *in vitro* and *in vivo* evaluation. The generation of $^1O_2$ could be determined by calculating the singlet oxygen quantum yield (SOQ, $\varnothing_\Delta$) by using DMA as the $^1O_2$ trap.

DMA was a florescence dye and its fluorescence would be lost by reacting with $^1O_2$ to form a nonfluorescent endoperoxide. By measuring the loss of fluorescence of DMA, the $^1O_2$ generation kinetics could be determined and is was used to calculate $\varnothing_\Delta$ according to the equation (2-1). As shown in **Figure 3.3E**, slight fluorescence recovery of PhA-NG in 1% Tween 80 could not effectively generate $^1O_2$ since only a minor fluorescence loss of DMA occurred. A similar result was also observed when adding 10% serum to the nanogel because of the low activation of the nanogel. In contrast, after incubation of the nanogel with GSH (10 mM) for 1 h, an increase loss of fluorescence of DMA was observed and the loss was continuously enhanced as the elongation of incubation time which produced more activated PhA. After 5 h of incubation which accounted of more than 90% PhA activation, the nanogel reached a very similar $^1O_2$ generation kinetics as free PhA, with a SOQ equal to 0.49 which was about 94% SOQ of the free PhA (0.52), indicating that the nanogel could rapidly induce high PDT effect at tumor site where GSH level was elevated.

3.3.3 Intracellular uptake and localization

Due to the short lifetime of $^1O_2$,[28] it needs to be intracellularly generated to take PDT into effect in treating cancer cells. This required PhA-NG should have a high cellular uptake. In order to improve it, the nanogel was decorated with a targeting ligand. Here, we chose head and neck squamous cell carcinoma (HNSCC) to explore the PDT efficacy of the nanogel because most HNSCC cases are localized, making PDT laser easily reaches the tumor. Additionally, PDT is advantageous over surgery in treating HNSCC since it causes minimal damage to cosmetic appearance and tissue function.

Due to the high overexpression of EGFR in HNSCC,[29] Anti-EGFR Affibody® molecule was selected as the targeting ligand to modify PhA-NG because of its relative small size compared to Anti-EGFR antibody and easy preparation for nanogel modification. The affibody could be facilely activated by dithiothreitol to expose cysteine residue and reacted with PhA-NG by thiol-maleimide Michael addition reaction. The reacting ratio between the affibody and PhA-NG were varied in order to obtain PhA-ENG with different surface ligand densities. The cellular uptake efficiency of the PhA-ENG was firstly evaluated using flow cytometry in UMSCC 22A cell, a head and neck cancer cell line which has been extensively reported overexpression of EGFR.[30] As shown in **Figure 3.4A**, free PhA had highest uptake because it could easily pass through cell membrane via simple diffusion.[31] For nanogels, their cellular uptake efficiency was dramatically different. Compared to the relative low uptake of PhA-NG, all three targeting nanogels exhibited enhanced uptake efficiency due to the facilitation of ligand-receptor interaction. However, the affibody modification density on the nanogel significantly determined their uptake behaviors. Only PhA-ENG modified with intermediate density of affibody (5×) showed the highest uptake efficiency. Higher (25×) or lower (1×) targeting density both would not exhibit the highest capability for nanogels to enter the cells because of too strong or too weak interaction between ligand and receptors.[32] Confocal laser scanning microscopy (CLSM) was further used to study the uptake behavior of the nanogels. In consistence with flow cytometry result, CLSM reconfirmed that Anti-EGFR Affibody® molecule could effectively improve the cellular uptake of PhA-ENG (**Figure 3.4B**). In the following experiments, PhA-ENG represented

the Anti-EGFR Affibody modified nanogel with the intermediate ligand density, otherwise noted.

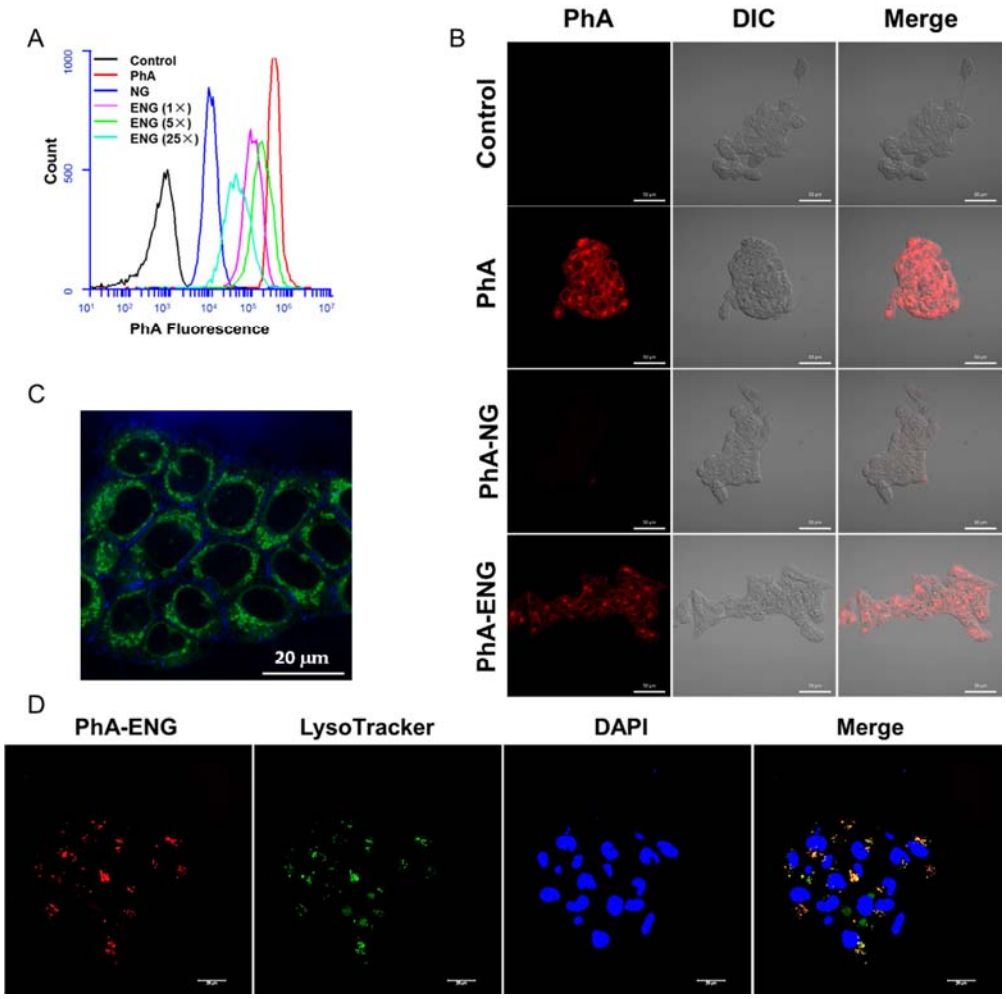

Figure 3.4 Cellular uptake and intracellular localization of nanogels. (A) Flow cytometry of PhA, PhA-NG and PhA-ENG with different ligand density. UMSCC 22A cell was incubated with different treatment for 3 h at 800 nM PhA. (B) Confocal images of PhA, PhA-NG and PhA-ENG (5×), UMSCC 22A cell was also incubated with different treatment for 3 h at 800 nM PhA. All scale bars are equal to 50 μm. (C) Co-localization of PhA-ENG (5×) with mitochondria. Mitochondria was stained with MitoTracker Green (MTG). Blue: nanogel, Green: MTG. Scale bar=20 μm. (D) Co-localization of PhA-ENG (5×) with endosomes/lysosomes. Endosomes/lysosomes were stained with Lysotracker Green (LTG). Red: nanogel, Green: LTG, Blue: nuclei. Scale bars are 20 μm.

As the PDT efficacy of chlorophyllide derivatives was reported relevant to the extent of co-localization with mitochondria.[33,34] we subsequently investigated that whether the nanogel could also deliver PhA to mitochondria. Surprisingly, the nanogel could not localize to mitochondria, as shown in **Figure 3.4C** since no overlay between green (mitochondria) and blue color (nanogel) was observed. Also no PhA nuclear localization was observed since no blue color showed up in the nuclei areas (black voids surrounded by green color in **Figure 3.4C**). Further experiment found that the nanogel was located in endosomes/lysosomes as the nanogel's fluorescence (red) coincided with endosomes/lysosomes labeled with LysoTracker (green), revealed by CLSM in **Figure 3.4D**. These findings were in line with several early reports which also found that pheophorbide a derivatives preferred to stay in intracellular membranes and lysosomes.[34,35]

3.3.4 In vitro phototoxicity

To evaluate whether the enhanced cellular uptake and endosomes/lysosomes co-localization would induce efficient PDT effect of nanogels in cell killing, MTT assay was carried out to assess the cell viability after PDT in UMSCC 22A cells. Prior to irradiation with 670 nm laser (800 mJ/cm^2), UMSCC 22A was incubated with free PhA, PhA-NG and PhA-ENG for 24 h. Cells treated with the same dose of free drug and nanogels but without laser irradiation were set as control. As shown in **Figure 3.5A**, without laser irradiation, nanogels had no obvious toxicity to cells since negligible cytotoxicity was observed at all doses for the control cells, suggesting that the nanogels itself was safe. When the cells received laser irradiation (800 mJ/cm^2), a dose dependent cytotoxicity was occurred (**Figure 3.5B**). PhA-ENG exhibited enhanced cytotoxicity at almost all

tested doses compared to non-targeted nanogel which had very limited cell killing effect even at the highest PhA concentration due to its difficulty in entering the cells. PhA-ENG also showed a similar cell killing effect (>95%) to free PhA at 800 nM PhA equivalent concentration, proving that enhanced cellular uptake could be translated to higher PDT efficacy. To be noted, the laser power we used here (800 mJ/cm^2) was less than others reported,[34] which further evidenced the high PDT effect of PhA-ENG nanogel.

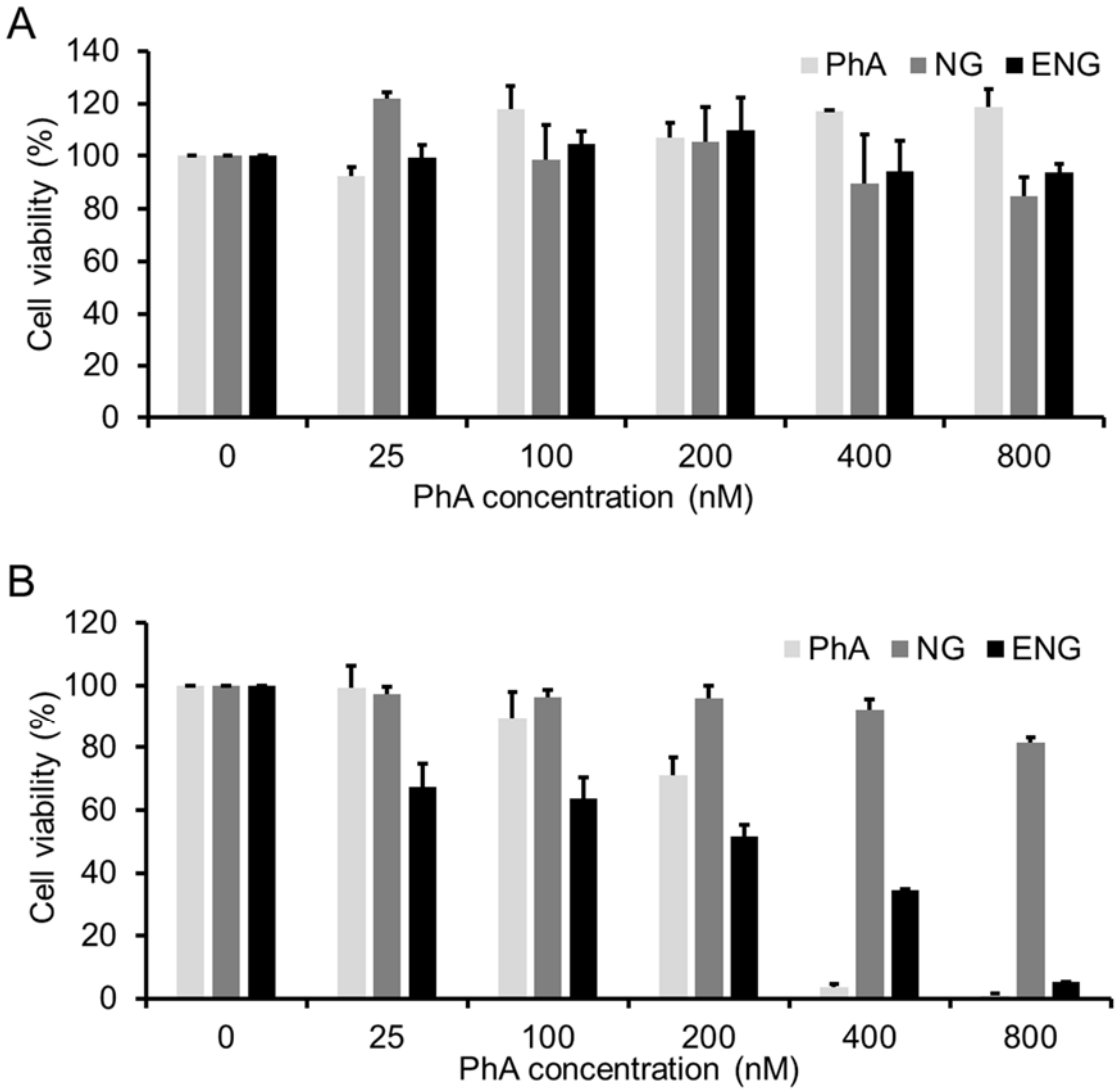

Figure 3.5 *In vitro* cytotoxicity of PhA, Pha-NG and PhA-ENG in UMSCC 22A at the absence (A) and presence (B) of a 670 nm laser (800 mJ/cm^2).

3.3.5 Biodistribution and in vivo PDT

As *in vitro* data showed that PhA-ENG had high cellular uptake and PDT efficacy, its PDT efficacy and tumor homing ability were further evaluated *in vivo*. We firstly tested the serum stability of the nanogel in 10% FCS by DLS for up to 7 days. **Figure 3.6A** showed that the nanogel was very stable and only had a slight size increase. The *in vivo* PDT effect of PhA nanogels was then studied in HNSCC xenograft mice model which was established by inoculating UMSCC 22A cells in both flanks of athymic nude mice. When the tumor grew to 50-150 mm^3, free PhA, PhA-NG and PhA-ENG were administered to the mice by retro-orbital injection (PhA dose equal to 1 mg/kg). The biodistribution of nanogels and free PhA were visualized using a non-invasive fluorescence imaging system. As shown in **Figure 3.6B**, compared to free PhA, both nanogels exhibited high fluorescence intensity in tumor sites at 24 h after injection, indicating that the nanogels could accumulate in the tumor by EPR effect and they were activated to restore high fluorescence in tumor-specific high GSH environment. PhA-ENG had even higher fluorescence than its non-targeting counterpart, proving that the targeting ligand really facilitated the tumor accumulation of the nanogel *in vivo*. To be noted here , free PhA also showed slight localization to tumor, probably because that a partial of the free drug aggregated or bound to serum proteins to form particles in circulation system, which also entered tumor by EPR effect. However, the free PhA excreted from the body very fast since very weak fluorescence was detected in the mouse after 24 h treating with free PhA. On the contrary, the nanogel showed high fluorescence intensity throughout the whole mouse body, indicating the high circulation time for the nanogels.

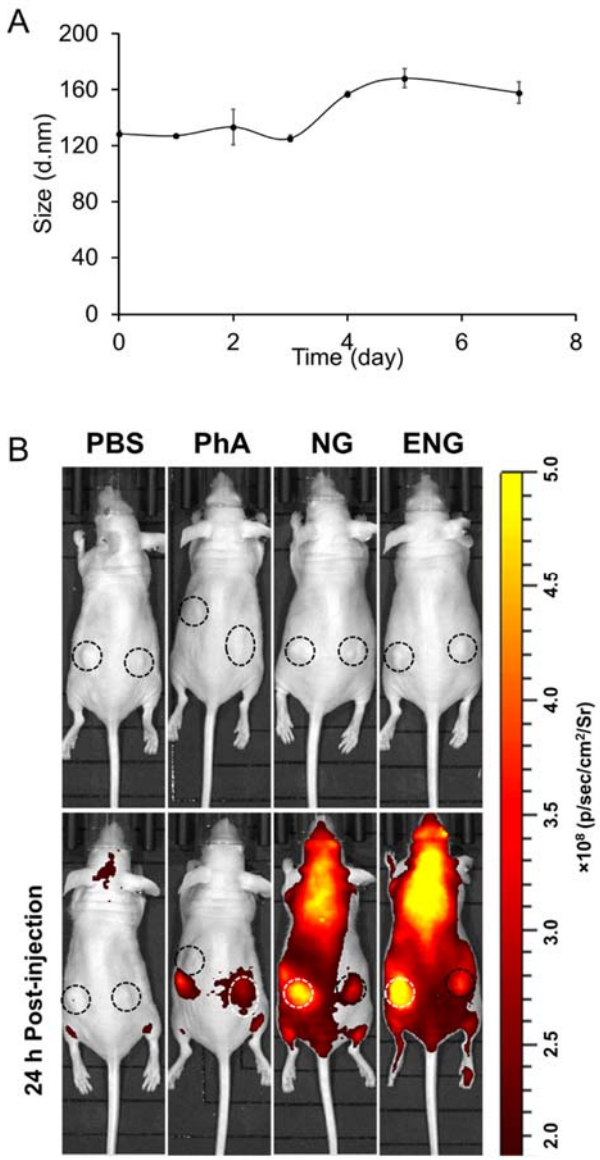

Figure 3.6 *In vivo* distribution of PhA nanogels. (A) Serum stability of PhA-NG. PhA-NG was diluted in 10% serum condition and incubated at 37 ºC for up to 7 days. (B) Biodistribution of PhA, PhA-NG and PhA-ENG 24 h post-injection. UMSCC 22A xenograft mice were administrated with PhA, PhA-NG and PhA-ENG by retro-orbital injection. The mice was imaged 24 h after injection with an IVIS Lumina III In Vivo Imaging System (Ex=620 nm, Em=670 nm). Circles reveal the location of tumor. White circle indicated the tumor receiving PDT, the laser power was 11.4 J/cm^2.

At 24 h post injection, the tumor was exposed to a 670 nm laser (11.4 J/cm^2). As shown in **Figure 3.7A**, laser irradiation effectively reduced the tumor volumes, and PhA-ENG had the highest PDT therapeutic efficacy. This was probably because of the

substantial accumulation of PhA-ENG in tumor under the assistance of the targeting ligand, rapid activation of its photoactivity by the high GSH level in tumor stroma and cytosol, and efficient generation of singlet oxygen to kill cancer cells and reduce tumor volume.

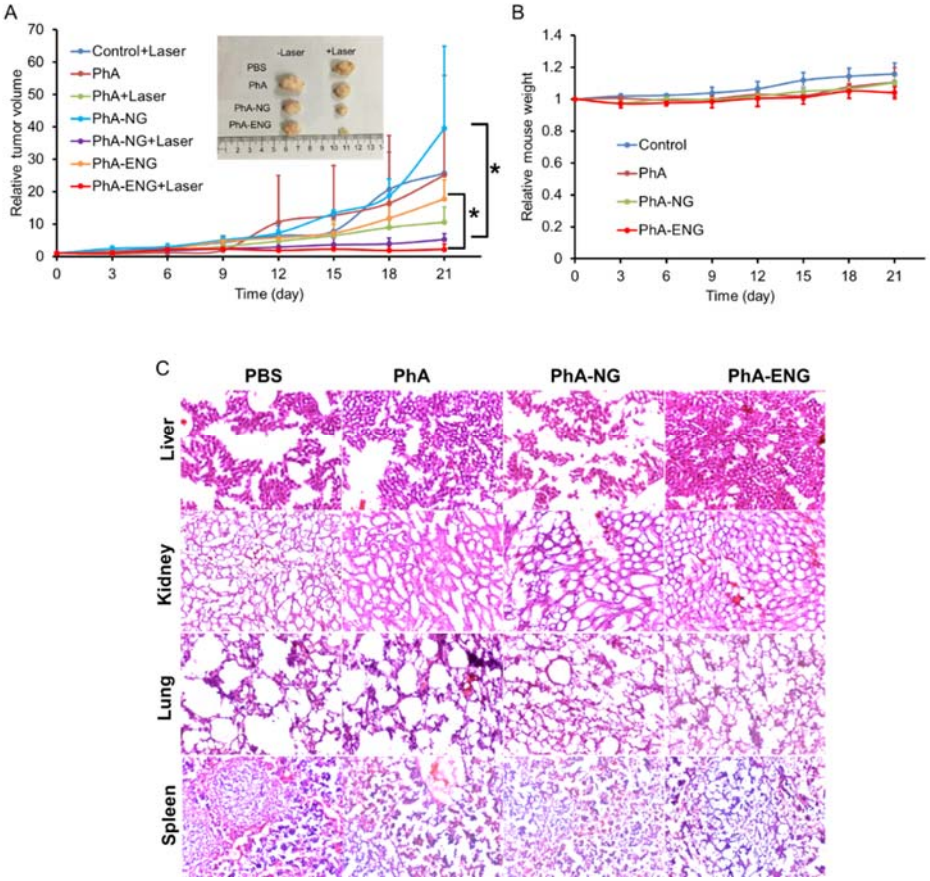

Figure 3.7 Antitumor activity of free PhA and PhA nanogels. UMSCC 22A xenograft mice were administered free PhA, PhA-NG and PhA-ENG by retro-orbital injection (1 mg/kg PhA equivalents). 24 h post injection, mice were irradiated with a 670 nm laser (200 mJ/cm^2). (A) Tumor growth curves; Inset showed the tumor sizes of different treatments 21 days after PDT. (B) The effect of different treatments on mouse bodyweight (bars represent ± SD); (C) Representative H&E staining images for liver, kidney, lung and spleen.

The *in vivo* toxicity of the nanogels was also investigated. Within the duration of 21 days after PDT treatment, no apparent bodyweight change was observed for all four groups (**Figure 3.7B**). Organs including liver, lung, kidney and spleen were also

harvested 21 days after the treatment for histologic analysis. No obvious sign of toxic side effect were also found in these organs. All these results suggested that the PhA nanogel was safe and effective for head and neck cancer therapy.

3.4 CONCLUSIONS

A self-quenching bioactivatable nanogel was developed and synthesized for targeted photodynamic therapy. The nanogel was fabricated by crosslinking PhA conjugated polymer through disulfide bonds. The aggregation of PhA in the nanogel resulted in a fluorescence quenching and the reduced singlet oxygen generation. Due to its responsiveness to redox potential, both the fluorescence intensity and singlet oxygen generation capacity can be restored in the tumor stroma and cytosol. The GSH mediated activation of photoactivity made the nanogel very safe for *in vivo* application since the nanogel would remain in its inactivated status and inhibit its phototoxicity to normal tissues due to the low GSH level there. While in high GSH level environment like tumor, the photoactivity of the nanogel would be activated and efficiently produce singlet oxygen for PDT. The nanogel was further decorated with Anti-EGFR Affibody to improve its tumor targeting efficiency and PDT effect in HNSCC due to the overexpression of EGFR in the tumor. The *in vitro* and *in vivo* data revealed that the affibody could effectively enhanced the cellular uptake and tumor homing ability of the nanogel, respectively, which subsequently resulted in high PDT efficacy. All these data demonstrated the high potential of the PhA nanogel as a safe and effective drug carrier for cancer therapy.

3.5 REFERENCES

(1) S. S. Lucky,K. C. Soo and Y. Zhang, *Chem. Rev.,* 2015, **115**, 1990-2042.

(2) D. K. Chatterjee,L. S. Fong and Y. Zhang, *Adv. Drug Delivery Rev.,* 2008, **60**, 1627-1637.

(3) D. E. J. G. J. Dolmans,D. Fukumura and R. K. Jain, *Nat. Rev. Cancer,* 2003, **3**, 380-387; P. Agostinis,K. Berg,K. A. Cengel,T. H. Foster,A. W. Girotti,S. O. Gollnick,S. M. Hahn,M. R. Hamblin,A. Juzeniene,D. Kessel,M. Korbelik,J. Moan,P. Mroz,D. Nowis,J. Piette,B. C. Wilson and J. Golab, *CA Cancer J. Clin.,* 2011, **61**, 250-281.

(4) A. Master,M. Livingston and A. Sen Gupta, *J. Controlled Release,* 2013, **168**, 88-102.

(5) C. Hur,N. S. Nishioka and G. S. Gazelle, *Digest. Dis. Sci.*, **48**, 1273-1283.

(6) K. Kostovic,Z. Pastar,R. Ceovic,Z. Bukvic Mokos,D. Stulhofer Buzina and A. Stanimirovic, *Coll. Antropol.,* 2012, **36**, 1477-1481.

(7) W. Jerjes,T. Upile,S. Akram and C. Hopper, *Clin. Oncol-uk.,* 2010, **22**, 785-791.

(8) N. Brasseur,R. Ouellet,C. La Madeleine and J. Van Lier, *Brit. J. Cancer,* 1999, **80**, 1533.

(9) C. J. Rijcken,J.-W. Hofman,F. van Zeeland,W. E. Hennink and C. F. van Nostrum, *J. Controlled Release,* 2007, **124**, 144-153.

(10) C. Kojima,Y. Toi,A. Harada and K. Kono, *Bioconjugate. Chem.,* 2007, **18**, 663-670.

(11) H. He,A. W. Cattran,T. Nguyen,A.-L. Nieminen and P. Xu, *Biomaterials,* 2014, **35**, 9546-9553.

(12) Y. Cheng,A. C. Samia,J. D. Meyers,I. Panagopoulos,B. Fei and C. Burda, *J. Am. Chem. Soc.,* 2008, **130**, 10643-10647; H. Y. Yoon,H. Koo,K. Y. Choi,S. J. Lee,K. Kim,I. C.Kwon,J. F. Leary,K. Park,S. H. Yuk and J. H. Park, *Biomaterials,* 2012, **33**, 3980-3989.

(13) T. J. Dougherty,M. T. Cooper and T. S. Mang, *Laser. Surg. Med.,* 1990, **10**, 485-488.

(14) K. Ogawa and Y. Kobuke, *Anticancer Agents Med. Chem.,* 2008, **8**, 269-279.

(15) S. Hackbarth,V. Horneffer,A. Wiehe,F. Hillenkamp and B. Röder, *Chem. Phys.,* 2001, **269**, 339-346.

(16) L.-B. Meng,W. Zhang,D. Li,Y. Li,X.-Y. Hu,L. Wang and G. Li, *Chem. Commun.,* 2015, **51**, 14381-14384.

(17) L. Li,M. Nurunnabi,M. Nafiujjaman,Y. Y. Jeong,Y.-k. Lee and K. M. Huh, *J. Mater. Chem. B,* 2014, **2**, 2929-2937.

(18) B. Jang and Y. Choi, *Theranostics,* 2012, **2**, 190-197.

(19) W. Chen,P. Zhong,F. Meng,R. Cheng,C. Deng,J. Feijen and Z. Zhong, *J. Controlled Release,* 2013, **169**, 171-179.

(20) I.-h. Oh,H. S. Min,L. Li,T. H. Tran,Y.-k. Lee,I. C. Kwon,K. Choi,K. Kim and K. M. Huh, *Biomaterials,* 2013, **34**, 6454-6463.

(21) B.-c. Bae and K. Na, *Biomaterials,* 2010, **31**, 6325-6335.

(22) K. Bahadur and P. Xu, *Adv. Mater.,* 2012, **24**, 6479-6483.

(23) R. B. KC,B. Thapa and P. Xu, *Mol. Pharmaceutics,* 2012, **9**, 2719-2729.

(24) M.Gregori,A. Orlando,F. Re,S. Sesana,L. Nardo,D. Salerno,F. Mantegazza,E. Salvati,A. Zito and F. Malavasi, *J. Pharm. Sci.,* 2016, **105**, 276-283.

(25) R. I. Nicholson,J. M. W. Gee and M. E. Harper, *Eur. J. Cancer,* 2001, **37**, 9-15.

(26) W. L. Kim,H. Cho,L. Li,H. C. Kang and K. M. Huh, *Biomacromolecules,* 2014, **15**, 2224-2234.

(27) I. Eichwurzel,H. Stiel and B. Röder, *J. Photochem. Photobiol. B, Biol.,* 2000, **54**, 194-200.

(28) P. R. Ogilby, *Chem. Soc. Rev.,* 2010, **39**, 3181-3209.

(29) A. R. Hansen and L. L. Siu, *J. Clin. Oncol.,* 2013, **31**, 1381-1383.

(30) S. E. Weigum,P. N. Floriano,N. Christodoulides and J. T. McDevitt, *Lab Chip,* 2007, **7**, 995-1003.

(31) F. Rancan,M. Helmreich,A. Mölich,N. Jux,A. Hirsch,B. Röder,C. Witt and F. Böhm, *J. Photochem. Photobiol. B, Biol.,* 2005, **80**, 1-7.

(32) D. R. Elias,A. Poloukhtine,V. Popik and A. Tsourkas, *Nanomedicine,* 2013, **9**, 194-201.

(33) I. J. MacDonald,J. Morgan,D. A. Bellnier,G. M. Paszkiewicz,J. E. Whitaker,D. J. Litchfield and T. J. Dougherty, *Photochem. Photobiol.,* 1999, **70**, 789-797.

(34) M. Jakubowska,M. Szczygieł,D. Michalczyk-Wetula,A. Susz,G. Stochel,M. Elas,L. Fiedor and K. Urbanska, *Photodiagn. Photodyn. Ther.,* 2013, **10**, 266-277.

(35) J.-Y. Matroule,G. Bonizzi,P. Morlière,N. Paillous,R. Santus,V. Bours and J. Piette, *J. Biol. Chem.,* 1999, **274**, 2988-3000.

CHAPTER 4

TRIPLE-RESPONSIVE EXPANSILE NANOGEL FOR TUMOR AND MITOCHONDRIA TARGETED PHOTOSENSITIZER DELIVERY[2]

4.1 INTRODUCTION

Photodynamic therapy (PDT) is a treatment procedure that uses a light to activate a photosensitizer (PS) to produce singlet oxygen for killing cancer cells or curing acne. [1] Since the onset of PS toxicity can only be triggered by the irradiation of light, PDT generally is considered as a safe alternative for chemotherapy in the treatment of cancer, and does not induce side effects. A lot of evidences indicate that PDT- induced apoptosis is due to the damage of mitochondria and suggest that mitochondria are the target for PDT. [2] Therefore, the efficacy of PS would be greatly enhanced if it can be delivered specifically to the mitochondria of cancer cells. In fact, research revealed that Pc 4, a silicon phthalocyanine PS, can spontaneously partition to mitochondria due to its high hydrophobicity, which makes it an ideal PS for maximizing PDT efficacy. [3] However, the clinical application of Pc 4 based PDT has not been widely accepted due to its poor water solubility and erratic tissue retention, especially in the skin which results in unwanted tissue damage upon the exposure to sunshine.

---

[2]H.He, W.C. Alexander, T. Nguyen, AL. Nieminen and P. Xu. 2014. *Biomaterails*. 35:9546-9553.

Reprinted here with permission of publisher.

Over past decades, many types of nanoparticle carriers have been developed for targeted delivery of Pc 4 to tumor by taking advantage of the leaky vascular structure in tumor tissue through so called enhanced permeability and retention (EPR) effect. Such systems include polymeric micelles, mesoporous silica nanoparticles, and gold nanoparticles, which can load hydrophobic Pc 4 through hydrophobic interaction. [4] Although with the help of various ligand-receptor interactions most nanoparticles achieved enhanced cellular uptake of Pc 4, there was occasional disconnection between the uptake of PS and their PDT efficacy. Higher uptake of PS did not result in better cell killing, possibly due to the fact that those encapsulated Pc 4 could not effectively escape from lysosome and then transfer to mitochondria. [3,5]

Therefore, we hypothesize that a nano-carrier which can escape from lysosome, quickly expand its size to release Pc 4 into cytosol would be able to deliver Pc 4 to mitochondria. Expansile nanoparticles (eNP), which can enlarge their size in response to pH, have been explored as drug carriers to control the drug release at targeted sites and achieved enhanced therapeutic effect. [6] Nanogels fabricated from pyridyl disulfide containing polymers have been applied in various drug delivery systems due to their easy functionalization. [7] Recently, our group reported a multicompartment nanogel made of poly[(2-(pyridin-2-yldisulfanyl)-co-[poly(ethylene glycol)]] (PDA-PEG) polymer, which showed self-expanding property in reducing environment and size increasing from 115 nm to 262 nm in 5 h. [8] In addition, the release of its payload was dependent on its environmental pH and redox potential. The abundance of pyridine segments endowed the proton sponge effect of the polymer and helped its escaping from lysosome.

To extend the sensitiveness of the nanogel to temperature, a thermal responsive polymer, poly (N-Isopropyl methacrylamide) (PNiPMA), was incorporated into the PDA-PEG by free radical polymerization to yield a pH, redox potential, and thermal triple-responsive polymer PDA-PEG-PNiPMA as described in **Figure 4.1**. A triple-responsive nanogel (TRN) was fabricated with the help of predesigned amounts of tris(2-carboxyethyl)phosphine (TCEP).

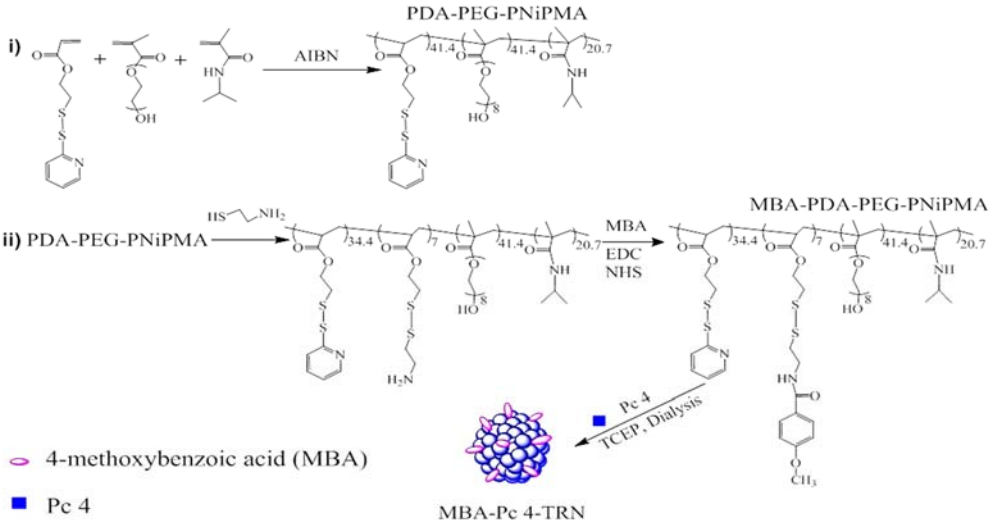

Figure 4.1 Schematic illustration of the synthesis of MBA-PDA-PEG-PNiPMA polymer and the fabrication of MBA-Pc 4-TRN nanogels.

4.2 EXPERIMENTS

4.2.1 Materials and reagents

Aldrithiol-2 and Silica gel (Spherical, 100 μm) were purchased from Tokyo Chemical Industry Co., LTD (Harborgate Street, Portland, OR). 2-mercaptoethenol, DL-dithiothreitol (DTT), tris(2-carboxyethyl)phosphine (TCEP), 2, 2-Azobisisobutyronitrile (AIBN) and Poly(ethylene glycol)methacrylate (Mn = 360 Da) were purchased from Sigma-Aldrich Chemical Co. (St. Louis, MO). Penicillin (10,000 U/mL), streptomycin (10,000 μg/mL), 0.25% trypsin-EDTA, Dulbecco's Modified Eagle Medium (with L-

glutamine) and fetal bovine serum (FBS) were obtained from American Type Culture Collection (ATCC, Manassas, VA)**.** 2,4,6-Trinitrobenzene sulfonic acid (TNBSA) was purchased from Thermo Scientific. Silicon phthalocyanine (Pc 4) was acquired from NCI (NSC 676418). All the other solvents used in this research were purchased from Sigma-Aldrich Chemical Co. (St. Louis, MO) and used without further purification unless otherwise noted.

4.2.2 Synthesis of PDA-PEG-PNiPMA polymer

PDA-PEG-PNiPMA polymer was synthesized by free radical polymerization as shown in **Figure 4.1**. PDA monomer was prepared following our previously reported method [8]. Typically, PDA (241.3 mg, 1 mmol), Poly(ethylene glycol)methacrylate (Mn = 360 Da) (360 mg, 1 mmol) and *N*-isopropylmethacrylamide (NiPMA, 63.6 mg, 0.5 mmol) were dissolved in 10 mL degassed anisole. 2, 2-azobisisobutyronitrile (AIBN, 14 mg, 0.085 mmol) in 1 mL degassed anisole was then added, and the reaction mixture was stirred for 24 hours at 65 °C. The final product was precipitated (3×) in ice cold ether and dried for 48 hours in vacuum. The structure of PDA-PEG-PNiPMA was confirmed by ^{1}H-NMR (**Figure 4.2A**). Gel permeation chromatography (viscotek GPCmax VE 2001 GPC solvent/sample module, Viscotek VE 3580 RI detector and 270 Dual Detector) using THF as mobile phase was empolyed to charactrize the polymer and found PDA-PEG-PNiPMA has an absolute molecular weight of 27,557 Da (Mw) and polydispersity (PDI: 1.35) (**Figure 4.2B**). For the quantification of side chain functionality, PDA-PEG-PNiPMA (1.0 mg/mL) was dissolved in DMSO and incubated with dithiothreitol (DTT, 10 mM) for 1 hour at room temperature, and then the amount of 2-pyridinethione

released was quantified through UV-Vis spectrophotometer at λ = 375 nm (ε, molar absorption coefficient = 8080 $M^{-1}cm^{-1}$).

4.2.3 Synthesis of MBA-PDA-PEG-PNiPMA

PDA-PEG-PNiPMA was further modified with sigma-2 receptor targeting motif (4-Methoxybenzoic acid (MBA)). Briefly, cysteamine (0.404 mg, 20% PDA function groups) in 500 μL DMSO was added dropwise into 20 mg PDA-PEG-PNiPMA in 500 μL DMSO and the reaction mixture was kept at room temperature overnight. After overnight reaction, the product was dialyzed towards DMSO using Spectra/Por® dialysis tube (MWCO: 1000 Da). The concentration of amine group in the polymer after dialysis was quantified by TNBSA assay. MBA (1.66 mg in 100 μL DMSO, 50% PDA function group) was firstly activated by EDC (4.2 mg in 50 μL DMSO) and NHS (2.5 mg in 50 μL DMSO), and then added into 20 mg cysteamine modified PDA-PEG-PNiPMA polymer. The reaction was kept overnight at room temperature. The amine concentration in PDA-PEG-PNiPMA polymer after MBA conjugation was also quantified by TNBSA assay to determine the MBA conjugation efficiency. TNBSA assay result revealed that 16% MBA (to PDA ratio) has been successfully conjugated to the polymer.

4.2.4 TRN nanogel fabrication

Briefly, PDA-PEG-PNiPMA and MBA-PDA-PEG-PNiPMA were mixed to obtain different MBA ligand density for TRN. The polymer mixture (5 mg) was dissolved in 300 μL DMSO. Pc 4 (250 μg) was dissolved in 100 μL DMSO and then added into the polymer mixture. For the fabrication of TRN with 30% cross-linking density, tris (2-carboxyethyl) phosphine hydrochloride (TCEP, 0.384 mg in 20 μL DMSO) was added to the above mixture. The reaction mixture was equilibrated for 15

min and then dropped into 4 mL ddH_2O under stirring and kept stirring for aerial oxidation overnight. After the oxidation, the nanogel was then dialyzed towards PBS of pH 7.4 (10 mM) for 10 h to remove unreacted TCEP, MBA and organic solvent. Finally, the nanogel was filtered (0.45 μm syringe filter) and stored in 4 °C. The morphology, size distribution and the surface charge (ζ-potential), of the nanogel were determined by a Hitachi H8000 transmission electron microscopy (TEM) and dynamic light scattering (DLS) as previously reported. [9]

4.2.5 Pc 4 nanogel drug concentration determination and release kinetic assay

Pc 4 shows maximum absorbance at peak 670 nm. Therefore, Pc 4 concentration in nanogels was measured at 670 nm by UV-Vis spectroscopy. Pc 4 nanogel 2 μL was diluted with 980 μL DMSO (diluted 50×) and measured by UV-Vis. Drug concentration was then calculated by calibration curve. Pc 4-TRN was suspended in PBS of pH 7.4 (10 mM) at the final concentration of 10 μg/mL. To mimic the drug release process of Pc 4-TRN during blood circulation and inside lysosome, Pc 4-TRN was dialyzed towards 40 mL PBS (pH 7.4, 10 mM, 1% Tween 80) and acetate buffer (pH 5.0, 1% Tween 80) at 37 °C, respectively. At pre-determined time intervals, 1 mL dialysis buffer was removed and replaced with 1 mL fresh buffer. The samples were stored at -20 °C till measurement. After collecting all samples, 100 μL each sample was loaded into 96 well plate (Costar, black, clear bottom) and Pc 4 concentration was quantified by fluorescence (Ex 610 nm, Em 680 nm, SpectraMax M2 Multi-Mode Microplate Reader). A calibration curve was constructed by adding known concentrations of Pc 4 to PBS pH 7.4 (10 mM, 1% Tween 80) acetate buffer (pH 5.0, 1% Tween 80). To simulate the process of Pc 4-TRN escaping from lysosome and transfer to cytosol, the pH of releasing buffer was adjusted to 5.0 at

first 2 h. After that, the pH of the releasing buffer was adjusted to 7.2 and kept at this pH for remaining experiment, GSH (final concentration was 10mM) was added into the buffer at the same time. As a control group, no GSH was added into buffer; however, the pH of the buffer was also adjusted to 7.2 and kept at this pH for the remaining experiment. At pre-determined time intervals, samples were retreated and Pc4 concentration was measured by fluorescence as previously described.

4.2.6 Cellular uptake of TRN observed by confocal microscopy

UMSCC22A cells (200,000 cells/dish) were cultured on 35 mm^2 Petri dishes (MatTek, MA, USA) for overnight. The media were replaced with fresh media containing 16% MBA-Pc 4-TRN, Pc 4-TRN, and free Pc 4 (equivalent to 200 nM Pc 4). After 4 or 20 h of incubation under a humidified atmosphere of 95/5% air/CO_2, cells were washed by PBS(3×), fixed with formaldehyde (4.5% in PBS) and stained with Hoechst 33342 (final concentration 1μg/mL). Then cells were analyzed under a confocal microscope (LSM 510, Carl-Zeiss Inc.).

4.2.7 Quantification of intracellular Pc 4 amount

UMSCC22A cells (100,000 cells/well) were cultured on 24-well plate for overnight. Culture media were replaced with fresh media containing free Pc4 drug, MBA (16, 8, 4, 1, and 0%) Pc 4-TRN nanogels (equivalent to 200 nM Pc 4). After incubation under a humidified atmosphere of 95/5% air/CO_2 for 4 and 20 h, respectively, cells were washed by PBS(3×) and lysed in 0.5% SDS. Cell lysates were collected and Pc 4 concentration was quantified by fluorescence (Ex 610 nm, Em 680 nm). Total protein concentrations of cell lysates were measured by BCA kit following manufacturer's

instruction (Thermo Fisher Scientific). The ratio between Pc 4 and protein was used to evaluate the ability of UMSCC22A cells take up Pc 4 and Pc 4-TRN of different MBA density.

4.2.8 Immunohistochemistry analysis

Human tissues were collected under IRB protocol approved by the Institutional Review Board of the Medical University of South Carolina. FFPE sections of human head and neck tumor tissue microarray were de-paraffinized in xylene, rehydrated in alcohol, and processed as follows: The sections were incubated with target retrieval solution (Dako S2368) in a steamer (Oster CKSTSTMD5-W) for 45 min, 3% hydrogen peroxide solution for 10 min and protein block (Dako X0909) for 20 min at room temperature. After overnight incubation with sigma-2 antibody (Sigma HPA002877) in a humid chamber at 4 °C, biotinylated anti-rabbit secondary antibody (Vector, PK-6101) and ABC reagent (Vector, PK-6101) was added for 30 min. Immunocomplexes of horseradish peroxidase were visualized by DAB (Dako, K3468) reaction, and sections were counterstained with hematoxylin before mounting.

4.2.9 Western Blot Analysis

UMSCC22A cell extracts were prepared in ice-cold RIPA lysis buffer (150 mM NaCl, 1 mM EGTA, 1% sodium deoxycholate, 1% Triton X-100, 0.1% SDS, 1% NP40, 50 mM Tris-Cl, pH 7.4) supplemented with a cocktail of protease inhibitors (Roche Diagnostics) and centrifuged. Proteins (75 μg) in sample buffer (Invitrogen) supplemented with 10% SDS and 10% β-mercaptoethanol were resolved on NuPAGE® Tris-bis 4%-12% polyacrylamide gels (Invitrogen). Proteins were transferred to PVDF membranes (EMD Millipore) and probed with anti-sigma-2 (PGRMC1) (1:1000) (Cell

Signaling). Membranes were developed by the Enhanced Chemiluminescence Detection System (Thermo Fisher Scientific), and band intensities were quantified using a Caresteam 4000 PRO image station (Woodbridge, CT).

4.2.10 Sub-cellular co-localization of TRN

UMSCC22A cells (150,000 cells/dish) were cultured onto glass-bottomed MatTek dishes and incubated with MBA-Pc 4-TRNs at indicated times. Before imaging, medium was changed to fresh medium supplemented with Insulin-Transferrin-Selenium-X (ITX) reagent [insulin (10 µg/ml), transferrin (5.5 µg/ml), selenium (6.7 ng/ml), ethanolamine (0.2 mg/ml)] (Gibco) but omitting FBS. To assess co-localization of nanoparticles with mitochondria, cells were loaded with 500 nM tetramethylrhodamine methylester (TMRM). Medium was then changed with fresh medium containing 50 nM TMRM. To assess co-localization of MBA-Pc 4-TRNs with lysosomes, cells were loaded with 500 nM LysoTracker Green (LTG). Dishes were placed in an environmental chamber at 37 ºC on the stage of a Zeiss LSM 510 laser scanning confocal microscope (Zeiss, Thornwood, NY). A 63 X N.A. 1.4 oil immersion planapochromat objective was used for all experiments. LTG, TMRM and Pc 4 fluorescence was imaged using 488 nm excitation/500–530-nm emission, 543 nm excitation/565-615 nm emission and 633 nm excitation/650-710 nm emission, respectively. ImageJ software was used to post-process the images and calculate the co-localization coefficients.

4.2.11 Photodynamic therapy

Cell cultures were incubated with 200 nM of MBA-Pc 4-TRN and Pc 4-TRN for 20 h before exposure to 200 mJ/cm^2 red light (670 nm) from an Intense-HPD 7404 diode

laser (North Brunswick, NJ). After exposure to red light, cells were incubated for various periods of time prior to analysis.

4.2.12 Assessment of Cell Death after PDT

Cell death was assessed by propidium iodide (PI) fluorometry using a multi-well fluorescence plate reader, as previously described [10]. Human head and neck cancer cells (UMSCC22A) were plated on 96-well plates (15,000 cells/well) in Dulbecco's Modified Eagle's Medium (DMEM) (Gibco) supplemented with 10% fetal bovine serum (FBS) and penicillin/streptomycin (complete culture medium) in a humidified 37 ºC incubator at 5% CO2/95% air. Subsequently, cells were incubated with MBA-Pc 4-TRN and Pc 4-TRN (200 nM) for 20 h. Before exposure to light, cells were changed to fresh medium supplemented with PI (30 μM) and Insulin-Transferrin-Selenium-X (ITX) reagent [insulin (10 μg/ml), transferrin (5.5 μg/ml), selenium (6.7 ng/ml), ethanolamine (0.2 mg/ml)] (Gibco) but omitting FBS. PI fluorescence was measured at frequent intervals using 530 nm excitation (25 nm band pass) and 620 nm emission (40 nm band pass) filters. Between measurements, microtiter plates were placed in a 37 ºC incubator. At the end of the experiment, digitonin (200 μM) was added to each well to permeabilize all cells and label all nuclei with PI. Cell viability determined by PI fluorometry is essentially the same as cell viability determined by trypan blue exclusion. [10]

4.2.13 Biodistribution of MBA-Pc 4-TRN

All animal experiments followed the protocols approved by the MUSC Institutional Animal Care and Use Committee (IACUC). Head and neck tumor xenografts were created with UMSCC22A cells (3 x 10^6 cells/mouse) in male athymic *Nu/J* mice (6 weeks old, inbred homozygous) (Jackson Labs). Once tumor volumes reached 50-150

mm^3 measured with a caliper, mice were administered with MBA-Pc 4-TRN and free Pc 4 (1 mg/kg Pc 4) in PBS through the tail vein. Fluorescence images were taken with a Maestro 2 *in vivo* imaging system 72 h after dosing. Subsequently, mice were sacrificed at 96 h post-injection. Liver, spleen, heart, kidneys, lungs, and the tumor were collected and imaged.

Cell death was assessed by propidium iodide (PI) fluorometry using a multi-well fluorescence plate reader, as previously described [10]. Human head and neck cancer cells (UMSCC22A) were plated on 96-well plates (15,000 cells/well) in Dulbecco's Modified Eagle's Medium (DMEM) (Gibco) supplemented with 10% fetal bovine serum (FBS) and penicillin/streptomycin (complete culture medium) in a humidified 37 ºC incubator at 5% CO2/95% air. Subsequently, cells were incubated with MBA-Pc 4-TRN and Pc 4-TRN (200 nM) for 20 h. Before exposure to light, cells were changed to fresh medium supplemented with PI (30 μM) and Insulin-Transferrin-Selenium-X (ITX) reagent [insulin (10 μg/ml), transferrin (5.5 μg/ml), selenium (6.7 ng/ml), ethanolamine (0.2 mg/ml)] (Gibco) but omitting FBS. PI fluorescence was measured at frequent intervals using 530 nm excitation (25 nm band pass) and 620 nm emission (40 nm band pass) filters. Between measurements, microtiter plates were placed in a 37 ºC incubator. At the end of the experiment, digitonin (200 μM) was added to each well to permeabilize all cells and label all nuclei with PI. Cell viability determined by PI fluorometry is essentially the same as cell viability determined by trypan blue exclusion. [10]

4.3 RESULTS AND DISCUSSION

PNiPMA is a polymer which undergoes phase transition when the environmental temperature passing through its Low Critical Solution Temperature (LCST, around 43

°C), soluble in water at temperature lower than LCST while becoming hydrophobic at temperature higher than its LCST. [11] Nano/micro-particles containing PNiPMA shrink when the environment temperature is higher than its LCST. [12] To investigate the effect of crosslinking density (CD) of TRN on its transition temperature, the transmittance of TRN was recorded during the course of temperature increase. Transmittance measurement revealed that the addition of PNiPMA did endow the temperature sensitivity to the nanogel: TRN nanogel suspension decreased its transmittance and appeared cloudy at high temperature (**Figure 4.2C**). The transition temperature of TRN shifted from 30.5 °C to 47 °C as its CD increased from 20 to 40%, while no transition was recorded for TRN with 80% CD or higher. Therefore, TRNs with different transition temperatures can be attained by simply tuning CD during nanoparticle fabrication process.

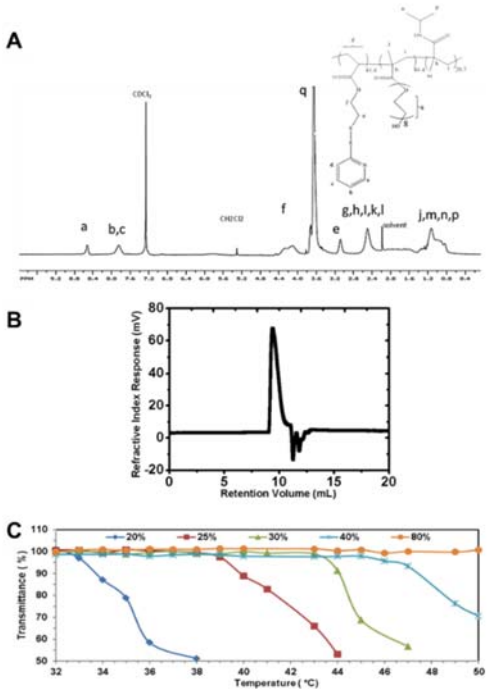

Figure 4.2 (A) ^{1}H NMR and (B) GPC spectra of PDA-PEG-PNiPMA polymer. (C) The relationship between TRN crosslinking density and its transition temperature. The transition temperatures were determined by measuring the change of transmittance for TRN PBS suspension at the nanogel concentration of 0.16 mg/ml during the increase of temperature

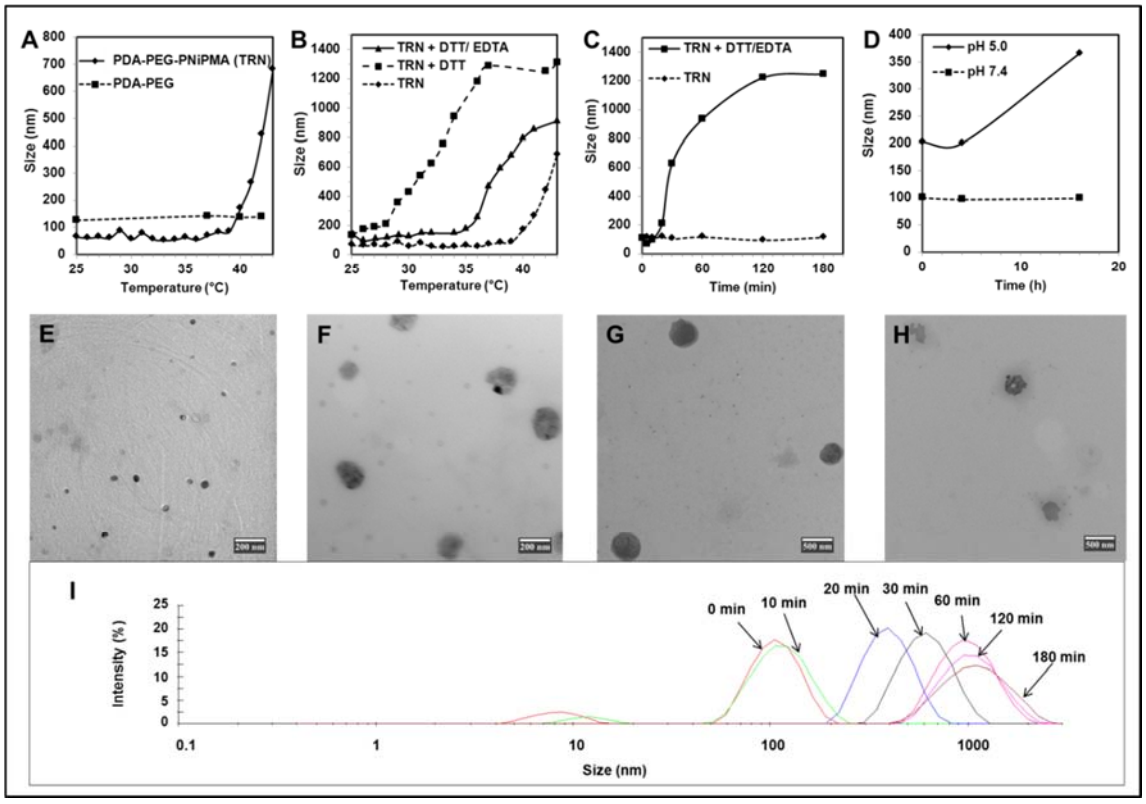

Figure 4.3 The z-average size of TRN in response to the change of temperature (A, B), the addition of 10 mM DTT (C), and the change of pH from 7.4 to 5.0 (D) acquired by DLS. All the size measurements were carried out at 37 °C unless otherwise specified. TEM images of control TRN at room temperature (E), heated at 42 °C (F), treated with 10 mM DTT for 2 h at 37 °C (G), and incubated in pH 5.0 buffer (H). Images were taken with a Hitachi H8000 TEM. Scale bars are 200 nm in (E) and (F), and 500 nm in (G) and (H). The size distribution of TRN in response to the addition of 10 mM DTT over time (I).

Using the fabrication protocol described above, Pc 4 loaded TRN with a transition temperature slightly higher than body temperature can be easily produced from PDA-PEG-PNiPMA with 30% CD. Compared with its counterpart fabricated from PDA-PEG polymer, the loading efficiency of Pc 4 increased from 13 to 40% for TRN, which may be due to the newly formed PNiPMA layer served as a buffer zone between the hydrophobic PDA and the hydrophilic PEG. To investigate how the TRN responses to the changes in temperature, redox potential, and pH after the loading of Pc 4, the sizes and morphologies

of the TRN were measured with dynamic light scattering (DLS) and observed with transmittance electron microscopy (TEM), respectively [9]. The size of the TRN was 108.1 ± 11.1 nm with a PDI of 0.163 (**Figure 4.3A**). Zeta sizer found that TRN carried slightly negative surface charge (-5.62 ± 1.40 mV). TEM revealed that TRNs were spherical (**Figure 4.3E**). TRN itself was stable in PBS and culture medium containing 10% FBS (**Figure 4.4**), and no obvious size change was observed after 3 days of incubation. In contrast to its PDA-PEG di-copolymer nanogel counterpart, which kept constant size in the whole tested temperature range, TRN with 30% CD dramatically increased its size at temperature higher than 39 °C (**Figure 4.3A**). It is worth noting that the size enlargement in response to the temperature increase is totally different from other PNiPMA containing particles, which shrink upon environment temperature higher than their LCSTs [12]. **Figure 4.3A** also showed that the addition of Pc 4 slightly decreased the transition temperature of TRN from 44 °C to 39 °C. The enlarged size of TRN shown in **Figure 4.3F** also evidenced the thermal expanding property of TRN.

To examine the redox potential effect on the transition temperature of TRN, 10 mM DTT was added during the heating process. To eliminate the possible effect caused by the intra-particle crosslinking of TRN after DTT treatment shown in **Figure 4.3B**, EDTA was added. **Figure 4.3B** revealed that the addition of 10 mM DTT/EDTA further decreased the transition temperature of TRN from 39 °C to 36 °C. It is known that cytosol has an elevated glutathione level (10 mM, much higher than that in the blood), which would result in the rapid intracellularly self-expanding of TRN at body temperature. [13]

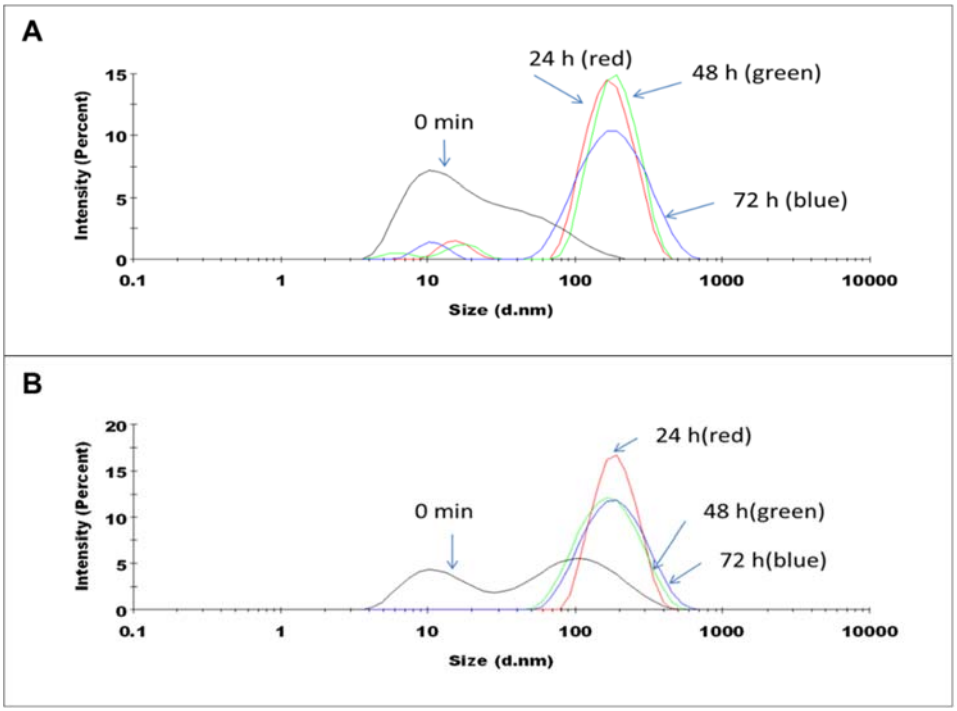

Figure 4.4 Stability of TRN at 37 °C over 3 days monitored by dynamic light scattering. (A) Size shifting of DMEM culture medium supplemented with 10% FBS; (B) Size shifting of TRN in DMEM culture medium supplemented with 10% FBS. There was no size difference between the culture medium with and without TRN addition, suggesting that TRNs are stable in the culture medium.

To further evaluate the sensitivity of TRN in response to reducing environment at body temperature, the size of TRNs suspended in media with or without 10 mM DTT/EDTA was monitored at 37 °C. As we expected, the size of TRN remained constant in PBS buffer (**Figure 4.3C**). To our surprise, under reducing environment, TRN swelled from 108 nm to 627 nm in 30 min and further expanded to larger than 1200 nm in less than 2 h (**Figure 4.3C, G,** and **I**), achieving more than 1000-fold size enlargement (in volume), which is more than 10-fold faster than its di-copolymer counterpart [8]. Besides its self-expansion in response to the increase of temperature and redox potential, DLS and TEM also revealed that the size of TRN was also sensitive to the change of pH. TRN

instantly expanded its size from 108 nm to 203 nm upon the decrease of pH from 7.4 to 5.0, and then further increased to 360 nm in 16 h (**Figure 4.3D** and **4.3H**).

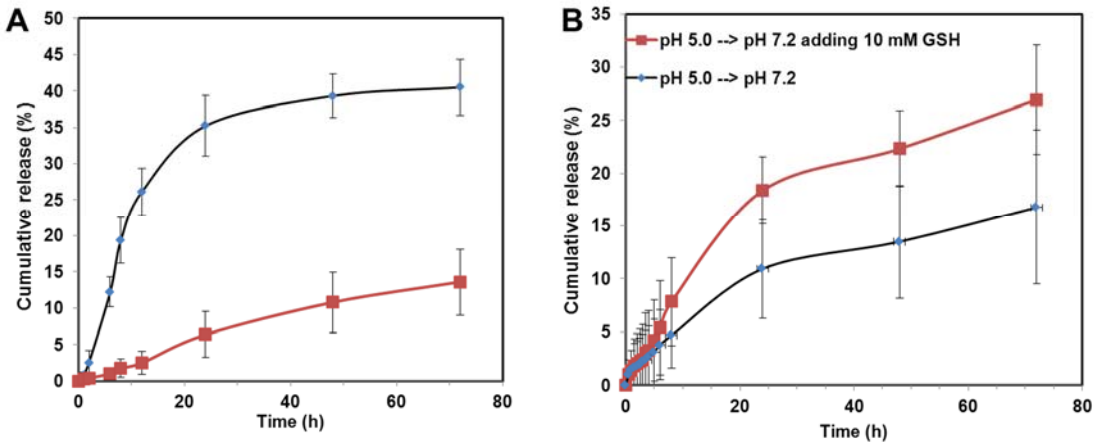

Figure 4.5 The Pc 4 release kinetics of TRN at different conditions. (A) Pc 4-TRNs were dialyzed against pH 5.0 and 7.4 buffer at 37 °C; (B) Pc 4-TRNs were first dialyzed against pH 5.0 buffer for 2 h and then against pH 7.2 buffer for 70 h with or without the addition of 10 mM GSH. Data represent mean ± SD, n=3.

To verify that the stimuli triggered size enlargement of TRN will result in faster release of Pc 4, drug release assay was carried out in pH 7.4 and 5.0 buffers to mimic the extracellular and lysosomal environments, respectively. **Figure 4.5A** showed that TRN released only 13.6% of Pc 4 in pH 7.4 buffer over 3 days of incubation, indicating that TRN is a stable carrier during the circulation. As we expected the release of Pc 4 became much faster in the pH 5.0 environment (30.7% Pc 4 released in 24 h). To investigate the effect of redox potential sensitiveness of TRN on its payload release, TRN was first incubated in pH 5.0 medium for 2 h and then transferred to pH 7.2 medium supplemented with 10 mM GSH to mimic the process of TRN escaping from lysosome to cytosol. **Figure 4.5B** revealed that the addition of GSH significantly accelerated the drug releasing process.

Head and neck squamous cell carcinoma (HNSCC) was selected to explore the PDT efficacy of TRN because most HNSCC cases are localized. [14] In addition, the treatment for HNSCC should not compromise the function and cosmetic appearance of corresponding tissues. All these make PDT, which causing minimal scar and loss of function of treated sites, a better alternative for surgery to treat HNSCC. Sigma-2 receptor is overexpressed in many cancers, including skin cancer, lung cancer, and breast cancer, and has been extensively explored as a target for tumor specific drug delivery. [15,16] However, thus far, no research investigated the expression of sigma-2 receptor in head and neck cancer. The expression of sigma-2 receptor in HNSCC was evaluated with immunohistochemistry in a human tissue array. High density of brown staining in the tumor tissue (**Figure 4.6A**) and little staining in the normal tissue (**Figure 4.6B**) indicated that sigma-2 receptor does overexpress in human head and neck tumor tissue, which makes it a valid target for tumor specific drug delivery. The quantitative analysis of the DAB-stained tissues revealed that human HNSCC expressed > 3-fold of sigma-2 receptor than normal tissues (**Figure 4.6C)**. After that, we further confirmed that sigma-2 receptor is expressed in UMSCC22A head and neck cancer cells by Western immunoblotting (**Figure 4.6D**). Thus, UMSCC22A cell line was selected to validate our hypothesis *in vitro*.

To endow head and neck tumor targeting effect for TRN, a sigma-2 receptor targeting ligand, 4-methoxybenzoic acid (MBA), [16] was grafted onto PDA-PEG-PNiPMA with the help of 1-Ethyl-3-[3-dimethylaminopropyl] carbodiimide (EDC) and N-hydroxysuccinimide (NHS) (**Figure 4.2A**). MBA-Pc 4-TRNs with different MBA densities were fabricated by adjusting the molar ratio of MBA-PDA-PEG-PNiPMA to

PDA-PEG-PNiPMA. To investigate the targeting effect of MBA on the cellular uptake of Pc 4 loaded TRN, confocal microscopy was employed. Red fluorescence signal (Pc 4) was observed among all treatments (**Figure 4.6E**). Compared with free Pc 4, non-targeted TRN showed similar capacity in carrying Pc 4 into UMSCC22A cells during 20 h of incubation. As we expected, the functionalization of TRN with MBA significantly enhanced its cellular uptake. To further quantify the intracellular Pc 4 amount after 20 h of incubation, the cells were harvested and lysed to measure the intracellular Pc 4 amount. MBA-TRN with 16% ligand density achieved about 1.8-fold of Pc 4 uptake compared with that of non-targeted TRN (**Figure 4.6F**). The higher the MBA density, the better its cellular uptake, which suggest that the modification of MBA did facilitate the sigma-2 receptor mediated endocytosis for Pc 4 loaded TRN.

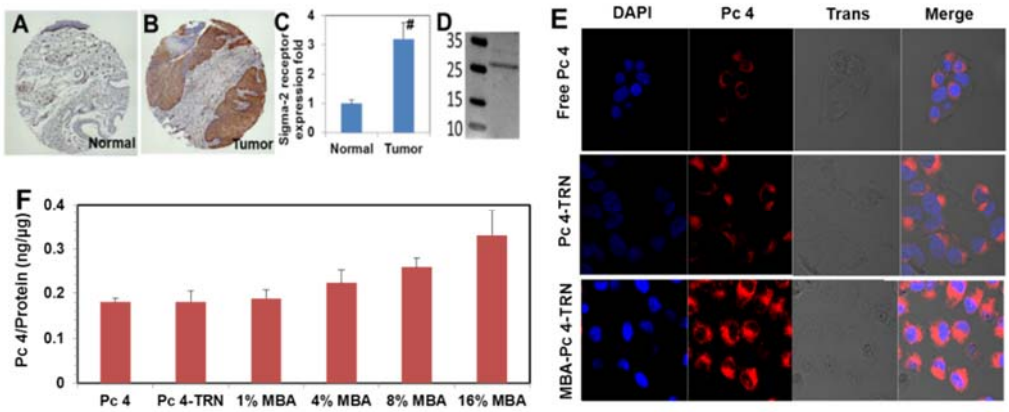

Figure 4.6 The expression of sigma-2 receptor in head and neck cancer and its effect on the cellular uptake of MBA-Pc 4-TRN. The expression of sigma-2 receptor in normal tissue (A) and human head and neck cancer tissue (B). Representative images shown. Sigma-2 receptor positive tissue areas were detected with immunohistochemistry and quantified as percent of total tissue and expressed as fold of normal tissue (mean ± SE, n >30, # $p < 0.001$) (C); The expression of sigma-2 receptor in UMSCC22A cell line detected by Western immunoblotting (D); Confocal images of UMSC22A cells treated with Pc 4 or Pc 4 loaded TRN (E). Cells were cultured with Pc 4 or Pc 4 loaded TRN (red) for 20 h. Cell nuclei were stained with DAPI (blue). Images from left to right were taken from DAPI, Pc 4, transmittance, and the overlay of the previous three channels; (F) Intracellular amount of Pc 4 for cells treated with Pc 4-TRNs containing different MBA densities (mean ± SD, n = 3).

Since TRN was taken up by cells *via* endocytosis, we assessed the sub-cellular localization of MBA-Pc 4-TRN in UMSCC22A cells after it entered cells by confocal microscopy. Cells were incubated with 200 nM Pc 4-TRN (blue) for 2, 3, and 20 h and subsequently co-loaded with LysoTracker Green (LTG, green) and tetramethylrhodamine methylester (TMRM, red) to label endosomes/lysosomes and mitochondria, respectively. After 2 h, the presence of small round green/light cyan spheres representing lysosomes indicate that Pc 4-TRN began to enter the lysosomes but very few co-localization of Pc 4-TRN with mitochondria (red) was observed (**Figure 4.7A**). After 3 h, much more cyan spheres appeared, suggesting more TRN entered lysosomes; furthermore, the color of mitochondria turned from red to magenta, indicating strong co-localization between mitochondria and Pc 4 (**Figure 4.7B**). After 21 h, blue fluorescence became diffused, showing the expanding of TRN resulted in the release of Pc 4 (**Figure 4.7C**). Moreover, mitochondria exhibited stronger magenta fluorescence, indicating more Pc 4 transferred to mitochondria. It is also worth mentioning that we also observed some enlarged lysosome (cyan dots in **Figure 4.7B** and **4.7C**), suggesting the expanding of TRN inside the lysosome during its intracellular traffic. To further quantitatively monitor the intracellular trafficking of TRN, images ($n > 15$) taken at different time points were analyzed by ImageJ to calculate the Pearson's co-localization coefficient for lysosome and Pc 4 (Pc 4/L), as well as Pc 4 and mitochondria (Pc 4/M). **Figure 4.7D** shows that more TRNs entered lysosomes after 2 h of incubation than that of 1 h ($p< 0.05$). The stronger co-localization of Pc 4 and mitochondria occurred after 3 h of incubation ($p< 0.01$). Since more TRN entered cancer cells (**Figure 4.8**) after 20 h of incubation, the co-

localization of Pc 4/L further increased; as a consequence, more Pc 4 partitioned to mitochondria after it was freed from TRN.

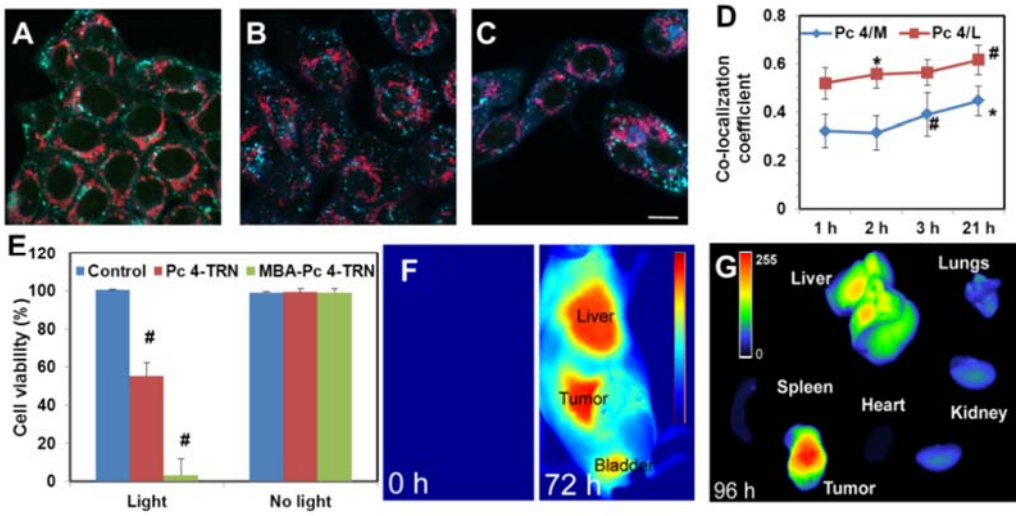

Figure 4.7 Subcellular co-localization of Pc 4 loaded TRN (red) with lysosome and mitochondria recorded at 2 h (A), 3 h (B), and 21 h (C) by confocal microscopy. LysoTracker Green (LTG, green) and tetramethylrhodamine methylester (TMRM, red) were used to label endosomes/lysosomes and mitochondria, respectively. Scale bar in (C) is 10 μm; (D) The trend for the Pc 4 co-localizing with lysosome (Pc4/L) and mitochondria (Pc 4/M) (mean ± SD, n> 15; * p< 0.05; # p< 0.01); (E) The PDT efficacy in killing UMSCC22A cells 12 h after irradiation (mean ± SD, n=3; # p< 0.01); (F, G) Biodistribution of MBA-Pc 4-TRN *in vivo*. Xenografts were created with UMSCC22A cells in nude mice. MBA-Pc 4-TRN was administered *via* tail vein. Mice were imaged before (F, left) and 72 h after drug administration (F, right). At 96 h, organs and tumor were dissected from the mouse treated with MBA-Pc 4-TRN and imaged *ex vivo* (G). Representative images shown.

To validate whether the enhanced uptake of Pc 4 and effective mitochondria targeting could be translated into better PDT efficacy in cell killing, cell viability after PDT was assessed by propidium iodide (PI) fluorometry. [10] UMSCC22A cells were incubated with non-targeted and targeted Pc 4-TRN for 20 h prior to receiving PDT. Cells treated with the same dose of nanoparticle receiving no light were employed as control. **Figure 4.7E** showed that PDT of MBA-Pc 4-TRN killed almost all cancer cells12 h post irradiation, while only 44.5% cells were killed in the non-targeted TRN

treated group. Combining cellular uptake data from **Figure 4.6E** and **4.6F**, we concluded that better cellular uptake of Pc 4 did translate into better PDT cell killing efficacy. Furthermore, no cytotoxicity appeared in either TRN groups without applying light irradiation, indicating MBA-Pc 4-TRN and nano-carrier itself were safe.

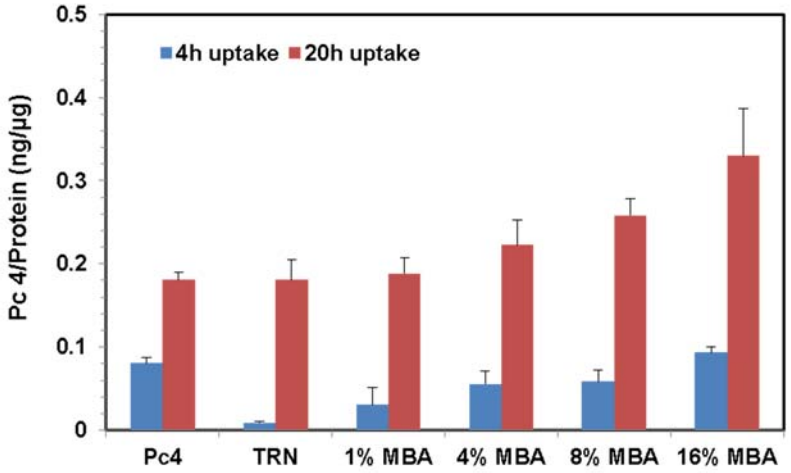

Figure 4.8 Cellular uptake of Pc 4 after 4 and 20 h of culture. Data represent mean ± SD, n=3.

To evaluate the tumor specific targeting effect of MBA-Pc 4-TRN, head and neck cancer xenograft mice model was employed. Mice were administered with MBA-Pc 4-TRN through the tail vein injection. Fluorescence images were taken with an *in vivo* fluorescence imaging system. At 72 h post-injection, MBA-Pc 4-TRN signal mainly appeared in the regions of tumor and liver, some in the bladder but very little in other tissues (**Figure 4.7F**). The *ex vivo* images obtained from dissected organs at 96 h post Pc 4 injection revealed that the majority of MBA-Pc 4-TRN was still retained in the tumor, while liver showed much less fluorescence signal compared to that of 72 h time point (**Figure 4.7G**). As expected, spleen, heart, lungs and kidney retained very little Pc 4, which is significantly different from other Pc 4 loaded carrier systems. [17,18]

PDT causing minimal scar and loss of function of treated sites, has been proposed as an alternative for surgery to treat HNSCC. However, the clinical application of PDT has been hindered due to the poor water solubility and non-specific skin retention of PS, as well as low PDT efficacy. To address that, we designed a thermal, pH, and redox potential triple-responsive expansile nanogel system (TRN), which swells at a temperature higher than its transition temperature, acidic pH, and reducing environment. *In vivo* biodistribution experiment revealed that TRN could specifically target tumor tissue with the synergetic outcome of EPR effect and sigma-2 receptor targeting effect (**Figure 4.7G**). The immunohistochemistry analysis of HNSCC human tissue array found that human HNSCC expressed > 3-fold of sigma-2 receptor than normal tissues (**Figure 4.6C)**. In addition, Western immunoblotting confirmed that sigma-2 receptor is expressed in UMSCC22A head and neck cancer cells (**Figure 4.6D**), which makes UMSCC22A cell line a valid model for the study of sigma-2 receptor targeted therapy. Based on the experimental observations, we proposed the following pathway for MBA-Pc 4-TRN: (i) MBA-Pc 4-TRN entered head and neck cancer cells by sigma-2 receptor mediated endocytosis with the help of sigma-2 receptor ligand, MBA (**Figure 4.6E** and **F)**; (ii) After that, MBA-Pc 4-TRN was transferred to endosome and then lysosome, where it has low pH. Partial of Pc 4 could be released from TRN due to the acidic pH (**Figure 4.5A**); (iii) Due the proton sponge effect of pyridine segments in PDA and the expansile property of TRN at low pH (**Figure 4.3D** and **H**), TRN and freed Pc 4 could escape from lysosome and enter cytosol; (iv) Since cytosol has an elevated GSH concentration, which can trigger the dramatic size expansion of TRN (**Figure 4.3C, G, I,** and **4.7B, C**) and induce the release of Pc 4 (**Figure 4.5B**); (v) Due to its hydrophobicity, Pc 4

spontaneously transferred to mitochondria (**Figure 4.7C** and **D**). Therefore, MBA-Pc 4-TRN exhibited enhanced cell killing effect after PDT (**Figure 4.7E**).

Due to the advantages of PDT mentioned above, several of PS nano-carrier systems have been developed for HNSCC treatment [27-32].[17-21] Among them, only a few were evaluated *in vivo*. Wang et al. showed that an integrin β1 binding fibronectin-mimetic peptide increased the accumulation of Pc 4 loaded iron oxide nanoparticle in HNSCC tumor[19]. However, this strategy also caused significantly higher Pc 4 retention in lung, liver, kidney, and skin tissues. In order to shorten the waiting time between drug administration and PDT treatment, Cheng et al. attached Pc 4 to gold nanoparticles through N-Au bonds.[18] Although the waiting period was reduced from 2 days to 2 h, this gold-Pc 4 system still couldn't solve the high lung and kidney retention associated with Pc 4. Since EGFR is overexpressed in most HNSCC, Master et al. functionalized PCL-PEG micelles with a EGFR targeting peptide, GE11. With the help of GE11, the targeted micelles exhibited higher cellular uptake and cell killing effect than the non-targeted ones.[20] Though, the high skin Pc 4 retention issue remaining unaddressed. To tackle the non-specific retention of Pc 4, we integrated a triple-responsive nanogel system with a sigma-2 receptor targeting ligand, MBA. MBA functionalized Pc 4-TRN showed much better cellular uptake than Pc 4-TRN and killed more head and neck cancer cells after PDT. Because the existence of a dense PEG layer on the surface of TRN, which prevents non-specific bindings, only negligible amount of Pc 4 retained in lung, kidney, and other tissues. Therefore, MBA-Pc 4-TRN achieved HNSCC tumor specific targeting effect.

4.4 CONCLUSIONS

In summary, a thermal, pH, and redox potential triple-responsive expansile nanogel system (TRN) has been developed. The transition temperature of TRN could be tuned from 30.5 °C to 47 °C by adjusting its crosslinking density. Due to the synergistic effect of its redox potential and thermal responsiveness, TRN could expand from 108 nm to over 1200 nm within 2 h in a reducing environment at body temperature, achieving more than 1000-fold size enlargement (in volume). Pc 4 loaded TRNs are stable (both size and retaining loaded drug) in a physiological condition, while quickly releasing Pc 4 at lysosomal pH and reducing cytosol environment attributed to its rapid swelling response upon the trigger of acidic pH, high temperature, and elevated GSH. MBA functionalized Pc 4-TRN could effectively enter UMSC22A cancer cells with the help of sigma-2 receptor and transfer Pc 4 to its target, mitochondria. Consequently, PDT of MBA-Pc 4-TRN showed significant higher toxicity than its non-targeted counterpart and killed almost all cancer cells. Furthermore, *in vivo* biodistribution study proved that MBA-Pc 4-TRN could effectively target head and neck tumor tissue and be retained there for 4 days. Based on the unique responsiveness and promising *in vitro* and *in vivo* results from TRN, further studies will focus on the mechanisms for TRN escaping from lysosome and employing the system for *in vivo* tumor growth inhibition effect for head and neck cancer.

4.5 REFERENCES

(1) N. L. Oleinick,R. L. Morris and T. Belichenko, *Photochem. Photobiol. Sci.,* 2002, **1**, 1-21.

(2) M. Lam,N. L. Oleinick and A. L. Nieminen, *J. Biol. Chem.,* 2001, **276**, 47379-47386.

(3) A. M. Master,M. E. Rodriguez,M. E. Kenney,N. L. Oleinick and A. S. Gupta, *J. Pharm. Sci.,* 2010, **99**, 2386-2398.

(4) Z. Jiang,T. Yang,M. Liu,Y. Hu and J. Wang, *Biosens. Bioelectron.,* 2014, **53**, 340-345; A. M. Master,M. Livingston,N. L. Oleinick and A. Sen Gupta, *Mol Pharm,* 2012;Y. Cheng,J. D. Meyers,A.-M. Broome,M. E. Kenney,J. P. Basilion and C. Burda, *J. Am. Chem. Soc.,* 2011, **133**, 2583-2591.

(5) A. M. Master,Y. Qi,N. L. Oleinick and A. S. Gupta, *Nanomedicine,* 2012, **8**, 655-664.

(6) A. P. Griset,J. Walpole,R. Liu,A. Gaffey,Y. L. Colson and M. W. Grinstaff, *J. Am. Chem. Soc.,* 2009, **131**, 2469-2471; R. Liu,D. M. Gilmore,K. A. Zubris,X. Xu,P. J. Catalano,R. F. Padera,M. W. Grinstaff and Y. L. Colson, *Biomaterials,* 2013, **34**, 1810-1819; R. Liu,O. V. Khullar,A. P. Griset,J. E. Wade,K. A. Zubris,M. W. Grinstaff and Y. L. Colson, *Ann. Thorac. Surg.,* 2011, **91**, 1077-1083; discussion 1083-1074; K. A. Zubris,R. Liu,A. Colby,M. D. Schulz,Y. L. Colson and M. W. Grinstaff, *Biomacromolecules,* 2013, **14**, 2074-2082.

(7) J.-H. Ryu,S. Jiwpanich,R. Chacko,S. Bickerton and S. Thayumanavan, *J. Am. Chem. Soc.,* 2010, **132**, 8246-8247;D. C. Gonzalez-Toro,J. H. Ryu,R. T. Chacko,J. Zhuang and S. Thayumanavan, *J. Am. Chem. Soc.,* 2012, **134**, 6964-6967.

(8) R. Bahadur K. C and P. Xu, *Adv. Mater.,* 2012, **24**, 6479-6483.

(9) P. Xu,E. Gullotti,L. Tong,C. B. Highley,D. R. Errabelli,T. Hasan,J. X. Cheng,D. S. Kohane and Y. Yeo, *Mol Pharm,* 2009, **6**, 190-201.

(10) A. L. Nieminen,G. J. Gores,J. M. Bond,R. Imberti,B. Herman and J. J. Lemasters, *Toxicol. Appl. Pharm.,* 1992, **115**, 147-155.

(11) K. von Nessen,M. Karg and T. Hellweg, *Polymer,* 2013, **54**, 5499-5510.

(12) M. M. Rahman,M. M. Chehimi,H. Fessi and A. Elaissari, *J. Colloid Interf. Sci,* 2011, **360**, 556-564; Y. Matsumura and K. Iwai, *Polymer,* 2005, **46**, 10027-10034.

(13) F. Q. Schafer and G. R. Buettner, *Free. Radical. Bio. Med,* 2001, **30**, 1191-1212.

(14) M. Biel In *Photodynamic Therapy*; Gomer, C. J., Ed.; Humana Press: 2010; Vol. 635, p 281-293.

(15) H. Kashiwagi,J. McDunn,P. Simon,P. Goedegebuure,J. Xu,L. Jones,K. Chang,F. Johnston,K. Trinkaus,R. Hotchkiss,R. Mach and W. Hawkins, *Mol. Cancer,* 2007, **6**, 48; R. Mach,C. Smith,I. al-Nabulsi,B. Whirrett,S. Childers and K. Wheeler, *Cancer Res.,* 1997, **57**, 156-161;Y. Yang,Y. X. Hu,Y. H. Wang,J. Li,F. Liu and L. Huang, *Mol. Pharmaceutics,* 2012, **9**, 2280-2289; Y. Yang,J. Li,F. Liu and L. Huang, *Mol. Ther.,* 2012, **20**, 609-615.

(16) S. Chono,S. D. Li,C. C. Conwell and L. Huang, *J. Controlled Release,* 2008, **131**, 64-69.

(17) L. V. Halig,D. Wang,A. Y. Wang,Z. G. Chen and B. Fei, *Proc SPIE,* 2013, **8672**.

(18) Y. Cheng,C. S. A,J. D. Meyers,I. Panagopoulos,B. Fei and C. Burda, *J. Am. Chem. Soc.,* 2008, **130**, 10643-10647.

(19) D. Wang,B. Fei,L. V. Halig,X. Qin,Z. Hu,H. Xu,Y. A. Wang,Z. Chen,S. Kim and D. M. Shin, *ACS nano,* 2014, **8**, 6620-6632.

(20) A. Master,A. Malamas,R. Solanki,D. M. Clausen,J. L. Eiseman and A. Sen Gupta, *Mol. pharmaceutics,* 2013, **10**, 1988-1997.

(21) H. Ding,R. Mora,J. Gao and B. D. Sumer, *Otolaryngol Head Neck Surg.,* 2011, **145**, 612-617; E. M. Cohen,H. Ding,C. W. Kessinger,C. Khemtong,J. Gao and B. D. Sumer, *Otolaryngol Head Neck Surg.,* 2010, **143**, 109-115.

CHAPTER 5

MUSSEL INSPIRED PLGA/POLYDOPAMINE CORE-SHELL NANOPARTICLE FOR LIGHT INDUCED CANCER THERMOCHEMOTHERAPY

5.1 INTRODUCTION

Photothermal therapy (PTT) has been extensively explored for cancer treatment by coupling localized near-infrared (NIR) irradiation and locally accumulated photothermal converting agents (PTCAa).[1] By far, most developed PTCAs are made of metal based nanostructures, such as gold nanorod, gold nanocage, CuSx nanocrystal.[2,3] By manipulating their shape, size, and geometry, the localized surface plasmon resonance peak of these nanostructures can be tuned to a tissue transparent window (650-900 nm), where light can penetrate deeply.[4] Because of that, upon NIR irradiation, PTCAs generate heat and can be applied for photothermal therapy.[3,5] Due to the slow or non-degradable nature of these PTCAs, they are retained in many organs after finishing their mission. The subsequently long-term safety concerns have thwarted their clinical PTT application.[6]

Poly(lactic-co-glycolic acid) (PLGA) is a FDA approved biodegradable material, which has been extensively explored as a drug carrier for cancer targeted therapy.[7] Since PLGA is not responsive to pH and redox potential, the release of payload from PLGA based carriers is mainly controlled by the degradation rate of the polymer. To endow light triggerable release capacities to these carriers, PLGA nanoparticles have been coated or

embedded with various metal based PTCAs.[8] However, the inherited non-degradable nature of those PTCAs remains a challenge for their clinical translation.

Inspired by the robust adherent property of mussel, polydopamine recently has been coated onto various surfaces to facilitate the functionalization of the templates.[9] Hereby, we developed a biodegradable photothermal converting nanomaterial based on a PLGA/polydopamine core/shell structure (**Figure 5.1A**). To be more effective in killing cancer cells, doxorubicin (DOX) was encapsulated into the nanoparticle. We expect that NIR irradiation can induce photothermal effect, and subsequently trigger the release of the encapsulated DOX to exhibit both photothermal therapy and chemotherapy for cancer (**Figure 5.1B**).

5.2 EXPERIMENTS

5.2.1 Materials and Reagents

Poly(lactic-co-glycolic acid) (PLGA, 50/50, 16 kDa) was purchased from Lakeshore Biomaterials, Inc. (Birmingham, AL, USA). Polyvinyl alcohol (PVA, Mw=9000-10000 Da), (3-(4,5-dimethylthiazol-2-yl)-2,5-diphenyltetrazolium bromide (MTT), Poly(ethylene glycol) methyl ether thiol (PEG-SH, Mn= 2000 Da), Propidium Iodide (PI), Dopamine hydrochloride were purchased from Sigma Aldrich Chemical Co. (St. Louis, MO, USA). Penicillin (10,000 U/mL), streptomycin (10,000 mg/mL), 0.25% trypsin-EDTA, Dulbecco's Modified Eagle Medium (with L-glutamine) and fetal bovine serum (FBS) were obtained from American Type Culture Collection (ATCC, Manassas, VA, USA). Doxorubicin (DOX) was purchased from AK Scientific, Inc. (Union City, CA, USA). Cetuximab was acquired from ImClone LLC (Princeton, NJ, USA). Calcein AM was purchased from Thermo Fisher Scientific, Inc. (Waltham, MA, USA).

5.2.2 DOX@PLGA nanoparticle fabrication

DOX encapsulated PLGA nanoparticle was fabricated by emulsion method. In briefly, 5 mg DOX was firstly dissolved in 1 mL CH_3OH with 25 μL triethylamine and mixed with 5 mL CH_2Cl_2 containing 200 mg PLGA. The mixture solution was then poured into 20 mL 5% PVA solution on ice, followed by ultrasonication for 15 min (Misonix Sonicator, XL-2015, 80% power). After sonication, the emulsion solution was added into 100 mL ddH_2O and stirred overnight to evaporate the organic solvent. The DOX@PLGA nanoparticle was firstly centrifuged at 1000 g for 10 min to remove big aggregates and then centrifuged at 16000 g for 15 min to collect the particles. The particles were washed by ddH_2O for three times to remove excessed PVA and non-encapsulated DOX and redispersed in 10 mL ddH_2O and keep at 4 ºC for further use.

5.2.2 Dopamine coating

The coating of dopamine on the DOX@PLGA nanoparticle was according previous reported.[10] Briefly, 6 mg DOX@PLGA was centrifuged and redispersed in 12 mL tris buffer (10 mM, pH 8.5) with 6 mg dopamine. The mixture was kept stirring for 3 h at room temperature in an opened glass vial. The solution turned its color from yellowish brown to dark brown, indicating the successful coating of polydopamine on the DOX@PLGA nanoparticle. Finally, the DOX@PLGA/PD nanoparticle was collected by centrifuging at 16000 g for 10 min and washed for three times and redispersed in 6 mL tris buffer (20 mM, pH 8.5) for the subsequent surface modification.

5.2.3 PEG and anti-EGFR antibody decoration

DOX@PLGA/PD nanoparticle suspension (2 mL) prepared above was mixed with 4 mg thio-PEG2000 or 4 mg Anti-EGFR antibody (Cetuximab) in 2 mL PBS buffer,

respectively, and stirred for 30 min. The pH of mixture was immediately adjusted to 7.0. The PEG and EGFR antibody decorated nanoparticles were collected by centrifuging at 16000 g for 10 min at 4 ºC and washed 2 times to yield DOX@PLGA/PD-PEG and DOX@PLGA/PD-C. The resulting nanoparticles were redispersed in 500 μL ddH_2O or DMEM culture medium and stored at 4 ºC. For EGFR antibody conjugation efficiency measurement, the supernatant of EGFR antibody decorated nanoparticle was collected and the unconjugated EGFR antibody was quantified by Bio-Rad assay and was used to calculate the EGFR conjugation efficiency. The result revealed that the EGFR antibody conjugation efficiency was about 60%.

5.2.4 Nanoparticle characterization

The DOX concentration in the nano-suspension was measured by fluorescence intensity (Ex=485 nm, Em=595 nm) by dissolving nanoparticles in DMSO and calculated according pre-known calibration curve. The UV-Vis spectrum of DOX@PLGA nanoparticle before and after dopamine coating was recorded. To quantify the loading efficiency and content, nanoparticles were freeze dried to get the weight amounts. The morphology of DOX@PLGA/PD, DOX@PLGA/PD-PEG and DOX@PLGA/PD-C were observed by TEM and the hydrodynamic size and zeta potential of nanoparticles were measured by DLS. For DLS measurement, nanoparticles were dispersed in 1 mM PBS 7.4 (0.2 mg/mL). The glass transition temperatures of the nanoparticles were measured by differential scanning calorimetry (Q2000, TA Instruments, heated from 25 ºC to 80 ºC with a heat flow rate of 1 ºC/min).

5.2.5 Serum stability

To investigate the serum stability, DOX@PLGA, DOX@PLGA/PD-PEG, and DOX@PLGA/PD-C were diluted in 10% FCS (equivalent DOX concentration was 15 μg/mL) and incubated at 37 ºC up to 7 days. The sizes of the nanoparticles were monitored by DLS to evaluate their stability in serum containing buffer.

5.2.6 Photothermal conversion and efficiency calculation

To test the photothermal effect of DOX@PLGA/PD-PEG nanoparticles, 50 μL nanoparticles with DOX concentration equal to 2, 5, 10, 25 and 50 μg/mL were irradiated with a 808 nm NIR laser (2.83 W/cm^2, Scorpius-D IR Portable Laser, Laserglow Technologies) for 10 min. The temperatures of the nanoparticles were measured every 1 min by FLIR thermal camera (FLIR i7, FLIR® Systems, Inc). For photothermal conversion efficiency measurement, DOX@PLGA/PD-PEG nanoparticle (50 μL, DOX equivalent to 10 μg/mL) was firstly irradiated at 808 nm for 9 min, and the temperature was record every 10 sec. After that, the laser was removed and the decreasing of the temperature of the nanoparticle was continued to measure every 10 s up to 9 min. Finally the photothermal conversion efficiency (η) was calculated according previous report as 16.9% for DOX-PLGA/PD-PEG.

5.2.7 In vitro DOX release

The release profile of the DOX from the nanoparticles were measured at pH 5.0 and pH 7.4 with or without laser irradiation. In brief, DOX@PLGA/PD-PEG nanoparticle was centrifuged and re-dispersed in 500 μL acetate buffer (10 mM, pH 5.0) and PBS buffer (10 mM, pH 7.4), respectively, and incubated at 37 ºC. Both buffers were

supplemented with 2% Tween 80 to create a sink condition by improving the solubility of DOX. The initial DOX concentration in the suspension was 20 μg/mL. Each pH group included six parallel samples. At pre-determined time points, all samples were centrifuged at 16000 g for 10 min. After that, 250 μL supernatants were carefully retrieved and refilled with 250 μL fresh buffers to redisperse the nanoparticles. At 24 h and 32 h post incubation, three samples in each pH group were irradiated under 808 nm laser for 10 min while the other three samples were kept at 37 ºC. All samples were continuously incubated up to 72 h. After that, the releasing of DOX from the nanoparticles were quantified by a microplate reader ((Ex=495 nm, Em=595 nm, Beckman Coulter DTX 880 Multimode Detector, Beckman Coulter, Inc).

5.2.8 Confocal microscopy

UMSCC 22A cells (200,000cells/dish) were seeded in 35mm^2 Petri dishes (Mat Tek, MA, USA) overnight. After that, DOX, DOX@PLGA/PD-PEG and DOX@PLGA/PD-C nanoparticles were added into the dishes at the DOX equivalent concentration of 2 μg/mL. In order to study the effect of free anti-EGFR antibody on the uptake of DOX@PLGA/PD-C nanoparticle, cells were pretreated with free anti-EGFR antibody (200 μg/mL) for 30 min before adding the nanoparticles. All dishes were then incubated at 37 ºC for 3 h. After that, cells were washed by PBS (3×), fixed with formaldehyde (4.5 % in PBS), and stained with Hoechst 33342 (final concentration 1μg/mL). Cells were analyzed under a confocal microscope (LSM 700, Carl-Zeiss Inc.).

5.2.9 Flow cytometry

UMSCC 22A cells (300,000cells/well) were seeded in 6-well plates overnight. After that, DOX, DOX@PLGA/PD-PEG and DOX@PLGA/PD-C nanoparticles were

added at the DOX equivalent concentration of 1 μg/mL. In order to investigate the effect of EGFR receptor on the cellular uptake of DOX@PLGA/PD-C nanoparticle, cells were pretreated with free anti-EGFR antibody (200 μg/mL) 30 min before adding DOX@PLGA/PD-C nanoparticles. The plate was incubated at 37 ºC for 3, 6 and 12 h respectively. Then cells were washed, trypsinized and resuspended in PBS. DOX positive cell population was quantified at Ex=488 nm, Em=585 nm using flow cytometry (BD Accuri C6, BD Biosciences).

5.2.10 Live & dead cell assay

To study the photothermal cytotoxicity of the nanoparticles, Live and Dead cell assay was introduced. In briefly, UMSCC 22A cells (300,000cells/well) were seeded in 6-well plates and incubated under a humidified atmosphere of 95/5% air/CO_2 until 100% confluence. Then free DOX, PLGA/PD-PEG, DOX@PLGA/PD-PEG, and DOX@PLGA/PD-C were added to the plates. The equivalent DOX concentration was 10 μg/mL and the absorbance at 808 nm for all nanoparticles were kept the same. Cells were incubated at 37 ºC for another 2 h, and exposed to the 808 nm NIR laser for 30 min. Here we used longer irradiation time compared to the irradiation time in MTT assay because we wanted to make sure that obvious photothermal cytotoxicity could be observed immediately after laser irradiation. After that, cells were gently washed by PBS (2×) to avoid washing off dead cells. Calcein AM (0.2 μM) and propidium iodide (PI, 25 μg/mL) mixture solution (500 μL) was added and kept at room temperature for 30 min and then cells were observed directly by fluorescence microscopy (Olympus IX81, Olympus America Inc).

5.2.11 In vitro cytotoxicity

The cytotoxicity of nanoparticles were evaluated by MTT assay. UMSCC 22A cells were seeded in 96-well plate (20,000 cells/well) for 24 prior to the study. Then free DOX, DOX@PLGA/PD-PEG, and DOX@PLGA/PD-C with DOX concentration equivalent to 2, 5 and 10 μg/mL were added. The cells were then incubated 3 h in 95/5% air/CO_2 at 37 ºC, following the irradiation under the 808 nm laser for 10 min. After that, all wells were washed 2 times and replaced with fresh culture medium and kept incubation for another 24 h. Finally, MTT reagent (100 μL, 5 mg/mL) in medium) was added and incubated for 4h, following the addition of MTT stop solution and the measurement of the optical density of the medium using a microplate reader (ELX808, Bio-Tech Instrument, Inc) at λ = 595 nm.

5.2 12 Animal experiment

All animal experiments were conducted in accordance with NIH regulations and approved by the Institutional Animal Care and Use Committee of the University of South Carolina.

Tumor model

UMSCC 22A cells (3×10^6 cells in 100 μL DMEM medium) were inoculated subcutaneously in female Balb/c nude mice (8-10 week old, ~20 g, Jackson Laboratory). The tumor volume were measured by a digital caliper and calculated according to the following formula: Tumor volume = (tumor length) × (tumor width)^2/2. When the tumor reached to 50 mm^3, free DOX and DOX@PLGA/PD-C were intratumorally injected (40 μL, DOX concentration equivalent to 15 μg/mL). For control group, PBS was injected.

Mice were exposed to a 808 nm laser irradiation (2.78 W/cm^2) 3 h post injection for 10 min. The temperature of the mice during the irradiation were recorded by FLIR thermal camera. The tumor volumes (V) of the mice were measured every other day for 24 days. The relative tumor volume expressed as V/V_0 (V_0 was the tumor volume when the treatment was initiated) was used to represent the tumor size change during the whole treatment process. After 24 days, the mice were sacrificed and the blood, tumor, liver, heart, lung, kidneys and spleen were collected for further analysis. All organs were firstly fixed in 10% neutral buffered formalin for 48 h and then washed with PBS and finally kept in 70% ethanol at 4 ºC.

Blood analysis

Whole blood (50 μL) of the mice were firstly collected in heparinized tubes and analyzed for white blood cells, red blood cells, neutrophils, etc. (VetScan HM5, Abaxis, Inc.).

TEM analysis for Heart tissue

To study the cardiotoxicity of DOX, hearts from the mice were analyzed by TEM. The formalin fixed samples were further fixed with 1% perosmic oxide for 2 h at 4 ºC, washed by water and then dehydrated in a serial of alcohol solutions, embedded, and sliced with the thickness between 50 and 70 nm. TEM analysis was performed on Hitachi H8000 operating at 200 kV.

Histological Examinations

The formalin fixed organs were embedded in OCT gel, sectioned into ~5 μm, stained with hematoxylin and eosin (H&E) and analyzed under light microscopy (Leica

DM1000 LED, Leica Microsystems Inc.). The histology was performed in a blinded fashion by professional personnel in the University of South Carolina.

5.3 RESULTS AND DISCUSSION

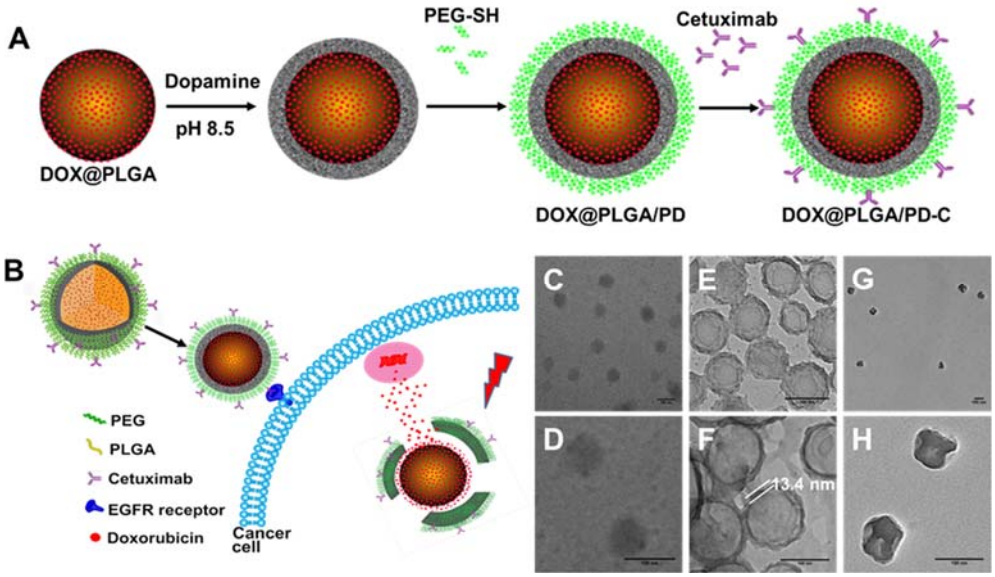

Figure 5.1 Schematic illustration of the fabrication of epidermal growth factor receptor targeted mussel inspired nanoparticle (A), and its proposed action pathway (B). TEM images of DOX@PLGA (C-D), DOX@PLGA/PD (E-F), and DOX@PLGA/PD after NIR irradiation (G-H). Scale bars are 100 nm in (C-H).

The DOX loaded PLGA nanoparticle (DOX@PLGA) was fabricated according to our published emulsion method,[11] and then coated with polydopamine (PD) under weak basic condition as shown in **Figure 5.1A.**The dark rings in **Figure 5.1E and 5.1F** proved the formation of a PD layer on the PLGA shell, which is about 13.38 nm. To enhance the stability and cancer cell targeting effect of the DOX@PLGA/PD nanoparticles, polyethylene glycol (PEG) and anti-EGFR antibody (Cetuximab) were conjugated onto the surface of the polydopamine (PD) (**Figure 5.1A**), respectively. Dynamic light scattering (DLS) found that the size of DOX@PLGA is about 110 nm (**Figure 5.2A**).

The coating of PD layer increased the size of DOX@PLGA/PD to 135 nm. The addition of PEG protection layer and Cetuximab slightly increased the size of DOX@PLGA/PD-C nanoparticles, which coincides with the observation of TEM (**Fig. 5.1**). Due to the high reactiveness of PD, PD based nanoparticle could react with serum protein and induce aggregation. To evaluate the stability of DOX@PLGA/PD-C nanoparticle during blood circulation, the size of the nanoparticle in 10% serum containing medium was monitored with DLS. Due to the existence of PEG protection layer, DOX@PLGA/PD-C was stable in culture medium containing 10% FBS (**Figure 5.2B**), and no obvious size change and aggregation were observed after one week of incubation. Zetasizer found that DOX@PLGA/PD-C carries negative surface charge (-14.6 ± 0.495).

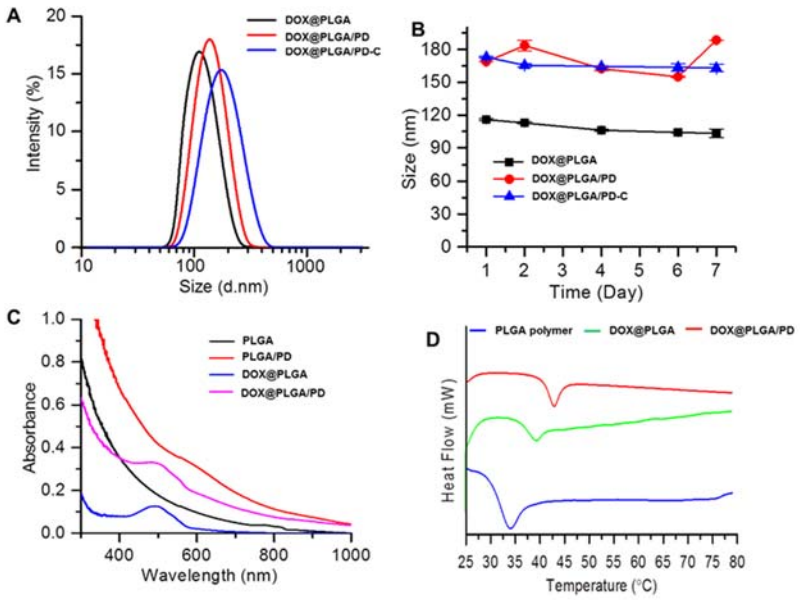

Figure 5.2 Physical properties of nanoparticles fabricated based on PLGA polymer. PLGA: PLGA nanoparticle; PLGA/PD: polydopamine coated PLGA nanoparticle; DOX@PLGA: DOX encapsulated PLGA nanoparticle; (A) The hydrodynamic size distributions of DOX@PLGA, DOX@PLGA/PD and DOX-PLGA/PD-C. (B) Serum stability of DOX@PLGA, DOX@PLGA/PD and DOX@PLGA/PD-C. Nanoparticles were dissolved in 10% FCS and incubated at 37 ºC for 7 days. (C) UV-Vis spectra of PLGA, PLDA/PD, DOX@PLGA and DOX@PLGA/PD. (D) The glass transition temperatures (Tg) of PLGA polymer, DOX@PLGA and DOX@PLGA/PD measured by DSC.

PLGA nanoparticle has little absorbance in the NIR region, while PD has been reported showing strong absorbance in that window.[12] The absorbance of PLGA nanoparticle shifted to the longer wavelength end after the coating of polydopamine (**Figure 5.2C**). Differential scanning calorimetry (DSC) revealed that PD coating significantly increased the glass transition temperatures (Tg) of PLGA nanoparticle from 39.42 To 42.97 ℃ (**Figure 5.2D**), suggesting that PLGA/PD nanoparticle could be a temperature sensitive carrier for targeted drug delivery.

It has been reported that polydopamine nanoparticle can generate heat upon NIR irradiation.[12] The coating of PD on the surface of PLGA nanoparticle boosted its absorbance in the NIR region (**Figure 5.2A**). To evaluate whether this increased absorbance in NIR region would endow PLGA/PD the ability to generate enough heat to elevate the solution temperature, the PLGA/PD nano-suspensions of different concentrations were irradiated with NIR laser (808 nm, 2.83 W/cm^2) for 10 min at predesigned time intervals and their temperatures were monitored with a FLIR i7 thermal imaging camera and recorded every minute. **Figure 5.3A** revealed that PLGA/PD could effectively heat the media and exhibited a concentration-dependent photothermal effect. At the OD of 0.75, PLGA/PD nanoparticle quickly heated the solution temperature to 45 ℃, indicating PLGA/PD is a good photothermal converting material. Based on the heating and cooling cycle shown in **Figure 5.3B**, we found the photothermal converting efficiency is 16.9%, just a slightly lower than that of gold nanorod (~22%) which are widely used for cancer therapy. Interestingly, for those experiments medium temperature reached higher than 60 ℃, we also noticed that medium temperature quickly reached its summit within 3 minutes and then exhibited as a plateau (**Figure 5.3A**), which is

different from most developed photothermal converting materials, their media temperatures always raise when the NIR irradiation is applied.[13] This unique dose dependent-peak temperature feature could be critical for photothermal therapy, during which burning adjacent healthy tissue should be avoided. To observe the morphology change after the NIR irradiation, we further examined DOX@PLGA/PD nanoparticles with TEM. Compared with the structure shown in **Figure 5.1F**, the size of the particles shrank after the irradiation (**Figure 5.1H**). Furthermore, the core/shell structure in **Figure 5.1F** was compromised (**Figure 5.1H**), indicating the breakage of the PD shell. We postulate that contraction of the particle size was due to the melting of the nanoparticle after it reaches Tg during the heating process, while the breakage of the PD shell was caused by the heterogeneous heat stress responses between the PLGA core and PD shell.

To investigate whether the coating of PD on the surface of PLGA nanoparticle could affect the release profile of its payload, anticancer drug doxorubicin (DOX) was adopted as a model drug. DOX@PLGA/PD nanoparticle was suspended in sodium acetate buffer (pH 5.0) and phosphate buffer (PBS, pH 7.4) to mimic the environments in the cytosol and lysosome, respectively. **Figure 5.3C** showed that DOX@PLGA/PD released 40.85% and 57.63% of its payload within 24 h of incubation in PBS and sodium acetate buffer, respectively. As we already proved that PLGA/PD nanoparticle could efficiently convert NIR laser irradiation into heat, we further investigated the effect of NIR irradiation on its release kinetics. Remarkably, **Figure 5.3C** showed that two pulses of 10 min of NIR irradiations induced 30% more DOX release for both pH conditions.

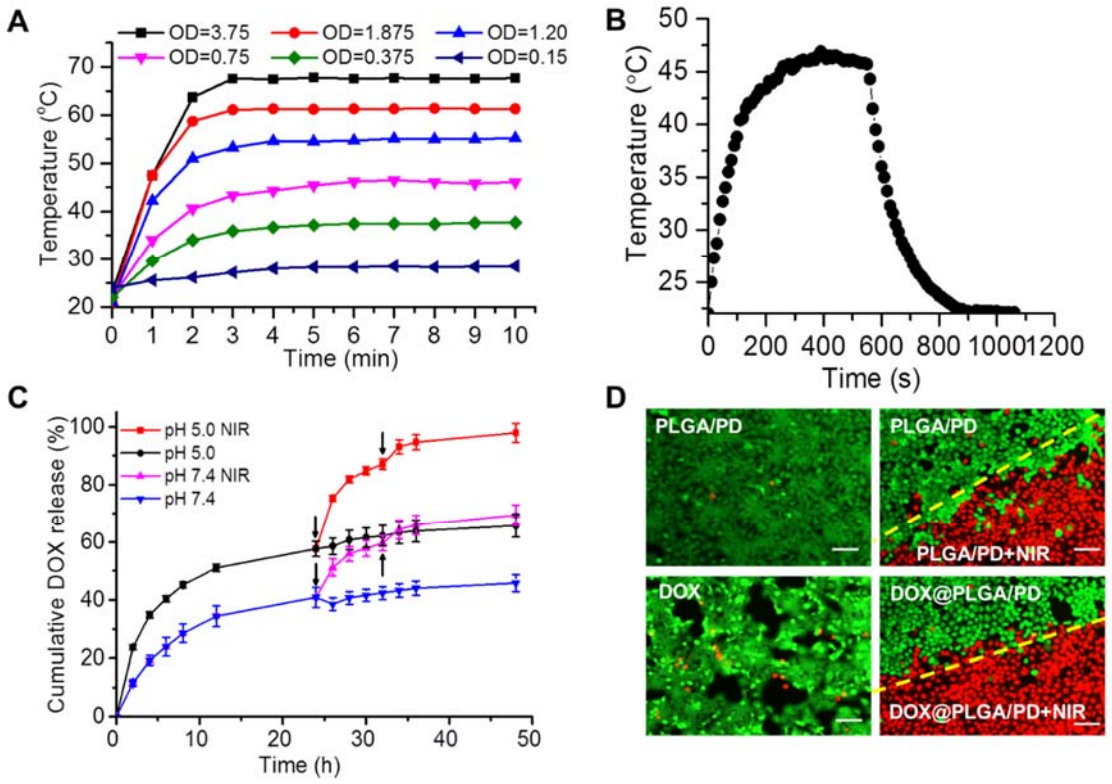

Figure 5.3 The photothermal effect of DOX@PLGA/PD on medium temperature elevation (A, B), drug release kinetics (C), and cell viability (D). Real-time temperature elevation of DOX@PLGA/PD at different concentrations after 808 nm irradiation (A). OD represents the absorbance at 808 nm. DOX@PLGA/PD nano-suspensions during 1 cycle of NIR irradiation and cooling (B). Nanoparticles were irradiated with a 808 nm NIR laser for 10 min (2.83 W/cm^2) and then cooled down for 10 min. DOX release profiles at different pHs with or without laser irradiation (C). Arrows indicate the application of NIR irradiation. The live/dead cell staining after receiving different treatments coupled with or without NIR irradiation (D).

To investigate the cell killing effect of NIR irradiation coupled with DOX@PLGA/PD on the head and neck cancer cells, live and dead cell assay was carried out immediately after the irradiation. As we expected, for cells co-incubated with PLGA/PD nanoparticle, nearly all non-irradiated cells were green (**Figure 5.3D**), while NIR irradiated cells were red. The distinct irradiation boundary as shown in red/green in the well treated with PLGA/PD nanoparticle and NIR irradiation suggests that NIR irradiation induced photothermal effect could effectively kill cancer cells while

PLGA/PD nanoparticle itself is non-toxic. Due to the relative short incubation time, most cells treated with DOX were alive. Therefore, no significant difference was observed between the cells treated with DOX@PLGA/PD and PLGA/PD.

EGFR receptor is overexpressed in many types of cancer, including colon cancer, lung cancer, glioblastoma multiforme, and head and neck cancer.[14] To enhance cellular uptake of DOX@PLGA/PD nanoparticles for UMSCC 22A head and neck cancer cells, EGFR receptor antibody, Cetuximab, was conjugated onto the surface of the particle. Confocal microscopy found that more red fluorescence signal in cells treated with Cetuximab conjugated DOX@PLGA/PD-C than its non-targeted counterpart (**Figure 5.4A**). In addition, the block of free Cetuximab significantly decreased the uptake of DOX@PLGA/PD-C nanoparticles, which EGFR receptor mediated endocytosis. The EGFR receptor mediated cellular uptake of DOX@PLGA/PD-C nanoparticles and blocking effect of free Cetuximab were also observed by flow cytometry (**Figure 5.4B**). It is worthy to mention that free DOX entered cancer cells faster than the DOX@PLGA/PD-C nanoparticles (**Figure 5.4B**).

To investigate whether the EGFR receptor enhanced cellular uptake of DOX@PLGA/PD-C nanoparticles and photothermal effect of the nanoparticle can be translated into higher efficacy in killing cancer cells, cell proliferation assay was employed. **Figure 5.4C** revealed that empty PLGA/PD nanoparticle itself is almost non-toxic, while effectively killing cancer cell when coupled with NIR irradiation. It is worth noting that the effect of NIR irradiation only became significant when PLGA/PD at the DOX corresponding of 5 μM or higher, at which PLGA/PD could generate enough heat to ablate cancer cells and augment drug release. The EGFR targeted nanoparticles

showed much higher efficacy in killing UMSCC 22A cells than their non-targeted counterparts. As expected, NIR irradiation significantly boosted the potency of DOX@PLGA/PD and DOX@PLGA/PD-C, which reflects the combination effect of photothermal effect and its subsequent induced quicker drug release. Free DOX exhibited higher cell killing effect than other treatments except at 10 μM dose.

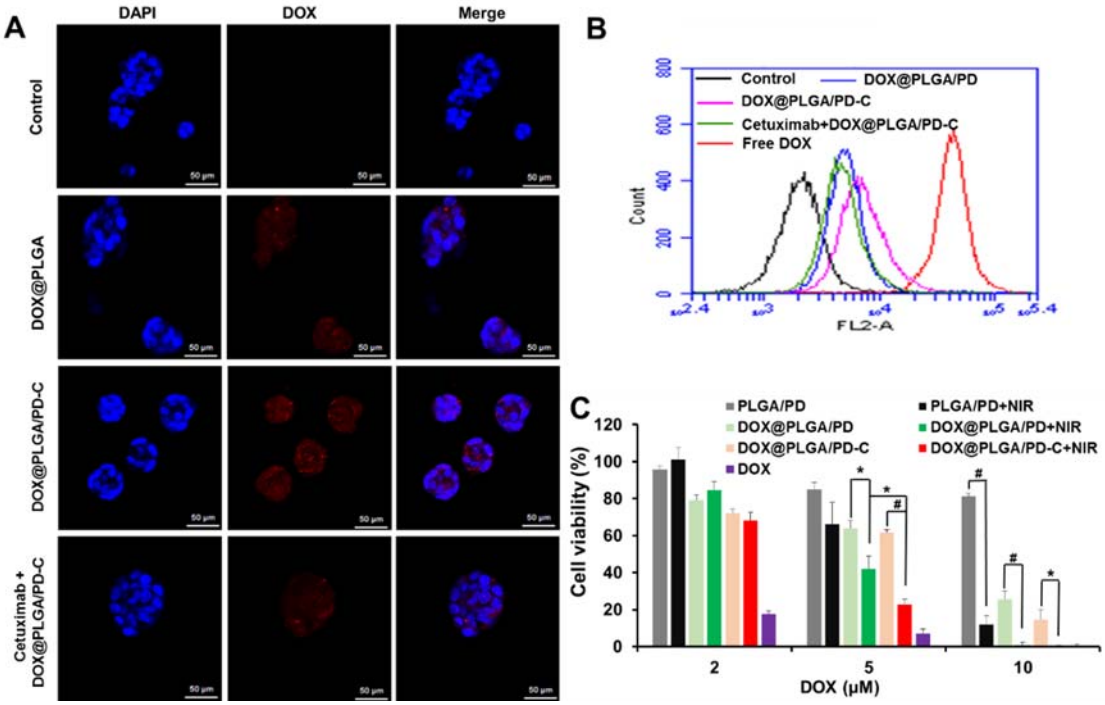

Figure 5.4 Confocal images (A), flow cytometry spectra (B), and cytotoxicity (C) of DOX@PLGA/PD-C treated UMSCC 22A cells. (A) All scale bars equal to 50 μm. Cells were co-incubated with various nanoparticles for 3 h before the MTT assay. Cells received NIR irradiation for 10 min, 2.83 W/cm^2. Data expressed as mean ± SD ($P < 0.05$ *; $P < 0.01$ #).

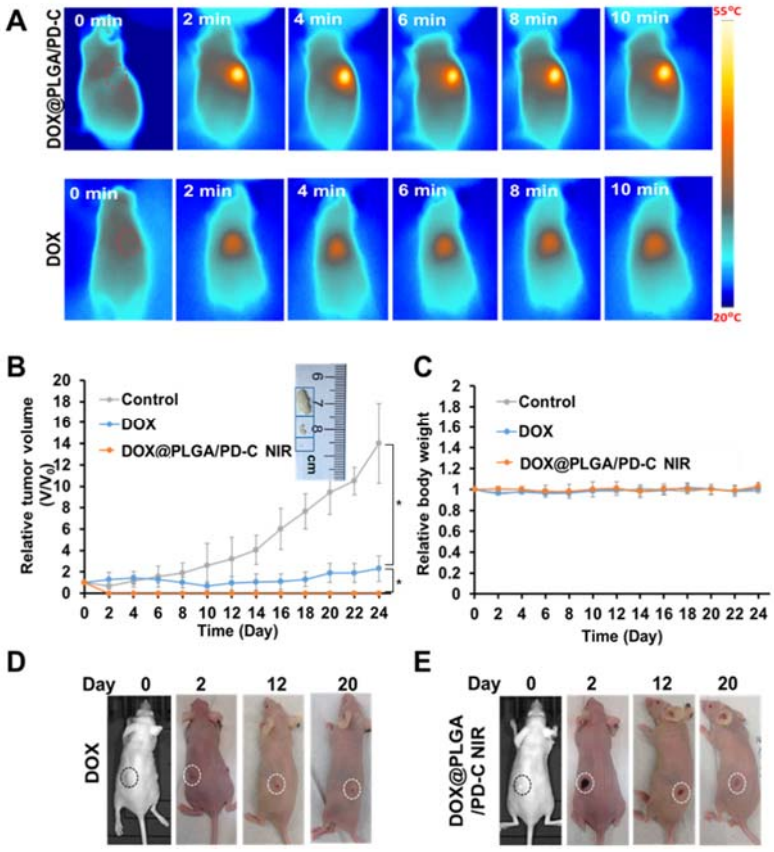

Figure 5.5 Tumor response after receiving different treatments. The tumor model was established by s.c. injection of UMSCC 22A cells into the flanks of mice. (A) Thermal image of mice after receiving NIR irradiation over 10 min (2.83 W/cm^2). (B) The tumor volume change profiles of mice after receiving different treatments. Data were expressed as mean ± SD, *$P < 0.05$. Insert shows the representative images of tumors harvested from different treatment groups at the end of the experiment. (C) The body weight curves of tumor-bearing mice after receiving different treatments. (D) Representative images of developed tumors after receiving DOX treatment. (E) Representative images of developed tumors after receiving DOX@PLGA/PD-C NIR treatment. Circles in (D) and (E) indicate the locations of tumor.

To investigate the tumor growth inhibitory effect of EGFR targeted DOX@PLGA/PD coupled with NIR irradiation, a subcutaneous head and neck cancer mouse model was introduced. To maximize the therapeutic effect of the treatment, free DOX and EGFR targeted DOX@PLGA/PD nanoparticles were administrated intratumorally. The thermal images shown in **Figure 5.5A** indicate that EGFR targeted

PLGA/PD could quickly elevate the temperature of tumor tissue to 55 ℃ within 2 min. Different from other photothermal systems,[15] the tissue temperature was maintained constant during the whole course of NIR irradiation. The tumor mass in the DOX@PLGA/PD-C coupled with NIR irradiation treatment group collapsed and formed a scar 2 days post treatment (**Figure 5.5E**). The scar gradually disappeared and the original tumor did not recur during a 24 days period (**Figure 5.5B and 5.5E**). Contrary to its strong potency shown in the *in vitro* study, free DOX treatment initially only slightly reduced tumor size (**Figure 5.5B and 5.5D)**. Furthermore, those tumors gradually bounced back 10 days post treatment. As expected, the non-treated tumors grew to 14 times of its initial size at the end of the experiment (**Figure 5.5B**). We did not observe significant body weight change in all groups (**Figure 5C**). The negligible tumor mass in **Figure 5.5B** and **5.5E** proved that DOX@PLGA/PD-C coupled with NIR irradiation is an effective approach for eradicating head and neck tumor.

Cardiotoxicity is a major side effect associated with DOX based chemotherapy.[16] To evaluate the safety of DOX@PLGA/PD-C coupled with NIR irradiation, hearts in the treated groups were collected and processed for TEM observation. TEM image (top panel of **Figure 5.6**) revealed that the membrane integrity and ordered structure of mitochondria in the heart tissue from the mice receiving free DOX treatment have been significantly compromised. To our surprise, no obvious structure abnormalness was observed in the heart tissue in the DOX@PLGA/PD-C coupled with NIR irradiation treatment group. Furthermore, no histopathological changes were observed in the liver tissues among all treatment groups. Similarly, blood components analysis did not detect significant alteration among all treatment groups (**Table. 5.1**). In addition, H&E staining

of the tumor tissue (low panel of **Figure 5.6**) showed that the control and DOX treated tumor kept the characteristics of squamous cell carcinoma, while the shrunk nuclei in the DOX@PLGA/PD-C coupled with NIR irradiation treated tumor proved its effectiveness. All these results indicate that DOX@PLGA/PD-C coupled with NIR irradiation is a safe tool for head and neck cancer therapy.

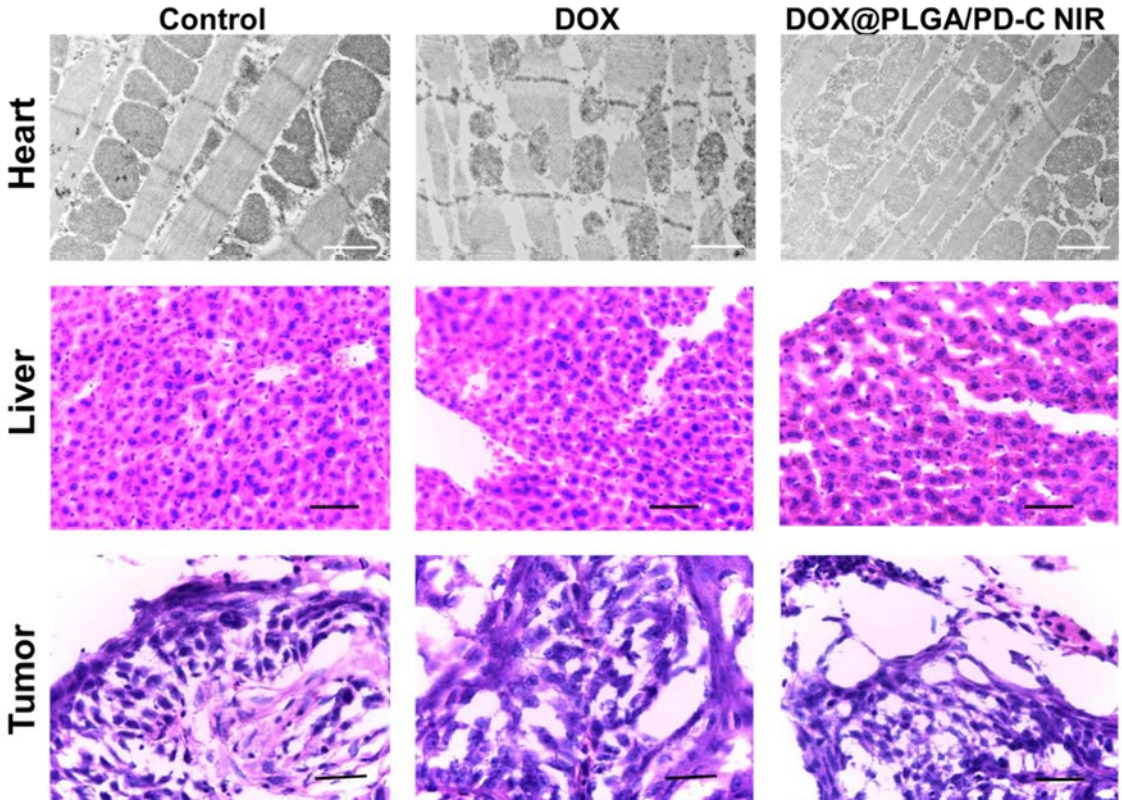

Figure 5.6 The TEM images of heart tissue sections and H&E staining images of liver and tumor tissue sections. Scale bars in the TEM images (top panel) and H&E staining sections (middle and bottom panels) are 1 μm and 50 μm, respectively.

Table 5.1 Blood test results of mice after different treatments

Parameters	Control	DOX	EGFR-PLGA-DOX
WBC (10^9/L)	6.03 ± 3.39	4.64 ± 2.69	6.53 ± 1.21
LYM (10^9/L)	1.8 ± 0.50	2.69 ± 1.14	3.60 ± 0.40
MON (10^9/L)	0.32 ± 0.19	0.34 ± 0.33	0.31 ± 0.15
NEU (10^9/L)	3.90 ± 2.80	1.61 ± 1.24	2.62 ± 1.00
LY (%)	37.87 ± 22.75	62.33 ± 10.83	56.00 ± 10.02
MO (%)	5.23 ± 0.47	6.03 ± 3.14	4.67 ± 1.36
NE (%)	56.90 ± 22.28	31.63 ± 7.85	39.30 ± 9.71
RBC (10^{12}/L)	8.21 ± 0.63	8.89 ± 0.93	8.85 ± 0.40
HGB (g/dL)	11.40 ± 0.89	13.53 ± 1.53	13.23 ± 0.85
HCT (%)	34.34 ± 2.66	38.62 ± 4.08	39.33 ± 3.15
MCV (fl)	42.00 ± 0.00	43.33 ± 0.58	44.00 ± 1.73
MCH (pg)	13.93 ± 0.21	15.23 ± 0.21	14.93 ± 0.32
MCHC (g/dL)	33.27 ± 0.76	35.00 ± 0.50	33.70 ± 0.62

5.4 CONCLUSIONS

In summary, we have developed a doxorubicin loaded biodegradable photothermal converting material based on a mussel inspired PLGA/polydopamine core/shell nano-structure for cancer photothermal therapy and chemotherapy. With the help of anti-EGFR antibody, the nanoparticle could effectively enter head and neck cancer cells and convert near infrared light to heat to trigger drug release from PLGA core for chemotherapy as well as ablate tumors by the elevated temperature. Since the nanoparticle was retained in the tumor tissue and subsequently released its payload inside the cancer cells, no any doxorubicin associated side effects were detected. Due to its unique biodegradable feature, the DOX@PLGA/PD-C nanoparticle is very promising to be clinically adopted for head and neck cancer treatment.

5.5 REFERENCES

(1) M. S. Khan,G. D. Vishakante and H. Siddaramaiah, *Adv. Colloid Interface Sci.,* 2013, **199**, 44-58.

(2) X. Liu,N. Huang,H. Li,H. Wang,Q. Jin and J. Ji, *ACS Appl. Mater. Interfaces,* 2014, **6**, 5657-5668; J. Chen,C. Glaus,R. Laforest,Q. Zhang,M. Yang,M. Gidding,M. J. Welch and Y. Xia, *Small,* 2010, **6**, 811-817; S. Wang,A. Riedinger,H. Li,C. Fu,H. Liu,L. Li,T. Liu,L. Tan,M. J. Barthel and G. Pugliese, *ACS nano,* 2015, **9**, 1788-1800.

(3) A. M. Alkilany,L. B. Thompson,S. P. Boulos,P. N. Sisco and C. J. Murphy, *Adv. Drug Delivery Rev.,* 2012, **64**, 190-199.

(4) X. Huang and M. A. El-Sayed, *Alexandria Journal of Medicine,* 2011, **47**, 1-9.

(5) K. C. Kwon,J. H. Ryu,J. H. Lee,E. J. Lee,I. C. Kwon,K. Kim and J. Lee, *Adv. Mater.,* 2014, **26**, 6436-6441; Z. Zhang,J. Wang and C. Chen, *Adv. Mater.,* 2013, **25**, 3869-3880; S. E. Skrabalak,J. Chen,L. Au,X. Lu,X. Li and Y. Xia, *Adv. Mater.,* 2007, **19**, 3177-3184; W. Dong,Y. Li,D. Niu,Z. Ma,J. Gu,Y. Chen,W. Zhao,X. Liu,C. Liu and J. Shi, *Adv. Mater.,* 2011, **23**, 5392-5397; M. S. Yavuz,Y. Cheng,J. Chen,C. M. Cobley,Q. Zhang,M. Rycenga,J. Xie,C. Kim,K. H. Song,A. G. Schwartz,L. V. Wang and Y. Xia, *Nat. Mater.,* 2009, **8**, 935-939; E. B. Dickerson,E. C. Dreaden,X. Huang,I. H. El-Sayed,H. Chu,S. Pushpanketh,J. F. McDonald and M. A. El-Sayed, *Cancer Lett.,* 2008, **269**, 57-66; C. Loo,A. Lin,L. Hirsch,M. H. Lee,J. Barton,N. Halas,J. West and R. Drezek, *Technol. Cancer Res. Treat,* 2004, **3**, 33-40.

(6) N. Khlebtsov and L. Dykman, *Chem. Soc. Rev.,* 2011, **40**, 1647-1671; S. Fraga,A. Brandão,M. E. Soares,T. Morais,J. A. Duarte,L. Pereira,L. Soares,C. Neves,E. Pereira and M. de Lourdes Bastos, *Nanomedicine.,* 2014, **10**, 1757-1766.

(7) B. Sun,B. Ranganathan and S.-S. Feng, *Biomaterials,* 2008, **29**, 475-486; Z. Zhang,S. H. Lee and S.-S. Feng, *Biomaterials,* 2007, **28**, 1889-1899; N. Karra,T. Nassar,A. N. Ripin,O. Schwob,J. Borlak and S. Benita, *Small,* 2013, **9**, 4221-4236.

(8) E. Fazio,A. Scala,S. Grimato,A. Ridolfo,G. Grassi and F. Neri, *J. Mater. Chem. B,* 2015, **3**, 9023-9032; J. Song,X. Yang,O. Jacobson,P. Huang,X. Sun,L. Lin,X. Yan,G. Niu,Q. Ma and X. Chen, *Adv. Mater.,* 2015, **27**, 4910-4917.

(9) Y. Liu,K. Ai and L. Lu, *Chem. Rev.,* 2014, **114**, 5057-5115; H.Lee,S.M. Dellatore,W. M. Miller and P. B. Messersmith, *Science,* 2007, **318**, 426-430; Q. Ye,F. Zhou and W. Liu, *Chem. Soc. Rev.,* 2011, **40**, 4244-4258.

(10) J. Park,T. F. Brust,H. J. Lee,S. C. Lee,V. J. Watts and Y. Yeo, *ACS nano,* 2014, **8**, 3347-3356.

(11) Y. Yang,N. Bajaj,P. Xu,K. Ohn,M. D. Tsifansky and Y. Yeo, *Biomaterials,* 2009, **30**, 1947-1953.

(12) Y. Liu,K. Ai,J. Liu,M. Deng,Y. He and L. Lu, *Adv. Mater.,* 2013, **25**, 1353-1359.

(13) J. Yang,J. Lee,J. Kang,S. J. Oh,H. J. Ko,J. H. Son,K. Lee,J. S. Suh,Y. M. Huh and S. Haam, *Adv. Mater.,* 2009, **21**, 4339-4342.

(14) R. I. Nicholson,J. M. W. Gee and M. E. Harper, *Eur. J. Cancer,* 2001, **37**, 9-15; J. Spano,R. Fagard,J.-C. Soria,O. Rixe,D. Khayat and G. Milano, *Ann. Oncol.,* 2005, **16**, 189-194; T. E. Taylor,F. B. Furnari and W. K. Cavenee, *Curr. Cancer Drug Targets,* 2012, **12**, 197.

(15) J. Advances In Colloid and Interface ScienceHu,X. Zhu,H. Li,Z. Zhao,X. Chi,G. Huang,D. Huang,G. Liu,X. Wang and J. Gao, *Theranostics,* 2014, **4**, 534.

(16) K. Chatterjee,J. Zhang,N. Honbo and J. S. Karliner, *Cardiology,* 2010, **115**, 155-162.

CHAPTER 6

SUMMARY AND FUTURE DIRECTIONS

6.1 SUMMARY

In this dissertation, we have mainly focused on the development of stimuli responsive nanoparticle for cancer targeted therapy. We fabricated several nanoparticles and investigated their responsiveness to various stimuli such pH, redox potential, temperature and light. Then we studied the influence of the stimuli on the drug release kinetics. Furthermore, we modified the nanoparticles with different targeting ligands and investigated the impact of targeting ligands on cellular uptake, intracellular distribution and anticancer efficacy of nanoparticles both *in vitro* and *in vivo*. Finally, we evaluated the systematic toxicity of the nanoparticles. The major conclusions of this dissertation are summarized as follows:

1. A polymer/copper combination has been developed and exhibits cancer cell-selective killing effect. Factors determined the selectivity of this polymer/copper combination are discovered, which include intracellular glutathione and gene expression regulation. By differentially alterating the expression level of oncogenes (CIRBP and STMN1) and tumor suppressor genes (CDKN1C and GADD45B) between normal and cancer cells, the PDA-PEG/Cu^{2+} exhibited high selectivity in killing a broad spectrum of cancer cells, including drug resistant one, while sparing normal cells.

2. A self-quenching bioactivatable nanogel has been developed for targeted photodynamic therapy (PDT). Under the help of targeting ligand, anti-EGFR affibody molecule, the nanogel can efficiently accumulate in the tumor and effectively enter cancer cells, where it can respond to intracellular elevated glutathione and restore its photoactivity to induce enhanced anticancer efficacy.
3. A thermal, pH, and redox potential triple-responsive expansile nanogel system (TRN) has been developed for targeted PDT. The nanogel can expand by responding to acidic pH, intracellular glutathione and high temperature and release its payload Pc 4 for PDT. Targeting ligand 4-methoxybenzoic acid (MBA) is conjugated to the nanogel and enhances the cellular uptake and tumor accumulation of the nanogel, which eventaully results in high PDT efficacy.
4. A mussel inspired PLGA/polydopamine core/shell nano-structure has been developed for cancer photothermal therapy and chemotherapy. With the help of anti-EGFR antibody, the nanoparticle can effectively enter head and neck cancer cells and convert near infrared light to heat to trigger drug release from PLGA core for chemotherapy as well as ablate tumors by the elevated temperature.

6.2 INNOVATION AND SIGNIFICANCE

The innovation and significance of researches in this dissertation are as follows:

1. The cancer-cell selective killing effect of PDA-PEG/Cu^{2+} is firstly discovered and used to treat cancer and effectively reduce side effects. The determinants

of its selectivity is also revealed at the first time. These findings might expedite the development of copper as a target for cancer therapy.

2. Bioactivatable and triple responsive nanogels have been developed for cancer targeted photodynamic therapy. These novel nanogels can smartly control the drug release and effectively improve the PDT efficacy as well reduce side effects.
3. A biodegradable polydopamine coated PLGA core-shell nanoparticle has been the first time to be used as thermochemotherapy. By using a near infrared light to trigger drug release for chemotherapy and to increase tumor temperature to ablate tumor to achieve thermotherapy, this nanoparticle achieves an extremely high anticancer efficacy. These findings might expedite the development of biodegradable nanoparticles to replace currently widely used metal nanoparticles for cancer photothermotherapy.

6.3 FUTURE DIRECTIONS

The future research will investigate the cell killing mechanism of PDA-PEG/Cu^{2+} in molecular level both *in vitro* and *in vivo*. The pharmacokinetics, *in vivo* anticacner efficacy as well as systemic toxicity of this polymer/copper combination will also need to be extensively evaluated to determine whether the PDA-PEG/Cu^{2+} can be translated into a safe and effective cancer treatment tool.

For both bioactivatable and triple responsive nanogel, their pharmacokinetics and systemic toxicity will be studied. To evaluate the anticancer efficacy of triple responsive nanogel, the tumor inhibitory experiment will be conducted in the near future. The laser

power for both nanogels will also optimized to achieve high PDT efficacy and minimize the damage to normal tissues.

For polydopamine coated PLGA nanoparticle, its size will be further decrease in future since smaller nanoparticle usually can achieve better anticancer performance *in vivo*. The thickness of polydopamine layer will be adjusted to realize better controlled drug release. Furthermore, systemic administration, instead of intratumoral injection which is used in this dissertation, will be employed to investigate the *in vivo* anticancer efficacy of the nanoparticle. The pharmacokinetics and systemic toxicity of the nanoparticle will be also studied.

APPENDIX

PERMISSION TO REPRINT

COPYRIGHT PERMISSION FOR CHAPTER 2

The Copyright permission for Chapter 2 is attached below.

[H. He, D. Altomare, U. Ozer, H. Xu, K. Creek, H. Chen and P. Xu, *Biomater. Sci.*, 2016, 4, 115] - Reproduced by permission of The Royal Society of Chemistry

Cancer cell-selective killing polymer/copper combination

H. He, D. Altomare, U. Ozer, H. Xu, K. Creek, H. Chen and P. Xu, *Biomater. Sci.*, 2016, **4**, 115
DOI: 10.1039/C5BM00325C

If you are the author of this article you do not need to formally request permission to reproduce figures, diagrams etc. contained in this article in third party publications or in a thesis or dissertation provided that the correct acknowledgement is given with the reproduced material.

Reproduced material should be attributed as follows:

- For reproduction of material from NJC:
  [Original citation] - Reproduced by permission of The Royal Society of Chemistry (RSC) on behalf of the Centre National de la Recherche Scientifique (CNRS) and the RSC
- For reproduction of material from PCCP:
  [Original citation] - Reproduced by permission of the PCCP Owner Societies
- For reproduction of material from PPS:
  [Original citation] - Reproduced by permission of The Royal Society of Chemistry (RSC) on behalf of the European Society for Photobiology, the European Photochemistry Association, and RSC
- For reproduction of material from all other RSC journals:
  [Original citation] - Reproduced by permission of The Royal Society of Chemistry

COPYRIGHT PERMISSION FOR CHAPTER 4

The Copyright permission for Chapter 4 is attached below.

Reprinted from *Biomaterials*, 35, H.He, A.W. Cattran, T. Nguyen, AL. Nieminen and P. Xu. Triple-responsive expansile nanogel for tumor and mitochondria targeted photosensitizer delivery, 9546-9553, Copyright (2014), with permission from Elsevier.

ELSEVIER LICENSE
TERMS AND CONDITIONS

Mar 21, 2016

This is a License Agreement between Huacheng He ("You") and Elsevier ("Elsevier") provided by Copyright Clearance Center ("CCC"). The license consists of your order details, the terms and conditions provided by Elsevier, and the payment terms and conditions.

All payments must be made in full to CCC. For payment instructions, please see information listed at the bottom of this form.

Supplier	Elsevier Limited The Boulevard,Langford Lane Kidlington,Oxford,OX5 1GB,UK
Registered Company Number	1982084
Customer name	Huacheng He
Customer address	715 Sumter Street COLUMBIA, SC 29208
License number	3833730463050
License date	Mar 21, 2016
Licensed content publisher	Elsevier
Licensed content publication	Biomaterials
Licensed content title	Triple-responsive expansile nanogel for tumor and mitochondria targeted photosensitizer delivery
Licensed content author	Huacheng He,Alexander W. Cattran,Tu Nguyen,Anna-Liisa Nieminen,Peisheng Xu
Licensed content date	November 2014
Licensed content volume number	35
Licensed content issue number	35
Number of pages	8
Start Page	9546
End Page	9553
Type of Use	reuse in a thesis/dissertation
Portion	full article
Format	both print and electronic
Are you the author of this Elsevier article?	Yes
Will you be translating?	No
Title of your thesis/dissertation	Stimuli responsive nanoparticle for cancer targeted therapy
Expected completion date	May 2016

Estimated size (number of pages)	200
Elsevier VAT number	GB 494 6272 12
Permissions price	0.00 USD
VAT/Local Sales Tax	0.00 USD / 0.00 GBP
Total	0.00 USD

Terms and Conditions

INTRODUCTION

1. The publisher for this copyrighted material is Elsevier. By clicking "accept" in connection with completing this licensing transaction, you agree that the following terms and conditions apply to this transaction (along with the Billing and Payment terms and conditions established by Copyright Clearance Center, Inc. ("CCC"), at the time that you opened your Rightslink account and that are available at any time at http://myaccount.copyright.com).

GENERAL TERMS

2. Elsevier hereby grants you permission to reproduce the aforementioned material subject to the terms and conditions indicated.

3. Acknowledgement: If any part of the material to be used (for example, figures) has appeared in our publication with credit or acknowledgement to another source, permission must also be sought from that source. If such permission is not obtained then that material may not be included in your publication/copies. Suitable acknowledgement to the source must be made, either as a footnote or in a reference list at the end of your publication, as follows:

"Reprinted from Publication title, Vol /edition number, Author(s), Title of article / title of chapter, Pages No., Copyright (Year), with permission from Elsevier [OR APPLICABLE SOCIETY COPYRIGHT OWNER]." Also Lancet special credit - "Reprinted from The Lancet, Vol. number, Author(s), Title of article, Pages No., Copyright (Year), with permission from Elsevier."

4. Reproduction of this material is confined to the purpose and/or media for which permission is hereby given.

5. Altering/Modifying Material: Not Permitted. However figures and illustrations may be altered/adapted minimally to serve your work. Any other abbreviations, additions, deletions and/or any other alterations shall be made only with prior written authorization of Elsevier Ltd. (Please contact Elsevier at permissions@elsevier.com)

6. If the permission fee for the requested use of our material is waived in this instance, please be advised that your future requests for Elsevier materials may attract a fee.

7. Reservation of Rights: Publisher reserves all rights not specifically granted in the combination of (i) the license details provided by you and accepted in the course of this licensing transaction, (ii) these terms and conditions and (iii) CCC's Billing and Payment terms and conditions.

8. License Contingent Upon Payment: While you may exercise the rights licensed immediately upon issuance of the license at the end of the licensing process for the transaction, provided that you have disclosed complete and accurate details of your proposed use, no license is finally effective unless and until full payment is received from you (either by publisher or by CCC) as provided in CCC's Billing and Payment terms and conditions. If full payment is not received on a timely basis, then any license preliminarily granted shall be deemed automatically revoked and shall be void as if never granted. Further, in the event that you breach any of these terms and conditions or any of CCC's Billing and Payment terms and conditions, the license is automatically revoked and shall be void as if never

granted. Use of materials as described in a revoked license, as well as any use of the materials beyond the scope of an unrevoked license, may constitute copyright infringement and publisher reserves the right to take any and all action to protect its copyright in the materials.

9. Warranties: Publisher makes no representations or warranties with respect to the licensed material.

10. Indemnity: You hereby indemnify and agree to hold harmless publisher and CCC, and their respective officers, directors, employees and agents, from and against any and all claims arising out of your use of the licensed material other than as specifically authorized pursuant to this license.

11. No Transfer of License: This license is personal to you and may not be sublicensed, assigned, or transferred by you to any other person without publisher's written permission.

12. No Amendment Except in Writing: This license may not be amended except in a writing signed by both parties (or, in the case of publisher, by CCC on publisher's behalf).

13. Objection to Contrary Terms: Publisher hereby objects to any terms contained in any purchase order, acknowledgment, check endorsement or other writing prepared by you, which terms are inconsistent with these terms and conditions or CCC's Billing and Payment terms and conditions. These terms and conditions, together with CCC's Billing and Payment terms and conditions (which are incorporated herein), comprise the entire agreement between you and publisher (and CCC) concerning this licensing transaction. In the event of any conflict between your obligations established by these terms and conditions and those established by CCC's Billing and Payment terms and conditions, these terms and conditions shall control.

14. Revocation: Elsevier or Copyright Clearance Center may deny the permissions described in this License at their sole discretion, for any reason or no reason, with a full refund payable to you. Notice of such denial will be made using the contact information provided by you. Failure to receive such notice will not alter or invalidate the denial. In no event will Elsevier or Copyright Clearance Center be responsible or liable for any costs, expenses or damage incurred by you as a result of a denial of your permission request, other than a refund of the amount(s) paid by you to Elsevier and/or Copyright Clearance Center for denied permissions.

LIMITED LICENSE

The following terms and conditions apply only to specific license types:

15. **Translation**: This permission is granted for non-exclusive world **English** rights only unless your license was granted for translation rights. If you licensed translation rights you may only translate this content into the languages you requested. A professional translator must perform all translations and reproduce the content word for word preserving the integrity of the article.

16. **Posting licensed content on any Website**: The following terms and conditions apply as follows: Licensing material from an Elsevier journal: All content posted to the web site must maintain the copyright information line on the bottom of each image; A hyper-text must be included to the Homepage of the journal from which you are licensing at http://www.sciencedirect.com/science/journal/xxxxx or the Elsevier homepage for books at http://www.elsevier.com; Central Storage: This license does not include permission for a scanned version of the material to be stored in a central repository such as that provided by Heron/XanEdu.

Licensing material from an Elsevier book: A hyper-text link must be included to the Elsevier homepage at http://www.elsevier.com . All content posted to the web site must maintain the copyright information line on the bottom of each image.

Posting licensed content on Electronic reserve: In addition to the above the following clauses are applicable: The web site must be password-protected and made available only to bona fide students registered on a relevant course. This permission is granted for 1 year only. You may obtain a new license for future website posting.

17. **For journal authors:** the following clauses are applicable in addition to the above:

Preprints:

A preprint is an author's own write-up of research results and analysis, it has not been peer-reviewed, nor has it had any other value added to it by a publisher (such as formatting, copyright, technical enhancement etc.).

Authors can share their preprints anywhere at any time. Preprints should not be added to or enhanced in any way in order to appear more like, or to substitute for, the final versions of articles however authors can update their preprints on arXiv or RePEc with their Accepted Author Manuscript (see below).

If accepted for publication, we encourage authors to link from the preprint to their formal publication via its DOI. Millions of researchers have access to the formal publications on ScienceDirect, and so links will help users to find, access, cite and use the best available version. Please note that Cell Press, The Lancet and some society-owned have different preprint policies. Information on these policies is available on the journal homepage.

Accepted Author Manuscripts: An accepted author manuscript is the manuscript of an article that has been accepted for publication and which typically includes author-incorporated changes suggested during submission, peer review and editor-author communications.

Authors can share their accepted author manuscript:

- immediately
  - via their non-commercial person homepage or blog
  - by updating a preprint in arXiv or RePEc with the accepted manuscript
  - via their research institute or institutional repository for internal institutional uses or as part of an invitation-only research collaboration work-group
  - directly by providing copies to their students or to research collaborators for their personal use
  - for private scholarly sharing as part of an invitation-only work group on commercial sites with which Elsevier has an agreement
- after the embargo period
  - via non-commercial hosting platforms such as their institutional repository
  - via commercial sites with which Elsevier has an agreement

In all cases accepted manuscripts should:

- link to the formal publication via its DOI
- bear a CC-BY-NC-ND license - this is easy to do
- if aggregated with other manuscripts, for example in a repository or other site, be shared in alignment with our hosting policy not be added to or enhanced in any way to appear more like, or to substitute for, the published journal article.

Published journal article (JPA): A published journal article (PJA) is the definitive final record of published research that appears or will appear in the journal and embodies all value-adding publishing activities including peer review co-ordination, copy-editing, formatting, (if relevant) pagination and online enrichment.

Policies for sharing publishing journal articles differ for subscription and gold open access

articles:

Subscription Articles: If you are an author, please share a link to your article rather than the full-text. Millions of researchers have access to the formal publications on ScienceDirect, and so links will help your users to find, access, cite, and use the best available version. Theses and dissertations which contain embedded PJAs as part of the formal submission can be posted publicly by the awarding institution with DOI links back to the formal publications on ScienceDirect.

If you are affiliated with a library that subscribes to ScienceDirect you have additional private sharing rights for others' research accessed under that agreement. This includes use for classroom teaching and internal training at the institution (including use in course packs and courseware programs), and inclusion of the article for grant funding purposes.

Gold Open Access Articles: May be shared according to the author-selected end-user license and should contain a CrossMark logo, the end user license, and a DOI link to the formal publication on ScienceDirect.

Please refer to Elsevier's posting policy for further information.

18. **For book authors** the following clauses are applicable in addition to the above: Authors are permitted to place a brief summary of their work online only. You are not allowed to download and post the published electronic version of your chapter, nor may you scan the printed edition to create an electronic version. **Posting to a repository:** Authors are permitted to post a summary of their chapter only in their institution's repository.

19. **Thesis/Dissertation**: If your license is for use in a thesis/dissertation your thesis may be submitted to your institution in either print or electronic form. Should your thesis be published commercially, please reapply for permission. These requirements include permission for the Library and Archives of Canada to supply single copies, on demand, of the complete thesis and include permission for Proquest/UMI to supply single copies, on demand, of the complete thesis. Should your thesis be published commercially, please reapply for permission. Theses and dissertations which contain embedded PJAs as part of the formal submission can be posted publicly by the awarding institution with DOI links back to the formal publications on ScienceDirect.

Elsevier Open Access Terms and Conditions

You can publish open access with Elsevier in hundreds of open access journals or in nearly 2000 established subscription journals that support open access publishing. Permitted third party re-use of these open access articles is defined by the author's choice of Creative Commons user license. See our open access license policy for more information.

Terms & Conditions applicable to all Open Access articles published with Elsevier:

Any reuse of the article must not represent the author as endorsing the adaptation of the article nor should the article be modified in such a way as to damage the author's honour or reputation. If any changes have been made, such changes must be clearly indicated.

The author(s) must be appropriately credited and we ask that you include the end user license and a DOI link to the formal publication on ScienceDirect.

If any part of the material to be used (for example, figures) has appeared in our publication with credit or acknowledgement to another source it is the responsibility of the user to ensure their reuse complies with the terms and conditions determined by the rights holder.

Additional Terms & Conditions applicable to each Creative Commons user license:

CC BY: The CC-BY license allows users to copy, to create extracts, abstracts and new works from the Article, to alter and revise the Article and to make commercial use of the Article (including reuse and/or resale of the Article by commercial entities), provided the user gives appropriate credit (with a link to the formal publication through the relevant DOI), provides a link to the license, indicates if changes were made and the licensor is not

represented as endorsing the use made of the work. The full details of the license are available at http://creativecommons.org/licenses/by/4.0.

CC BY NC SA: The CC BY-NC-SA license allows users to copy, to create extracts, abstracts and new works from the Article, to alter and revise the Article, provided this is not done for commercial purposes, and that the user gives appropriate credit (with a link to the formal publication through the relevant DOI), provides a link to the license, indicates if changes were made and the licensor is not represented as endorsing the use made of the work. Further, any new works must be made available on the same conditions. The full details of the license are available at http://creativecommons.org/licenses/by-nc-sa/4.0.

CC BY NC ND: The CC BY-NC-ND license allows users to copy and distribute the Article, provided this is not done for commercial purposes and further does not permit distribution of the Article if it is changed or edited in any way, and provided the user gives appropriate credit (with a link to the formal publication through the relevant DOI), provides a link to the license, and that the licensor is not represented as endorsing the use made of the work. The full details of the license are available at http://creativecommons.org/licenses/by-nc-nd/4.0.

Any commercial reuse of Open Access articles published with a CC BY NC SA or CC BY NC ND license requires permission from Elsevier and will be subject to a fee.

Commercial reuse includes:

- Associating advertising with the full text of the Article
- Charging fees for document delivery or access
- Article aggregation
- Systematic distribution via e-mail lists or share buttons

Posting or linking by commercial companies for use by customers of those companies.

20. **Other Conditions**:

v1.8

Questions? customercare@copyright.com or +1-855-239-3415 (toll free in the US) or +1-978-646-2777.